LEVERAGING BACKSCATTER FOR ULTRA-LOW POWER WIRELESS SENSING SYSTEMS

A Dissertation Presented

by

PENGYU ZHANG

Submitted to the Graduate School of the
University of Massachusetts Amherst in partial fulfillment
of the requirements for the degree of

DOCTOR OF PHILOSOPHY

May 2016

College of Information and Computer Sciences

LEVERAGING BACKSCATTER FOR ULTRA-LOW POWER WIRELESS SENSING SYSTEMS

A Dissertation Presented

by

PENGYU ZHANG

ACKNOWLEDGMENTS

I would not have been able to complete this thesis without the guidance of my advisor and the support of my friends and family. Professor Deepak Ganesan taught me key skills needed for any researcher: how to identify and formulate a research problem, tackle a research problem from a unique angle, think critically about a potential solution, develop a big research vision, etc. I especially thank Deepak for his hands-on advising when I started my Ph.D. study and had little knowledge of what is good research. I also appreciate Deepak for reminding me to take one step back from details and looking at the problem again.

I also enjoyed working with Professor Prashant Shenoy, Arun Venkataramani, and Ben Marlin in such a diverse and collaborative department. I would like to thank Professor Kevin Fu for being my synthesis advisor. I was fortunate to have discussions with Professor Dennis Goeckel who gave me lots of feedback from the perspective of wireless communication theory.

I have collaborated with researchers outside of UMass while on an internship at Microsoft Research Redmond. I would like to thank Bodhi Priyantha, Jie Liu, and Matthai Philipose for working closely with me on the mobile vision project. They taught me how to think about a project from the perspective of industry research.

I would like to thank Jeremy Gummeson and Negin Salajegheh for sharing hands-on experiences about building systems and doing system research. I am grateful for being able to have five years' discussion with Bo Jiang about how to use probability theory to analyze system performance. I also thank Pan Hu for teaching me hardware design principles.

My life in Amherst would not be so much fun if I did not have incredible friends from sensors research group, CS department, and other departments at UMass. I would like to thank Tingxin Yan, Abhinav Parate, Addison Mayberry, Moaj Musthag, Annamalai Natarajan, Yamin Tun, and other folks who made my life in Amherst wonderful.

I finally want to thank my parents who raised me up and have been supporting me for years. I felt lucky to spend my graduate school with my wife, Shaofang Wang, together. I am grateful for having our beautiful daughter Elly Zhang born in the middle of my Ph.D. study. I am looking forward to continuing our journey together.

ABSTRACT

LEVERAGING BACKSCATTER FOR ULTRA-LOW POWER WIRELESS SENSING SYSTEMS

MAY 2016

PENGYU ZHANG

B.Sc., TSINGHUA UNIVERSITY, BEIJING, CHINA

M.Sc., TSINGHUA UNIVERSITY, BEIJING, CHINA

Ph.D., UNIVERSITY OF MASSACHUSETTS AMHERST

Directed by: Professor Deepak Ganesan

The past few years have seen a dramatic growth in wireless sensing systems, with millions of wirelessly connected sensors becoming first-class citizens of the Internet. The number of wireless sensing devices is expected to surpass 6.75 billion by 2017, more than the world's population as well as the combined market of smartphones, tablets, and PCs. However, its growth faces two pressing challenges: battery energy density and wireless radio power consumption. Battery energy density looms as a fundamental limiting factor due to slow improvements over the past several decades ($3\times$ over 22 years). Wireless radio power consumption is another key challenge because high-speed wireless communication is often far more expensive energy-wise than computation, storage and sensing. To make matters worse, wireless sensing devices are generating an increasing amount of data.

These challenges raise a fundamental question — how should we power and communicate with wireless sensing devices. More specifically, instead of using batteries, can we leverage other energy sources to reduce, if not eliminate, the dependence on batteries? Similarly, instead of optimizing existing wireless radios, can we fundamentally change how radios transmit wireless signals to achieve lower power consumption?

A promising technique to address these questions is backscatter — a primitive that enables RF energy harvesting and ultra-low-power wireless communication. Backscatter has the potential to reduce dependence on batteries because it can obtain energy by rectifying the wireless signals transmitted by a backscatter reader. Backscatter can also work by reflecting existing wireless signals (WiFi, BLE) when these are available nearby. Because signal reflection only consumes μWs of power, backscatter can enable ultra-low-power wireless communication.

However, the use of backscatter for communicating with wireless sensing devices presents several challenges. First, decreasing RF power across distance limits the operational range of micro-powered backscatter devices. This raises the question of how to maintain a communication link with a backscatter device despite tiny amount of harvested power. Second, even though the backscatter RF front-end is extremely power-efficient, the computational and sensing overhead on backscatter sensors limit its ability to operate with a few μWs of power. Such overhead is a negligible factor of overall power consumption for platforms where radio power consumption is high (e.g. WiFi or Bluetooth based devices). However, it becomes the bottleneck for backscatter based platforms. Third, backscatter readers are not currently deployed in existing indoor environments to provide a continuous carrier for carrying backscattered information. As a result, backscatter deployment is not yet widespread.

This thesis addresses these challenges by making the following contributions. First, we design a network stack that enables continuous operation despite decreasing harvested power across distance by employing an OS abstraction — task fragmentation. We show that such a network stack enables packet transfer even when the whole system is powered by a 3cm$\times$3cm solar panel under natural indoor light condition.

Second, we design a hardware architecture that minimizes the computational overhead of backscatter to enable over 1Mbps backscatter transmission while consuming less than 100μWs of power, a two order of magnitude improvement over the state-of-the-art. Finally, we design a system that can leverage both ambient WiFi and BLE signals for backscatter. Our empirical evaluation shows that we can backscatter 500bps data on top of a WiFi stream and 50kbps data on top of a Bluetooth stream when the backscatter device is 3m away from the commercial WiFi and Bluetooth receivers.

TABLE OF CONTENTS

Page

ACKNOWLEDGMENTS . . . . **iv**

ABSTRACT . . . . **vi**

LIST OF TABLES . . . . **xv**

LIST OF FIGURES . . . . **xvi**

CHAPTER

1. INTRODUCTION **1**

1.1 Background and Motivation 1
1.2 Thesis Contribution 4

1.2.1 Contribution Summary 5
1.2.2 Thesis Overview 5
1.2.3 Network Stack for Micro-powered Sensors — QuarkNet 5
1.2.4 High Speed Ultra Low-power Backscatter — Ekho 6
1.2.5 Leveraging Ambient Wireless Signals — FS-Backscatter 7

2. BACKGROUND **8**

2.1 Backscatter system overview 8
2.2 Hardware overview 9

2.2.1 Backscatter radio analog RF front end 9
2.2.2 RF energy harvesting 10

2.3 Backscatter channel model 11

2.3.1 Backscatter link budget 11
2.3.2 Asymmetric forward and backward links 12

3. PUSHING THE OPERATING LIMITS OF MICRO-POWERED SENSORS 14

3.1 Background and Motivation 14
3.2 Case for μframes 18

3.2.1 Challenge 1: Variable energy per transmission 19
3.2.2 Challenge 2: Variable harvesting rate 21
3.2.3 Challenge 3: Time-decaying SNR 22
3.2.4 Challenge 4: Energy-induced reader to node losses 23

3.3 Fragmenting packets into μframes 24

3.3.1 Fragmentation at bit boundaries 25
3.3.2 Tuning inter-μframe gap 26

3.3.2.1 Gradient descent algorithm 26
3.3.2.2 Handling time-varying SNR 27
3.3.2.3 Duty-cycling the radio 27

3.3.3 Remote interrupts 28

3.3.3.1 Estimating μframe length 28
3.3.3.2 Estimating inter-μframe gap 29

3.4 QuarkNet for multi-node networks 30

3.4.1 Design Options 30
3.4.2 Variability-aware node scheduling 31

3.5 Implementation 32

3.5.1 Platforms 32

3.5.1.1 USRP Reader 32
3.5.1.2 Backscatter node 33

3.5.2 Trimming Overheads 33

3.5.2.1 Radio transition overhead 33
3.5.2.2 Pilot tone 34
3.5.2.3 Probing energy state 34

3.5.3 Protocols and Algorithms 34

3.6 Evaluation 35

3.6.1 Benefit of μframes 35

3.6.1.1 Minimum operating conditions 35
3.6.1.2 Increased operational range 36

3.6.2 Benefits of μframe adaptation 37

3.6.2.1 Convergence of gradient descent 37
3.6.2.2 Throughput benefits 37
3.6.2.3 Breaking down the benefits 39
3.6.2.4 QuarkNet vs battery-assisted alternatives 40

3.6.3 Reader-to-node communication 40
3.6.4 Evaluating the QuarkNet MAC layer 41
3.6.5 Microbenchmarks 42

3.7 Discussion 43

3.7.1 Interoperability with other PHY mechanisms 43
3.7.2 QuarkNets role with evolving technology 43
3.7.3 Fragmenting other tasks 44

3.8 Related Work 44

3.8.1 Computational RFIDs (CRFIDs) 45
3.8.2 EPC Gen 2 optimizations 45

3.9 Conclusion 46

4. HIGH SPEED ULTRA LOW-POWER BACKSCATTER 47

4.1 Background and Motivation 47
4.2 Case for Ekho 50

4.2.1 Backscatter radio RF front end 50
4.2.2 Why compute if its cheaper to transmit? 52

4.2.2.1 Computation vs Communication 52
4.2.2.2 Implications on architecture design 54

4.3 Investigating existing wireless sensing architectures 54

4.3.1 Poor energy efficiency 55

4.3.1.1 Sensor data acquisition 55
4.3.1.2 Data handling subsystem 56
4.3.1.3 Communication subsystem 58

4.3.2 Poor transmission efficiency 59
4.3.3 Summary 60

4.4 The Ekho platform 60

4.4.1 Eliminating computational blocks 61
4.4.2 The EkhoNet MAC layer 62

4.4.2.1 MAC Design Considerations 63
4.4.2.2 Channel-Utility-Energy aware Rate Selection 66

4.5 Implementation 68

4.5.1 Hardware 68
4.5.2 Software defined backscatter reader 69
4.5.3 MAC layer protocol 70

4.6 Evaluation 71

4.6.1 Experimental setup 71
4.6.2 Ekho power benchmarks 72
4.6.3 Whole-system power consumption 73
4.6.4 Evaluating EkhoNet's throughput 75

4.7 Related Work 78

4.7.1 Backscatter communication 78
4.7.2 Optimized sensing platforms 79

4.8 Discussion 80

4.8.1 FPGA v.s. MCU 80
4.8.2 Power benefits 80
4.8.3 Encoding 81
4.8.4 Applications 82

4.9 Conclusion 83

5. ENABLING PRACTICAL BACKSCATTER COMMUNICATION FOR ON-BODY SENSORS 84

5.1 Introduction 84
5.2 Case for FS-Backscatter 88

5.2.1 Infrastructure-assisted Backscatter 88
5.2.2 Infrastructure-less Backscatter 89

5.2.2.1 Low signal-to-noise ratio 91
5.2.2.2 Mobility-induced dynamics 91

5.2.3 FS-Backscatter: Key Ideas and Challenges 92

5.3 Frequency-Shifted Backscatter 94

5.3.1 FS-Backscatter on Commodity Radios 94

5.3.1.1 Packet-level FS-Backscatter 95
5.3.1.2 Bit-level FS-Backscatter 97
5.3.1.3 What if no channels are available? 98
5.3.1.4 Can we improve robustness by using multiple transmitters or receivers? 99

5.3.2 Low-power FS-Backscatter Tag 100

5.3.2.1 What is the power bottleneck? 101
5.3.2.2 Can we shift by 20MHz while consuming μWs? 102
5.3.2.3 Reducing operating voltage 105

5.4 Implementation 106
5.5 Evaluation 109

5.5.1 FS-Backscatter: Throughput and BER 109
5.5.2 Multiple Carriers and Receivers 112

5.5.2.1 Leveraging multiple carriers 112
5.5.2.2 Leveraging multiple receivers 113

5.5.3 Power consumption 113
5.5.4 FS-Backscatter vs BLE/Zigbee 114
5.5.5 Mobile and static deployment 116
5.5.6 Mutual Interference 117

5.6 Related Work 119
5.7 Conclusion 120

6. CONCLUSION AND FUTURE WORK 121

6.1 Thesis Summary 121
6.2 Future Work 122

6.2.1 Applications enabled by backscatter 123
6.2.2 Passive sensing via backscatter 123
6.2.3 Mobile health 124

BIBLIOGRAPHY **125**

LIST OF TABLES

Table **Page**

2.1 Parameters used for modeling bi-static and mono-static backscatter. 11

3.1 EPC Gen 2 vs Achievable Performance. 19

3.2 Overhead of μframe transmission. 43

4.1 Power consumption of accelerometer, audio, ecg, and image sensors. 48

5.1 Power consumed by commercial oscillators operating at different frequencies and different accuracies. 102

5.2 FS-Backscatter energy efficiency. Pkt refers to packet-level decoding, and Bit refers to bit-level decoding. 115

LIST OF FIGURES

Figure **Page**

1.1 The wireless sensing devices alone will surpass the smartphone, tablet, and PC market combined by 2017 [1]. 1

1.2 3× battery energy density improvement from 1990 to 2012. 2

1.3 Power consumption of several low-power wireless radios. 3

1.4 An overview of thesis. 6

2.1 Backscatter system architecture. 9

2.2 Backscatter communication analog RF front end. 10

2.3 Link budget of bi-static and mono-static backscatter. 12

3.1 Backscatter signaling at PHY. 18

3.2 Energy harvesting systems. 20

3.3 Factors that impact communication throughput. 21

3.4 Sleep gaps can be inserted into backscatter pulses at various position (lines with dots). 26

3.5 In-band remote interruptions from nodes. 29

3.6 The maximum range achieved by EPC Gen 2, Dewdrop, Buzz, QuarkNet, and a battery assisted node. QuarkNet operates at ranges close to the battery assisted node. 37

3.7 Throughput achieved for different sleep times (inter-μframe gaps). The sleep time chosen by QuarkNet is within 98% of the optimal. 38

3.8 For micro-powered devices, QuarkNet improves throughput by at least 3.3× over all other schemes, and even performs better than battery assisted nodes. The benefit comes from reducing overhead, and adapting μframe sizes to energy and SNR. 39

3.9 Throughput achieved by EPC Gen 2, Dewdrop, Flit, and QuarkNet across 30 locations. QuarkNet has at least 4.4× higher throughput than other schemes. 39

3.10 Throughput of reader-to-node communication. QuarkNet has 2× higher throughput than battery-assisted EPC Gen 2 Writes. 41

3.11 Throughput of 10 nodes is 5.4× higher when interleaved than when individually inventoried. 42

4.1 Backscatter communication basics. 51

4.2 1 bit adder and 1 bit shift register circuit. 52

4.3 Computational blocks on existing backscatter-based sensors. 55

4.4 Power consumed for handling timer interrupts at 4kHz. The MCU is unable to switch to sleep mode due to frequent interrupts. 56

4.5 The power consumption of DMA transfer at different frequencies. 57

4.6 Power consumption of DMA transfer at 100Hz. DMA is slow to return to sleep mode. 58

4.7 The key components of Ekho. 61

4.8 Efficiency of backscatter radio (in bits/joule). 64

4.9 SNR at different bit rates when device is placed 1m from a reader. 64

4.10 Mean Opinion Score (MOS) at different sampling rates for a microphone. 65

4.11 Ekho is implemented as a low-profile printed circuit board with small form factor. 69

4.12 Timeline of Ekho MAC. 70

4.13 Power reduction for sensing subsystem: a) sampling an accelerometer, b) sampling a microphone. 72

4.14 Power reduction for data transfer to network queue. 73

4.15 The power consumption of operating a backscatter radio. 74

4.16 Whole-system power consumption for operating an accelerometer sensor. 75

4.17 Whole-system power consumption for operating an audio sensor. 75

4.18 Comparing throughputs of EPC Gen 2, QuarkNet on Moo vs Ekho across 30 locations. 76

4.19 Boxplot of the MOS scores for 10 Ekho nodes with microphones at 3 locations (3 ft, 6 ft, 9 ft). 78

4.20 SNR of transmitting encoded and raw data across 20 locations 82

5.1 Throughput of WiFi Backscatter across distance with 3dBi Omni-directional [7] and 9dBi directional [17] antennas. 90

5.2 SNR and SINR of backscatter across distance. 92

5.3 Received WiFi signal strength in static and mobile deployment. 93

5.4 FS-Backscatter reflects a WiFi signal and a Bluetooth signal to adjacent non-overlapping channels. 93

5.5 FS-Backscatter throughput across distance when leveraging WiFi and Bluetooth signals. 96

5.6 FS-Backscatter spectrum when leveraging 2.4GHz WiFi channel 13 for carrying backscattered information. 99

5.7 Backscatter tag power consumption breakdown. 102

5.8 Ring oscillator circuit diagram. 103

5.9 Ring oscillator frequency when temperature changes. The normal range of skin temperatures is fairly tight (typically between 36.6^{o}C and 37.2^{o}C). 104

5.10 Packet-level decoder throughput on a WiFi signal when a tag experiences ±250kHz frequency offset. 105

5.11 FS-Backscatter tag diagram. 106

5.12 FS-Backscatter radio analog front end 107

5.13 FS-Backscatter throughput and BER across distance when leveraging WiFi and Bluetooth signals. 111

5.14 FS-Backscatter throughput benefit when leveraging multiple active transmitters and receivers. 112

5.15 Benchmarking the power consumption of a FS-Backscatter tag. 114

5.16 FS-backscatter throughput in static and mobile deployment. 116

5.17 Mutual interference between FS-Backscatter and WiFi. 118

CHAPTER 1
INTRODUCTION

1.1 Background and Motivation

The past few years have seen a dramatic growth in wireless sensing devices, with millions of wirelessly connected sensors becoming first-class citizens of the Internet. Figure 1.1 shows that the number of wireless sensing devices is expected to surpass 6.75 billion by 2017, more than the world's population as well as the combined market of smartphones, tablets, and PCs. However, the growth of wireless sensing devices faces two pressing challenges: battery energy density and wireless radio power consumption.

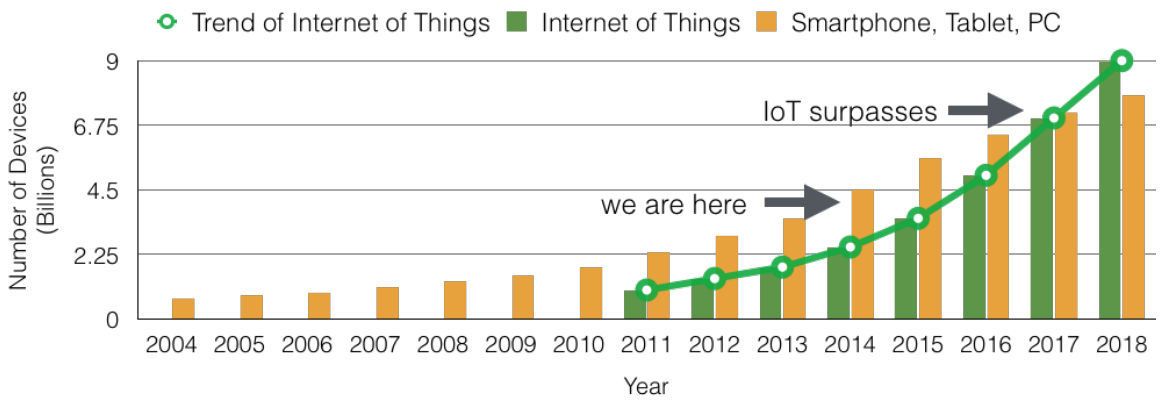

Figure 1.1. The wireless sensing devices alone will surpass the smartphone, tablet, and PC market combined by 2017 [1].

Battery energy density looms as a fundamental limiting factor in wireless sensing devices especially because improvements have been slow over the past several decades. Figure 1.2 shows that battery energy density has improved by only 3× over the past

22 years. Research forecasts, such as Forbes research, also identifies this limitation and says "*Currently, connected devices, such as Pebble and Galaxy Gear, run on batteries, which have limited shelf life. Given current energy availability, powering these devices will be impossible. Prolonged battery life that sources energy from unconventional power sources is a must for future development for the Internet of Things*" [8].

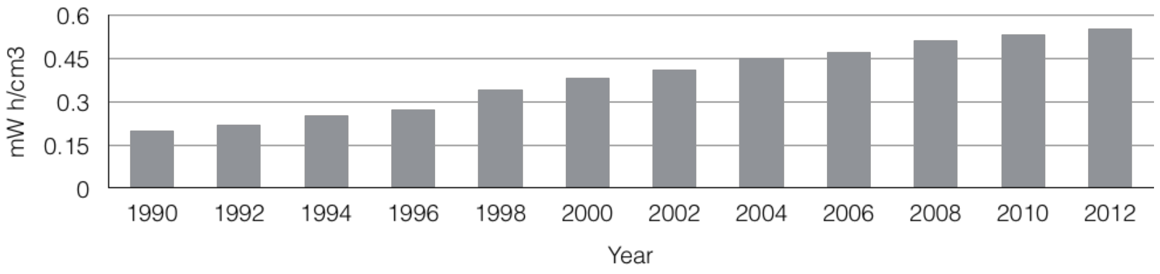

Figure 1.2. 3× battery energy density improvement from 1990 to 2012.

Wireless radio power consumption is another key challenge as high-speed wireless communication is often far more expensive energy-wise than computation, storage or sensing. Figure 1.3 shows the power consumption of a variety of wireless radios and other components of a wireless sensing device. Even Bluetooth Low Energy (BLE), which has the lowest power consumption among these radios, consumes 15mW during an active transmission, orders of magnitude higher than the power needed for computation (MSP430 MCU), storage (SRAM), or in many cases sensing (e.g. accelerometer). Therefore, there is a dire need to design novel wireless communication techniques to achieve higher data rates while simultaneously minimizing energy consumption.

These challenges raise a fundamental question — how should we power and communicate with wireless sensing devices. More specifically, instead of using batteries, can we leverage other energy sources to reduce, if not eliminate, the dependence on batteries? Similarly, instead of optimizing existing wireless radios, can we fundamentally change how radios transmit wireless signals to achieve lower power consumption?

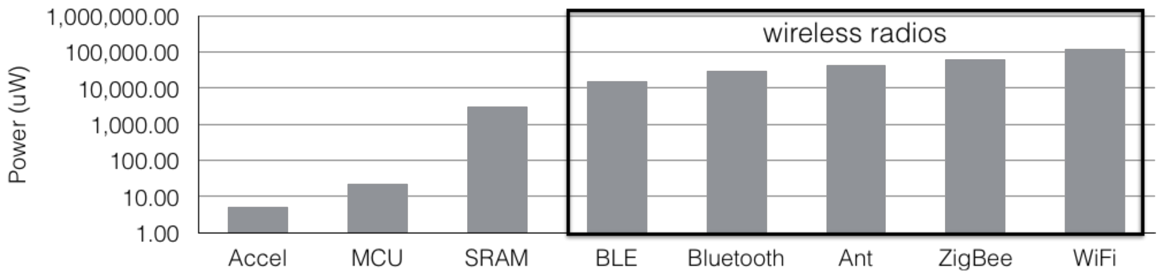

Figure 1.3. Power consumption of several low-power wireless radios.

A possible answer to these questions is backscatter — a primitive that enables RF energy harvesting and ultra-low-power wireless communication. Backscatter has the potential to reduce the dependence on batteries because it can obtain energy by rectifying a wireless signal transmitted by a backscatter reader or an ambient wireless radio, such as WiFi and Bluetooth. In addition, instead of directly transmitting high-power wireless signals, backscatter modulates information by reflecting existing wireless signals. Because signal reflection only consumes μWs of power, backscatter has the potential to enable ultra-low-power and high-speed wireless connection for wireless sensing devices.

However, the use of backscatter for wireless sensing devices presents several challenges. First, backscatter RF power decreases sharply across the distance, which limits the operational range of micro-powered backscatter devices. This trend is a result of path loss and can be modeled with the Friis model shown in equation 1.1 (in logarithmic form). In this model, P_T is the transmit power of the reader, λ is the carrier wave length, G_T is the transmit antenna gain, G_R is the receive dipole antenna gain of the backscatter device, d is the distance between the reader and the backscatter device, and L_P is the polarization loss. The amount of RF power, P_R, available for harvesting decreases as the distance d increases. As a result, a micro-powered backscatter device does not have enough energy for operation at a longer distance even though the SNRs of both backscatter reader-to-tag and tag-to-reader links are still sufficient for data communication.

$$P_R = P_T - 20\log(\frac{4\pi d}{\lambda}) + G_T + G_R - L_P P_R \propto \frac{1}{d^2} \tag{1.1}$$

Second, computational overheads on backscatter sensors limit their ability to operate at μWs of harvested power. These overheads include acquiring data from sensors, migrating sensor data to the radio, and executing network protocols. These overheads are negligible on platforms where wireless communication is expensive (e.g. WiFi-based sensors). However, because of the ultra-low power consumption of backscatter radios, they become the bottleneck on backscatter-based systems and increase power consumption while limiting throughput. Therefore, there is a dire need to systematically investigate the sources of these computational overheads and understand how to eliminate them.

Third, backscatter readers are not yet integrated into commonly used mobile and wearable devices nor deployed widely in urban settings. An alternative would be to leverage ambient signals (e.g. WiFi and BLE) that already exist. However, leveraging ambient signals for backscatter is hard primarily because an ambient signal itself causes substantial interference to a backscatter receiver. As a result, decoding weak reflected signal becomes harder. Another challenge comes from the bursty nature of an ambient signal where it is not always available for backscatter. As a result, we cannot directly use an off-the-shelf receiver (e.g. WiFi or BLE receiver) to decode backscattered information.

1.2 Thesis Contribution

My thesis tackles these challenges and seeks to enable the practical adoption of backscatter for wireless sensing systems.

1.2.1 Contribution Summary

Overall, the key systems and contributions of this thesis are:

- QuarkNet – A network stack that tackles the challenge of operating under decreasing harvested power across distance by employing task fragmentation. Our network stack enables packet transfer even when the whole system is powered by a 3cm×3cm solar panel under the natural indoor light.
- Ekho – A hardware architecture that minimizes the computational overheads of a backscatter system to enable ≥1Mbps backscatter transmission while only consuming ≤100μW of power, two orders of magnitude improvement over the state-of-the-art.
- FS-Backscatter — A system that can leverage ambient WiFi and Bluetooth signals in an environment for carrying backscattered information. Our system can achieve 500bps and 50kbps data rate when a backscatter tag is 5m away from the commercial WiFi and Bluetooth receivers respectively.

1.2.2 Thesis Overview

Figure 1.4 shows an overview of the thesis. It includes three components to tackle the three key challenges of backscatter systems.

1.2.3 Network Stack for Micro-powered Sensors — QuarkNet

In chapter 3, we present the design of a network stack to tackle the challenge of operating under decreasing harvested power across distance. Its design is based on the observation that communication often fails not because energy cannot be harvested but because packet transfer involves hundreds of instructions and cannot fit into the available energy budget. To address this problem, we develop a simple but powerful abstraction — by fragmenting any networking task into its smallest atomic units,

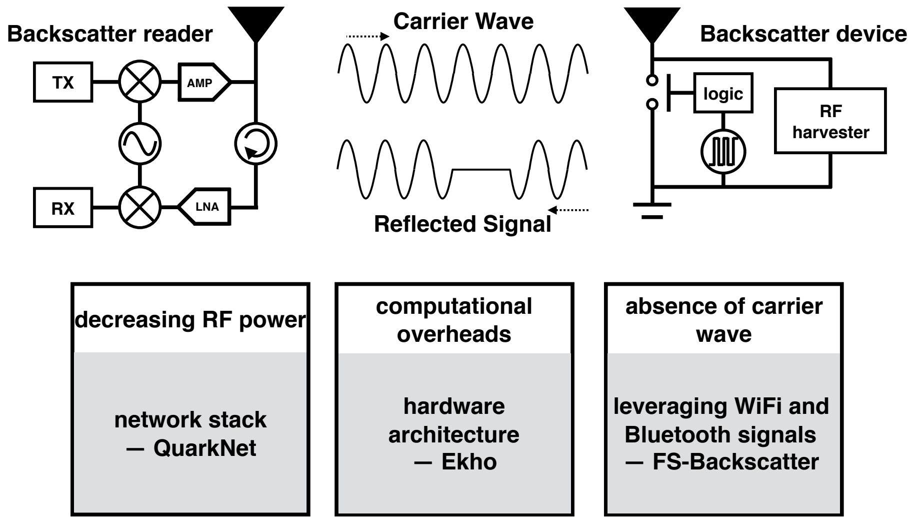

Figure 1.4. An overview of thesis.

and we can enable the system to scale down to resource impoverished regimes. Our network stack enables packet transfer even when the whole system is powered by a 3cm×3cm solar panel under natural indoor light condition.

1.2.4 High Speed Ultra Low-power Backscatter — Ekho

In chapter 4, we design a hardware architecture to minimize the computational overheads on backscatter sensors for achieving high-speed ultra low-power backscatter. A fundamental assumption that has driven the design of sensor networks for decades is that communication is the most power-hungry component of an individual sensor system. We argue that this assumption does not hold when it comes to passive radios such as backscatter, where communication is much cheaper energy-wise compared to computation. Therefore, we overturn the design principle governing wireless sensor design from one that focuses on minimizing communication to one focuses on optimizing the computational elements between the sensor and RF interface. We design a hardware sensing architecture that minimizes computational blocks between the sensors and the backscatter RF interface. We implement our architecture on an FPGA and show that we are able to achieve ≥1Mbps backscatter transmission while only consuming $\leq 100\mu$W of power, a two orders of magnitude improvement over the state of the art.

1.2.5 Leveraging Ambient Wireless Signals — FS-Backscatter

In chapter 5, we introduce FS-Backscatter, a system that can leverage ambient WiFi and Bluetooth signals for carrying backscattered information. A key feature of this system is that it enables backscatter decoding using commercial WiFi and Bluetooth radios. By eliminating the need of deploying backscatter readers, FS-Backscatter provides a promising solution for deploying backscatter on existing wireless sensing devices even though radios on these devices are not designed for backscatter. Decoding backscattered information on top of WiFi and Bluetooth signals is hard because the signal strength of WiFi and Bluetooth is usually several orders of magnitude higher than the reflected signal strength. To deal with such strong interference, we move the backscattered signal to an adjacent clean channel where the interference from the primary WiFi or Bluetooth channel is smaller. Our empirical evaluation shows that we can achieve $\sim$500bps and $\sim$50bps data transmission when the backscatter device is 5m away from the commercial WiFi and BLE receivers.

CHAPTER 2

BACKGROUND

This thesis discusses how and why a backscatter device experiences limited operational range, has a significant amount of computational overhead, and cannot obtain a continuous carrier wave in an ambient environment. All these challenges prevent us from deploying backscatter devices in the nearby environment. To understand these challenges, we present background material on backscatter systems to set the context for our contributions. More detailed related work sections are also provided in the remaining chapters.

Our background introduction starts from looking at the overall system architecture, which gives us an overview of a backscatter system. We then turn to study the hardware architecture of a backscatter device, which sets the context about why existing backscatter devices have a significant amount of computational overhead. We also investigate the channel model of backscatter communication, which helps us understand why SNR is not the limiting factor of the operational range of a micro-powered backscatter device. Let us now start from looking at an overview of backscatter systems.

2.1 Backscatter system overview

Figure 2.1 shows the architecture of a backscatter system. A backscatter reader, which has a form factor as large as an RFID reader or as small as a wearable device, sends out a continuous carrier wave. The carrier wave travels through a certain distance and reaches a backscatter device. A portion of the carrier power is converted by the backscatter device into DC current and is stored locally as harvested energy. Another portion is reflected back to the backscatter reader by toggling an RF transistor. When the backscatter device toggles the RF transistor, the amount of reflected signal changes. Such changes can be detected by the reader and is interpreted as the information transmitted by the backscatter device.

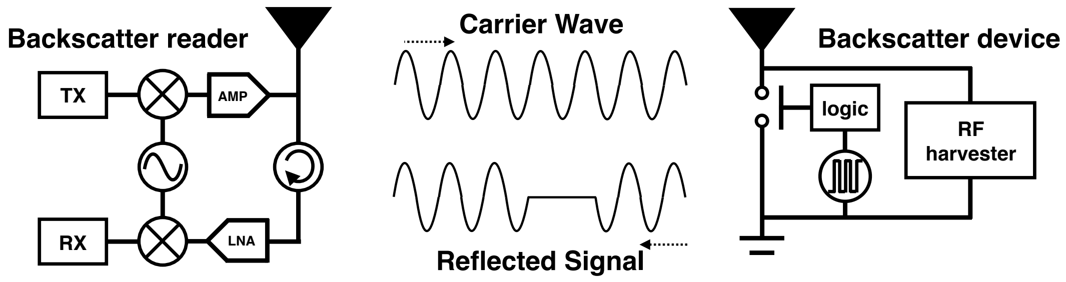

Figure 2.1. Backscatter system architecture.

2.2 Hardware overview

2.2.1 Backscatter radio analog RF front end

Backscatter radios are designed to enable ultra low power wireless communication. As shown in Figure 2.2, a reader provides a carrier wave, which can be modulated with information. To transmit data, a sensor toggles the state of a transistor to detune its antenna and reflect the carrier wave back to the reader with its information bits. Because the sensor does not actively generate an RF carrier signal unlike active radio systems, the power consumption of the backscatter radio is very low. In addition, the on-off transition overhead of backscatter radios is very low because backscatter radios do not have to warm up the RF analog circuits for data transmission, unlike active radio systems. As a result, there is little overhead incurred while transmitting via backscatter, even when transmitting at a high rate. For example, one key component of the backscatter analog RF front end of the WISP [18] is a MOSFET transistor (BF1212WR). Its power consumption follows the equation of $\frac{1}{2}CV^2F$ where C is the capacitance of the transistor, V is the digital drain-source voltage, and F is the frequency of operating the transistor. When this transistor is toggled at a slow rate of 10Hz, it consumes 55pW of power, and even when toggled at a high rate of 1MHz, it only consumes 5.5μW of power. Thus, backscatter radios consume of the order of μWs of power, even for high rate data transfer.

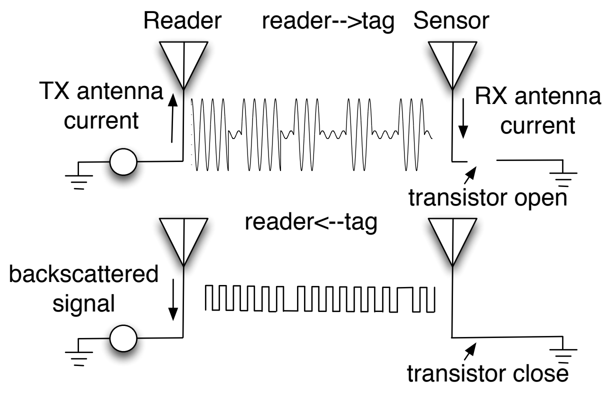

Figure 2.2. Backscatter communication analog RF front end.

2.2.2 RF energy harvesting

In addition to ultra low-power wireless communication, backscatter also enables wireless energy delivery. As shown in Figure 2.2, the backscatter reader provides a carrier wave, which can be rectified by the sensor to produce DC voltage. This voltage is boosted to an appropriate level by a charge pump at the sensor and accumulated in a small storage capacitor until the voltage reaches an appropriate threshold before any computation (or sensing) can begin. Once the voltage is sufficient to power the device, it can begin to receive and transmit data, both of which are done by modulating the same carrier wave.

Table 2.1. Parameters used for modeling bi-static and mono-static backscatter.

	Explanation
P_t	TX antenna transmit power
G_t	TX antenna gain
G_r	RX antenna gain
G_n	Sensor's backscatter antenna gain
λ	Wave length of carrier wave
D	Distance between transceiver and sensor
D_t	Distance between transmitter and sensor
D_r	Distance between receiver and sensor

2.3 Backscatter channel model

2.3.1 Backscatter link budget

Figure 2.3 shows the wireless channel link budget of bi-static and mono-static backscatter systems across distance. These two types of backscatter have different types of wireless channel link budget because they use different mechanisms for transmission and reception. For mono-static backscatter, TX and RX antennas are deployed in the same location or are hosted on the same object. In contrast, for bi-static backscatter, the deployment of TX and RX antennas are geophysically separated. The mathematical models of mono-static and bi-static backscatter are shown in equation 2.1 and equation 2.2 respectively. Table 2.1 summarizes the parameters used in the two models. For both models, the wireless link budget of backscatter decreases significantly even when the device is slightly further from the carrier wave transmitter because the strength of the backscattered signal decreases at the fourth power of distance.

$$P = \frac{P_t G_t G_r G_n}{(\frac{4\pi}{\lambda})^4 D^4} \tag{2.1}$$

$$P = \frac{P_t G_t G_r G_n}{(\frac{4\pi}{\lambda})^4 D_t^2 D_r^2} \tag{2.2}$$

To illustrate why we prefer bi-static backscatter, we consider the following scenario where a backscatter device moves away from a mono-static reader and a bi-static

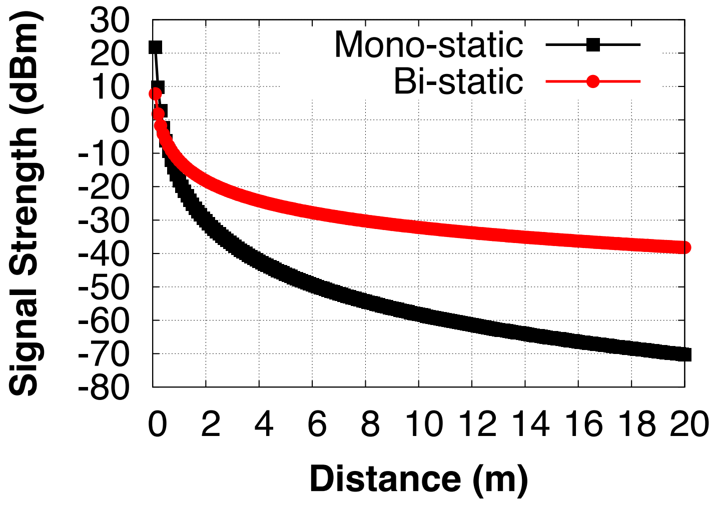

Figure 2.3. Link budget of bi-static and mono-static backscatter.

reader where the device is always 0.1m away from the RX antenna. We find two interesting observations from Figure 2.3. First, bi-static backscatter has higher link budget compared to mono-static backscatter when the sensor is more than 0.5m away from the carrier wave transmitter. This benefit comes from the geophysical separation between TX and RX antennas where one of them can be deployed close to the backscatter device. Second, distance has a larger impact on the signal strength of mono-static backscatter compared to a bi-static backscatter system. For example, at 2m, the signal strength of a mono-static backscatter system is 12 dB lower than a bi-static backscatter system. To make matters worse, this gap becomes larger at a longer distance. At 10m, this gap is 26 dB, much larger than the 2m case. Both observations suggest that we should use bi-static backscatter if possible.

2.3.2 Asymmetric forward and backward links

The forward (reader-to-sensor) and backward (sensor-to-reader) links in backscatter communication differ in several ways. First, the path loss is very different for the two links. The signal to noise ratio (SNR) for typical backscatter communication decays with the square of distance for the forward link and to the fourth power of distance for the backscatter link. Second, the encoding schemes for the links are different. In the EPC Gen 2 network stack, reader to sensor communications use pulse-interval encoding (PIE), which allows easy decoding, whereas sensor to reader communication uses more complex encodings (FM0, Miller2, Miller4, Miller8). Third, the antenna sensitivity at the sensor and reader are vastly different. A typical backscatter reader (e.g. Impinj [14]) uses a mono-static antenna for sending and receiving data, which has a sensitivity of -80 dBm. In contrast, an RFID-scale sensor (e.g. the Intel WISP [18]) uses a simple dipole antenna for data transfer, which is significantly less sensitive than the reader antenna. These factors contribute to different link qualities in the two directions. The forward link uses weaker encoding and is received by a less sensitive antenna, but has lower path loss. The backward link uses robust encoding and is received by a highly sensitive antenna, but has much higher path loss.

CHAPTER 3

PUSHING THE OPERATING LIMITS OF MICRO-POWERED SENSORS

Existing micro-powered sensors make a slew of design choices that limit the ability to scale down to severe energy harvesting environment. In this chapter, we address this issue with QuarkNet, a network stack that is designed to enable continuous communication even if there is only enough harvested energy to transmit a few bits at a time.

3.1 Background and Motivation

The idea of networks of perpetual self-powered sensing, communication and actuation devices that can fly in swarms, swim through the bloodstream, and navigate through pipes and debris has propelled the imagination of science fiction writers for decades, but reality is finally catching up. While practical instantiations of self-powered devices have largely been limited to RFID tags, a new generation of micro-powered devices promises to go beyond simple identification towards computation, sensing, and actuation. Among the key technology trends enabling this vision are advances in micro-harvesters that scavenge energy from light, electro-magnetic waves, vibrations, temperature, and other sources [24]. Such micro-harvesters enable platforms to cut their reliance on stored energy in batteries, thereby enabling true miniaturization and perpetual operation [89, 92].

While micro-powered devices present an exciting opportunity, they present tremendous challenges due to the amount of energy they harvest and the sizes of their energy reservoirs. The amount of harvested power using a micro-energy harvester is of the order of *nano*Watts to μWatts, which is three to six orders of magnitude lower than the average power draw of a Mote. At first glance, this seems to suggest that if we wait long enough, the device can trickle charge to accumulate sufficient energy to operate similar to a battery-powered device. But there are three problems. First, long delays before performing useful work are often unacceptable, particularly for continuous sensing and communication. Second, the voltage from the incoming energy source is often low, therefore accumulating energy into an energy reservoir requires boosting voltage which is wasteful compared to incoming energy (imagine pumping water up a hill to store for future use). Third, micro-powered platforms often have small energy reservoirs to reduce form-factor. For example, the Intel WISP [18] and Michigan Micro Mote (M^3) [61] have energy reservoirs that are 4 – 6 orders of magnitude smaller than a coin cell respectively.

The dual limitations of low harvesting rates and tiny energy reservoirs have profound implications on the design of a network stack for micro-powered devices. Every communication task needs to be small enough to fit within the available energy in the reservoir. Enabling communication despite such minuscule energy budgets is akin to working on a micro-sculpture — optimizations at the granularity of individual instructions, bits, on-off transitions, and analog-to-digital conversions are needed. To compound matters, small short-term variations in harvesting conditions that typically would be smoothed out by a larger energy reservoir begin to impact system operation, and can cause an order of magnitude variation in available energy for a task.

These challenges are not addressed by existing protocols such as EPC Gen 2. RFID tags operate solely on continuous harvested power without buffering energy, therefore EPC Gen 2 assumes a regime where the tag either has enough power to operate continuously, or not at all. In contrast, micro-powered devices can buffer energy, thereby enabling operation in regimes where there is insufficient power to operate continuously, but enough power to operate intermittently.

Recent systems such as MementOS [76] and Dewdrop [29] tackle this problem in different ways. Both these systems use backscatter similar to RFIDs, but the challenge is fitting the communication stack within the energy budget. MementOS introduces checkpoints within computation tasks such that it can recover from outages and continue execution. Dewdrop continually adapts task execution to harvesting conditions such that the efficiency of execution is optimized. To evaluate the ability of these systems to scale down, we consider two harvesting conditions — strong light (2000 lux) and natural indoor light (200 lux), both of which should, in principle, provide enough energy to operate a micro-powered sensor. But while both Mementos and Dewdrop operate under strong light, they are inoperable under natural light.

The inability of current systems to scale-down illustrates the central challenge in designing a network stack for micro-powered devices. A wireless network stack involves a variety of tasks that are simply too large to fit into the extreme energy constraints of this regime. Even the core primitive of a network stack — packet transfer — can involve hundreds of instructions and bits. In this work we ask the following question — what are the general principles that we, as systems designers, should use to enable these micro-powered platforms to communicate continuously despite trickles of energy, tiny energy reservoirs, and dynamic harvesting conditions?

We present QuarkNet, a network stack that embodies a simple but powerful abstraction — by fragmenting a backscatter network stack into its smallest atomic units, we can enable the system to scale down to resource-impoverished regimes. The fundamental building block of QuarkNet is the ability to dynamically fragment a larger packet transfer into μframes that can be as small as a single bit under severe energy constraints, and as large as the whole packet when sufficient energy is available. On top of this abstraction, we design a variety of innovative techniques to handle dynamic frames that can be abruptly terminated in low energy settings, maximize throughput by tracking harvesting dynamics in a low-overhead manner, interleave μframes across nodes to maximize throughput despite different harvesting rates, and minimize overhead across the entire stack.

Our results on a USRP reader and Moo nodes show that:

- The maximum communication distance achieved by QuarkNet is 21 feet, 3.5× longer than Dewdrop and 4.2× longer than EPC ID transfer. QuarkNet achieves close to the maximum achievable range, beyond which decoding even a single bit fails.

- The minimum illuminance required for QuarkNet to operate is 150 lux, which is 13× lower than the 2000 lux requirement of 12 byte EPC ID transfer. This suggests that μframe can operate when a device is powered by natural indoor illuminance, dramatically increasing utility of micro-powered devices for practical deployments.

- The throughput of QuarkNet for node to reader transfer is 18 kbps, 10.5× higher than EPC Gen 2, 5.8× higher than Dewdrop, and 3.3× higher than Flit. For reader to node transfer, we obtain throughput of 1.5 kbps, 2× higher than a battery-assisted device which uses the EPC Gen 2 write command.

- When ten nodes transmit simultaneously to a reader, we achieve a throughput of 16.5 kbps as a result of variability-aware scheduling and interleaving of μframes, which is 5.4× higher than the throughput when devices are inventoried individually. Flit and EPC Gen 2 obtain zero throughput in this case.

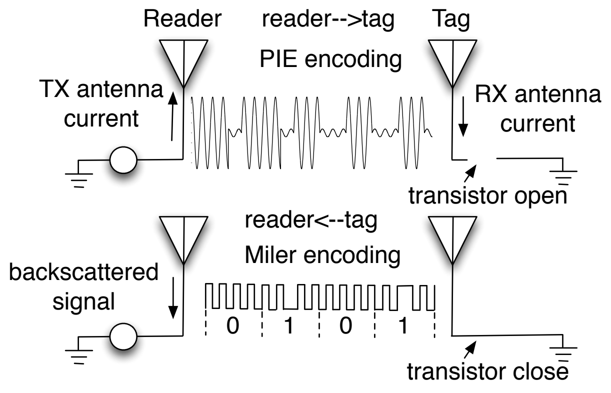

Figure 3.1. Backscatter signaling at PHY.

3.2 Case for μframes

A backscatter radio is designed to both provide power to a passive device as well as to enable communication. As shown in Figure 3.1, the reader provides a carrier wave, which can be reflected by a passive device back to the reader with its own information bits. This makes backscatter a considerably more energy-efficient communication mechanism compared to active radios, and ideally suited to the constraints of micro-powered devices. The Intel WISP [18] and UMass Moo [96] are examples of backscatter-enabled sensor platforms.

Despite the energy benefits of backscatter radios, existing network stacks achieve only short communication range and low throughput. We make an empiric argument these limitations are, in part, due to the design of the network stack. To do this, we compare the range and throughput of existing network stacks versus achievable performance. Our experiment uses a UMass Moo [96] and a USRP reader [30]. Since combining multiple micro-power sources can enable higher performance, broader operating conditions, and enable wider range of applications, we augment the Moo with a small solar panel [44, 24, 43]. We vary the distance from the reader by small steps, and at each step, we vary RF power from 17dBm to 26dBm, while not changing the light levels (normal indoor light).

Table 3.1. EPC Gen 2 vs Achievable Performance.

	Range(ft)	Throughput(kbps)	SNR(dB)
Gen 2	3.6±0.8	3.6±0.3	9.6±1
Optimal	18.6±3.3	21.7±3.7	6.9±0.9

To measure the achievable range, we look at the raw backscattered signal at the reader, and find the distance at which the reader is unable to decode even a single bit. This would be the edge of the communication range for our hardware platform.

Measuring the maximum achievable throughput is harder since it is influenced by several system parameters including voltage at the energy reservoir when communication starts, the length of each transmission unit, and control overheads associated with the protocol. We brute-force search across all possible voltages and packet lengths to find the setting that results in the maximum number of transistor flips at the node. We then convert the transistor flips to a maximum number of bits transmitted using the default Miller-4 encoding scheme, and assume zero control overhead for each packet, which gives us an estimate of the maximum throughput.

Table 3.1 shows the range and throughput while executing the EPC Gen 2 stack (used in Mementos [76], Dewdrop [29], and Blink [100]) versus achievable limits. We see that the achievable range is 18.6 feet, which is over 5× longer than the communication range of EPC Gen 2. Surprisingly, we find that EPC Gen 2 ceases to operate even when its SNR is 9.6dB, 1.4× higher than the optimal case. Similarly, we see that the achievable throughput is 21.7 kbps, whereas EPC Gen 2 achieves barely 1.7 kbps, an order of magnitude difference.

We now investigate the fundamental factors underlying this performance gap, and outline the core challenges that need to be addressed to bridge the gap.

3.2.1 Challenge 1: Variable energy per transmission

A key challenge in designing a backscatter network stack is handling variability in the amount of energy accumulated in the energy reservoir. To understand the

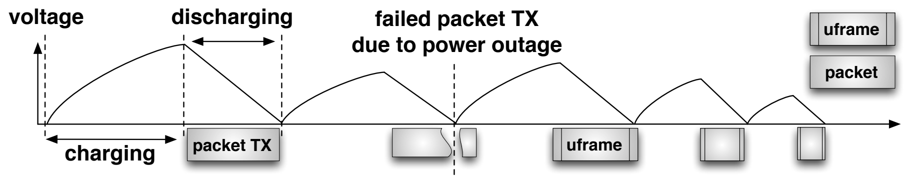

Figure 3.2. Energy harvesting systems.

reasons, let us look at how micro-powered devices work. As shown in Figure 3.2, micro-powered devices operate in a sequence of charge-discharge cycles since there is too little energy to continually operate the device. The device sleeps for a short period during which it harvests energy and charges a small energy reservoir, and then wakes up and transmits a packet during which the reservoir discharges.

There are several reasons why it is difficult to anticipate how much energy will be available in each discharge cycle. First, if harvesting conditions are too low, it is often too expensive to push more energy into a reservoir due to the inefficiencies of stepping up the voltage. As a result, the maximum amount of energy that can be accumulated depends on current harvesting conditions. Second, RF energy harvested by a node depends on how much energy is output by the reader. When a reader is doing nothing, the RF output power is roughly constant. However when a reader is communicating, this RF carrier wave is being modulated which changes the amount of harvested energy. In a multi-node network, the reader is communicating with different nodes, therefore harvesting rates continually vary at each node. Third, even if the node were to wait until it has a certain amount of energy prior to communication, this requires measurement of energy levels using analog-to-digital conversions (ADC). Each ADC operation consumes 327 uJ on the Moo platform [96], which is equal to the energy budget for transferring 27 bits of data. Such overhead is far too substantial on a micro-powered platform.

While choosing a smaller transmission unit might seem like a straightforward solution to this problem, this over-simplifies the design challenge. As the distance

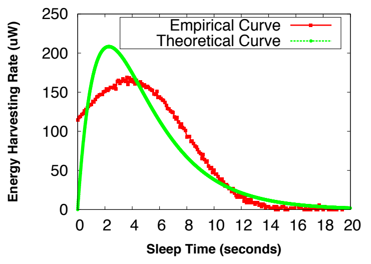

(a) Energy harvesting rate.

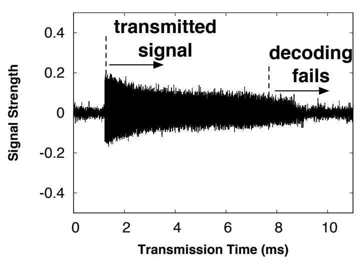

(b) Decreasing SNR over time.

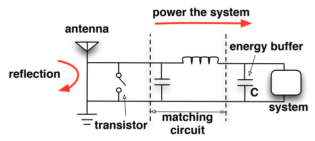

(c) RF matching circuit.

Figure 3.3. Factors that impact communication throughput.

between the node and reader increases to the limit of the achievable range in Table 3.1, the number of bits that can be successfully transmitted reduces. Thus, we need to use frames that may be as small as one or a few bits in size when the energy levels are low, which requires a network stack that can scale down to unprecedented levels. But such scale down often comes at the expense of throughput, which suffers due to the overheads associated with each transmission, including preambles, headers, and hardware transition overheads. To simultaneously optimize throughput, it is important to transmit as large a transmission as is possible given available energy. Thus, the problem faced by a node is that it needs to scale down its transmission unit to the bare minimum under poor harvesting conditions, while scaling up to improve throughput when the conditions allow.

3.2.2 Challenge 2: Variable harvesting rate

The energy harvesting rate has significant impact on the communication throughput, since higher harvesting rate means that more energy can be used for data transfer. While energy harvesting rate might seem like a characteristic of the harvesting source, system parameters have a surprisingly high impact. Figure 3.3(a) shows the empirically measured harvesting rate as we vary the amount of time for which the node replenishes energy between two transmissions. The results are counter-intuitive

— while one might expect more energy to be harvested over time, the harvesting rate drops to zero for longer sleep durations.

This observation can be explained analytically by looking at how capacitors buffer energy. The charging process of a capacitor follows its charging equation $V = V_{max}(1 - e^{-t_s/\tau})$, where t_s is the sleep time, τ is the RC circuit time constant, and V_{max} is the maximum voltage to which the capacitor can be charged under the current harvesting conditions. Its energy harvesting rate follows the equation: $H = C \times V_{max}^2 \times \tau^{-1}(1 - e^{-t_s/\tau})e^{-t_s/\tau}$. When the harvesting conditions are constant (i.e. V_{max} and τ are fixed), H is a concave function of t_s, which is shown both analytically and empirically in Figure 3.3(a). When harvesting conditions change, both V_{max} and τ change, therefore the maximum operating point changes as well. Thus, to optimize throughput, it is important to adapt to current harvesting conditions, and continually track the maximum harvesting point.

One factor that should not be overlooked is keeping the overhead of adaptation low. Most methods to track the charging rate of batteries and capacitors use analog-to-digital conversions to obtain the voltage at the energy reservoir. This overhead is minuscule for most platforms, but a significant part of the harvested energy in our case. Thus, it is important to minimize such overheads while adapting to harvesting conditions.

3.2.3 Challenge 3: Time-decaying SNR

A peculiar aspect of backscatter communication is that the signal to noise ratio (SNR) of the received signal at the reader degrades steadily as the size of the transmission unit increases. Figure 3.3(b) shows that the signal strength of a node response decreases gradually from 0.18 at 1.5ms to 0.05 at 8ms during the transmission process. While decoding the initial part of the transmission is straightforward due to high SNR, it becomes much more challenging after about 8ms since the SNR is too low for reliable decoding, resulting in packet losses.

In order to understand why this happens, let us look at how a backscatter radio works. A backscatter radio provides power to a passive device and enables communication. The reader provides a carrier wave, which can be reflected by a passive device back to the reader with its own information bits. The modulation is achieved by toggling the state of the transistor of a backscatter device shown in Figure 3.3(c). Since the same RF power source is shared by different system components, some fraction of the incoming power is used to operate the micro-powered device while the rest is reflected back to the reader for communication. The exact fraction depends on the state of the energy reservoir C and the state of the matching circuit, which is designed to charge the energy reservoir C when the voltage is low. Therefore, when the transmission begins, C is fully charged, the antenna resistance is mismatched with the resistance of other hardware components of the system. As a result, most of the incoming power will be reflected back to the reader, which receives a strong signal that can be easily decoded. As the transfer progresses, C slowly discharges, and the antenna resistance matches the resistance of the system load. Therefore, most of the incoming power is harvested to operate the system, and less RF power is reflected. This leads to decreased backscatter signal strength at the reader, and consequently, packet losses. Thus, to ensure that packets are received successfully, the tag needs to adapt the size of each packet such that the SNR at the tail of the packet is higher than the minimum decoding requirement.

3.2.4 Challenge 4: Energy-induced reader to node losses

While time-decaying SNR only presents a problem when a node communicates with a reader, reader to node communication presents other challenges. The central issue is that that the energy level on the receiving node might dip below the low watermark at any point during the reception, at which point the node has to shut off its RF circuit and go to sleep to recharge. The reader, however, does not know that the node has gone to sleep, and only realizes this fact after a timeout.

While such losses can be attributed to small energy harvesting variations at longer ranges, we observed to our surprise that such losses occur even when a tag is placed relatively close to the reader — 40% losses at 2 ft. The reason for this behavior is that data transfer from the reader to tag comes at the expense of RF power being transmitted to the tag. Since the reader is actively transmitting to the tag, the carrier wave from the reader to tag is intermittent, causing substantial variations in RF energy harvesting and consequently variations in energy levels at the tag.

The energy dynamics at the tag makes it difficult to use reader-side estimation to identify the best transmission unit to communicate with a tag. In addition, explicitly providing information to the reader about the current energy level has considerable overhead while not being robust to dynamics. Thus, the challenge we face is that the reader needs to have a way of knowing the instantaneous energy state at the tag, and detecting its shut-off point without using cumbersome protocol-level mechanisms to enable this information exchange.

3.3 Fragmenting packets into μframes

At the heart of QuarkNet is a simple hypothesis — by breaking down packet transmission into its smallest atomic units, which we refer to as μframes, we can enable the system to scale down to severely limited harvesting regimes. We address the challenges in enabling such extreme fragmentation both for node-to-reader and reader-to-node communication.

3.3.1 Fragmentation at bit boundaries

The first question we ask is: what are the practical considerations that determine how we can dynamically fragment a logical transmission unit (packet) into μframes? Ideally, we would want to insert fragment boundaries at arbitrary positions within a packet so that we can make μframes as small or large as needed, however, this makes decoding extremely error-prone.

To understand where to place fragmentation boundaries, we need to give some more detail about how backscatter modulation works. Figure 3.4 shows a sequence of backscatter pulses that compose bits in a packet. Backscatter modulation uses On-Off-Keying (OOK), therefore each bit is composed of a sequence of on and off pulses. As can be seen, the template for a '0' pulse and '1' pulse differ only slightly in the phase information of the pulses within the bit.

The key observation is that placing boundaries at certain points in a packet can be done without disrupting the phase information required for decoding, whereas other boundaries would disrupt decoding. For example, suppose that a fragment boundary is inserted between two adjacent bits, the phase information of each bit is maintained, thereby not impacting the ability to match the template to the bit. On the other hand, suppose that a fragment boundary is inserted within a single bit, the phase information within the bit is disrupted, thereby causing a mismatch at the decoder between received bit pulses and its template.

This leads us to a general principle for fragmenting a packet into μframes — μframe boundaries can be inserted between bits but not within a bit. The ability to fragment at any bit boundary gives us the requisite combination of fine-grained fragmentation as well as low decoding error.

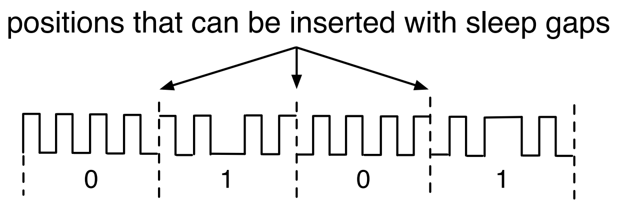

Figure 3.4. Sleep gaps can be inserted into backscatter pulses at various position (lines with dots).

3.3.2 Tuning inter-μframe gap

We now have a method for fine-grained fragmentation of larger packets, but how do we use this to dynamically fragment packets? How do we decide the length of each μframe and the sleep gap between μframes where the node replenishes energy?

We first answer this question for node-to-reader communication. In this case, we need to address two of the challenges discussed in §3.2: a) how to optimize throughput by operating at the optimal harvesting rate, and b) how to ensure the tail of each μframe transmitted from a node has sufficiently high SNR to be decoded at the reader.

3.3.2.1 Gradient descent algorithm

As can be seen in Figure 3.3(a), the harvesting rate curve is a concave function of the gap between μframes (under constant harvesting conditions). A fast and effective method for converging to the optimum of a concave function is to use gradient descent [9]. The gradient descent algorithm works as follows: first, we start with an initial guess about the optimal sleep gap. Second, we compute the gradient at this point, and look for the direction of the positive gradient. Third, we take a step along the direction of the positive gradient with step size proportional to the gradient. We repeat this process until convergence (i.e. step is smaller than a threshold). The algorithm takes large steps when the gradient is steep (i.e. point is far from optimal), and small as the gradient reduces (i.e. point is near optimal).

What if the harvesting conditions change and the curve itself shifts to create a new optimal harvesting point? Our gradient descent-based sleep gap adaptation algorithm operates continually — once it converges to the optimal, it periodically probes the gradient at the current optimal, and moves along the positive gradient if the optimal harvesting rate changes. In this manner, the algorithm seamlessly adapts to such dynamics.

3.3.2.2 Handling time-varying SNR

We need to add another constraint to to the gradient descent algorithm — the SNR at the tail of the frame should be higher than the decoding threshold at the reader, otherwise the frame cannot be decoded. This constraint is easy to add since it simply translates to a bound on the maximum length of the inter-μframe gap. Since the length of the gap directly impacts the length of the μframe, capping the inter-μframe gap ensures that the length of each μframe is lower than the decoding threshold. The only change to the gradient descent algorithm is that a step cannot exceed the maximum inter-μframe as determined by the SNR constraint.

3.3.2.3 Duty-cycling the radio

One important aspect of the inter-μframe gap is that we shut off the node's RF circuit for this length of time. In a multi-node environment, the reader is constantly talking to other nodes, so leaving the RF circuit on results in substantial reception overhead since backscatter is a broadcast-based protocol, and wakes up every node that has its radio circuit turned on. To avoid these costs, we turn off the RF circuit during the recharge cycle. Once the node has slept for the intended duration, it switches on its RF circuit. One side-effect of our decision to turn off the RF circuit during gaps is that the reader now has to be more careful to avoid transmitting to a node or scheduling a node for transmission while it is inactive. We return to this question in §3.4.2.

3.3.3 Remote interrupts

We now turn to μframe adaptation for communication from a reader to a node. As described in §3.2, the key challenge is that the reader cannot detect when a node's energy level drops below a low watermark, and it should stop transmitting. Similarly, once a node has gone to sleep, a reader does not know when it will wake up for the next μframe. Given these constraints, how can we enable reader-to-node communication?

3.3.3.1 Estimating μframe length

Our idea is to use a remote interruption mechanism, where a node issues an in-band interrupt during reader transmission, and informs the reader that it has reached a low-energy state. This remote interrupt is generated by toggling its transistor while receiving the current frame. In other words, the remote interrupt is a signal that is overlaid on the same time-slot and frequency signal as the message from the reader to node.

How can the reader decode an in-band interrupt from the node? The key insight is that the reader modulates the carrier by toggling the carrier wave whereas the node communicates back to the reader by changing the amplitude of the backscattered signal. In other words, both can occur simultaneously! Thus, when the reader is sending an ON pulse, the amplitude of the backscattered signal that it receives depends on whether the state of the transistor at the node is ON or OFF — the amplitude is higher when the node's transistor is ON and lower when it is OFF. When the carrier is OFF at the reader, then the state of the node's transistor does not matter since there is no backscattered signal. The reader can detect the remote interrupt by looking for a large signal variance in the carrier wave when the reader has the carrier wave turned on.

Figure 3.5 shows an example signal where toggling the transistor causes a large variance on the carrier wave, which is monitored by a reader and can be identified

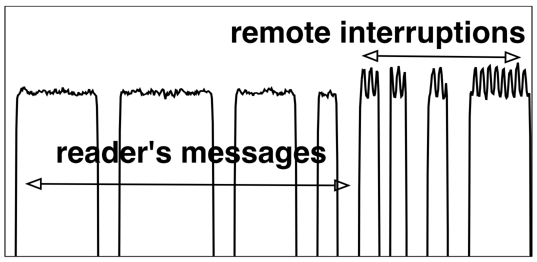

Figure 3.5. In-band remote interruptions from nodes.

by tracking the signal variance within a reader pulse. However, the signal variance is detected only when the carrier wave is on. As shown in the figure, a reader cannot observe the large signal variance when the carrier wave is off. Fortunately, the carrier wave is on for 50% of the time when the reader transmits 0s and 75% for 1s. Thus, as long as a remote interrupt is longer than 50% of the length of a '0' bit from a reader, it can reliably detect the interrupt and pause its transfer.

Finally, an auxiliary benefit of the remote interrupt is that it acts as an inexpensive μframe ACK from the node, which obviates the need for more explicit protocol-level mechanisms and reduces our overhead.

One limitation of our current design is that it is not robust to noise spikes in the frequency band. Such spikes can occur because of multiple readers transmitting to nodes since backscatter is a broadcast medium and reader-to-node communication has to be serialized. Robustness against external interference could be improved by making the remote interrupt longer and encoding the signal, but we do not do this in our current implementation.

3.3.3.2 Estimating inter-μframe gap

We now have a way for the node to interrupt a reader when it needs to replenish energy, but how long should the reader wait before initiating the next μframe transfer? Clearly, this duration should be at least as long as the inter-μframe gap that the node is using, otherwise the reader might be trying to communicate to a node that has its RF circuit turned off. We address this by using a simple probing-based approach at the reader — for each μframe gap that the reader selects, it knows whether the frame was received or not by checking the presence of a remote interrupt. If no remote interrupt is received, the reader knows the node does not receive the frame properly. The reader continually adjusts the gap to minimize missed frames at the node.

3.4 QuarkNet for multi-node networks

So far, we have focused on communication between a single node and reader. We now turn to the case where there are several nodes in the vicinity of a reader. The key difference between a single node and multi-node setting is that in the former, the reader stays idle during times when the node is asleep to replenish energy, whereas in the latter, these inter-μframe intervals present an opportunity to schedule another node's μframe transfer, thereby ensuring that throughput is maximized.

3.4.1 Design Options

Before launching into the details of our design, lets step back and look at the design options. Co-ordination mechanisms for backscatter networks are more restrictive than typical active radio-based networks for two reasons: a) nodes cannot overhear each other's transfer, hence carrier sense-based approaches are infeasible, and b) the stringent resource constraints of nodes render approaches that require complex coding and synchronization infeasible. As a result, existing proposals have focused on two classes of techniques — EPC Gen 2 and variants which use a sequence of random-access slots, and rateless transfer where nodes transfer concurrently, and the reader simultaneously and successively decodes all transmissions.

While the deficiencies of EPC Gen 2 for severely energy constrained regimes have been detailed earlier in this chapter, other alternatives and enhancements are surprisingly poor in dealing with this regime as well. In particular, consider two prominent recent techniques — Flit [45] and Buzz [86]. Our earlier work, Flit, re-purposes EPC Gen 2 slots for bulk transfer, thereby amortizing overhead, but it assumes that nodes are able to sustain a long stream of transfer, which we realized was not the case in severe harvesting conditions. Buzz uses rateless codes, but in-order to get these codes to work, it has to use synchronous single-bit slots across nodes. Each single-bit slot incurs substantial overhead due to slot indicators, and turning on and off the radio, which dramatically impacts performance. Given that existing approaches are not well-suited to our nodes, the question is what protocol to use for co-ordinating nodes.

3.4.2 Variability-aware node scheduling

Our scheduler is designed to interleave μframes from different nodes, thereby fully utilizing the inter-μframe gaps. The reader divides time into variable-sized μslots, during which it explicitly schedules a single node to transmit its μframe. The length of each μslot depends on the size of the μframe — a node-to-reader μframe terminates when the node reaches its low watermark energy level and the reader ACK is received, and a reader-to-node μframe terminates when the node issues a remote interrupt. In both cases, there is a maximum bound on the μframe size to deal with nodes that have plentiful energy.

While the μslot mechanism appears relatively straightforward, the main challenge is handling the fact that nodes turn off their RF circuit when they are asleep. As a result, if a node is scheduled too early by the reader, then it may not be awake to utilize the slot, but if it is scheduled too late, then it is not operating at its maximal harvesting rate.

To handle this, we use a token-based scheduler to deal with the stochastic nature of harvesting conditions, while optimizing throughput. For each node, the scheduler maintains a running estimate of the gap between μslots assigned to a specific node, and whether the μslot resulted in a successful transfer. It uses the estimate to select the inter-μframe gap that ensures a high likelihood of obtaining a node response.

The reader's estimate of the inter-μframe gap is used as input to a token bucket scheduler, which assigns tokens to nodes at a rate inversely proportional to its inter-μframe gap. Once a node has accumulated sufficient tokens, it is likely to have woken up after sleep, therefore the reader places the node into a ready queue since it is ready to be scheduled. The ready nodes can be scheduled based on a suitable metric — for example, the highest throughput node may be selected from the queue to maximize throughput, or the node that has received least slots may be selected for fairness.

3.5 Implementation

In this section, we describe key implementation details not covered in earlier sections. We use the USRP reader and UMass Moo for our instantiation of QuarkNet. The source code of QuarkNet is available at [13].

3.5.1 Platforms

3.5.1.1 USRP Reader

QuarkNet is built based on the USRP software radio reader developed by Buettner [30] with a ANT-NA-2CO antenna [15]. We modify the signal processing pipeline to enable variable sized μframe decoding, harvesting-aware tag scheduling, and detection of in-band remote interrupts. The RFX900 USRP RF daughterboard on our platform is only able to transmit 200mW of power, which is 5$\times$ smaller than the 1W of power issued by a commercial reader. Therefore, we attach a 3cm$\times$3cm solar panel to each Moo to increase the amount of harvested energy. The use of hybrid power (RF + ambient) is known to increase range from a reader, which enhances the regimes where backscatter can be used [44].

3.5.1.2 Backscatter node

The UMass Moo is a passive computational RFID that operates in the 902MHz $\sim$ 928MHz band. Perhaps the most challenging aspect of our implementation is debugging under extreme low energy conditions. Traditional methods for debugging embedded systems, such as using JTAG, supply power to the node and change its behavior. Instead, we instrument the Moo to toggle GPIO pins at key points during its execution, and a logic analyzer to record the toggle events. In many cases, however, it is difficult to insert sufficient instrumentation to have visibility while still working with tiny energy harvesting levels. Thus, intuition and experience is particularly important in designing systems for these regimes.

3.5.2 Trimming Overheads

One important aspect of our system is careful measurement and tuning of all overheads, which impacts our ability to scale-down to severe harvesting conditions.

3.5.2.1 Radio transition overhead

An important source of overhead is transition times for turning on or off the radio. Fortunately, since hardware timers are responsible for generating the pulses on the backscatter radio, sleep gaps can be inserted by clearing the hardware timers and turning the micro-controller into its low power mode. These operations are inexpensive energy-wise, and consume roughly the same amount of energy as a data frame of size 3 bits. Note that this observation does not hold for more complex active radios — for example, a WiFi radio takes 79.1ms to be on, and 238.1ms to be turned off [53], which is five orders of magnitude higher than the corresponding numbers for a backscatter radio.

3.5.2.2 Pilot tone

Each backscatter frame can potentially include a pilot tone in addition to the payload. A pilot tone is used when a tag changes its baud rate [80]. We focus on a minimalist protocol that uses a fixed baud rate, therefore we remove the pilot tone. The total overhead per μframe is 6 bits of preamble, in contrast to the 22 bits overhead of EPC Gen 2 (and variants such as Flit [45]).

3.5.2.3 Probing energy state

As mentioned earlier, analog-to-digital conversions are expensive, and should be avoided while tracking the maximum energy harvesting rate. Our key insight is that rather than measure the voltage on the node, we can leverage the existing low watermark threshold detector that is already present on such nodes. Such a detector is common on harvesting-based sensor platforms for two reasons: a) the platform needs to know when to save state and go to sleep to avoid an outage, and b) the platform needs to know when to wake up after sleep to continue operation. Thus, QuarkNet gets an interrupt both when the voltage crosses above the threshold, as well as when it drops below the threshold, and uses this information as a one-bit proxy for the actual voltage. The voltage threshold is chosen to be 2V which is slightly higher than 1.8V, the minimum voltage required for operating a micro controller. This information is input to a sleep time tracker, which determines how long to wait after crossing the threshold in the upward direction before initiating transfer. Our approach is 100$\times$ less expensive energy-wise than an ADC conversion.

3.5.3 Protocols and Algorithms

While we do not describe the complete protocol in the interest of space, more details as well as pseudocode for our algorithms can be found in our technical report [98].

3.6 Evaluation

The evaluation consists of three parts: 1) demonstrating the range and throughput benefit of μframe transmission, 2) benchmarking the performance of our reader-to-node communication, and 3) evaluating the benefit of interleaving μframes from multiple nodes.

3.6.1 Benefit of μframes

In this section, we validate our claim that the ability to breakdown packets into μframes that can be as small as a single bit can allow us to operate under lower energy conditions and achieve higher operating range. To focus on the effect of the choice of frame size, we strip off overheads (slot indicators, handshakes, etc) for all protocols that we compare.

3.6.1.1 Minimum operating conditions

We look at two harvesters — RF and solar — and ask what is the minimum power requirements for different approaches. We find that the minimum illuminance required for a 1 bit μframe is 150 lux, which is 13$\times$ lower than the 2000 lux budget of 12 byte packet transmission (the same packet size used by EPC Gen 2, Dewdrop, Flit, etc). We choose 12 byte packet size for EPC Gen 2-based protocols because the 12 byte EPC identifier needs to be transmitted in a singulation phase prior to executing Read or Write commands. Thus, this packet is the bottleneck for operation. To translate from lux to the typical energy available from indoor energy sources, we measure the natural indoor illuminance in 30 positions in an office room. We find that 92% the measured illuminance value is between 150 lux and 1000 lux. This suggests that μframes can operate in most of natural indoor illuminance conditions while a canonical 12 byte transfer scheme can almost never operate under natural indoor light.

The minimum RF power required for a 1 bit μframe is 13dBm, which is 20$\times$ smaller than the 26dBm budget of a 12 byte packet transmission that is the minimum needed for EPC Gen 2 and its variants to operate. Both experiments illustrate the benefits of using tiny μframes.

3.6.1.2 Increased operational range

Our second claim is that we can improve operational range by using μframes. Figure 3.6 shows the maximum range that is achieved by QuarkNet with 1 bit μframes, EPC Gen 2 with fixed 12 byte packets, Dewdrop with fixed 12 byte packets, Buzz with two slot choices, and a battery-assisted node which represents the best-case scenario. We adjust the RF power of the USRP RFID reader from 17dBm to 25.7dBm, which represents the range of RF power that can be generated by the USRP RFX900 daughterboard.

The results show that the communication range of QuarkNet is longer than other schemes across all RF power levels. At the lowest power level (17.5dBm), μframes do not improve range since the node is not able to decode the reader signal beyond 5ft. But as the RF level increases, the operational range increases dramatically, and is about 4$\times$ longer than EPC Gen 2 at the highest power. In fact, the performance of 1 bit μframe transfer while using harvested energy almost matches the performance of a battery-assisted node, which shows that we are able to reach the ceiling of operational range despite operating on micro-power.

Figure 3.6 also shows that Buzz [86] performs poorly compared to other schemes. This can be attributed to the fact that each one-bit slot in Buzz has substantial overhead — the reader sends a pulse, followed by one bit from the node, random number generation for deciding whether to transfer in the next slot, and a recharge period. Thus, while Buzz has high range in some settings, the overhead is too high to scale gracefully.

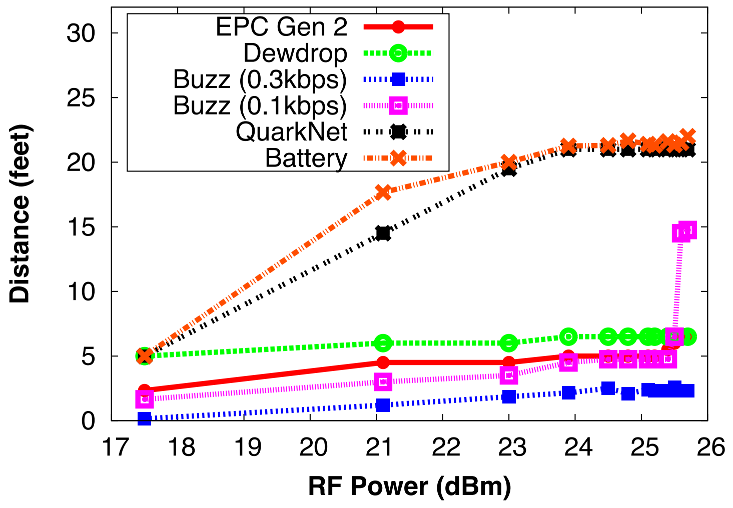

Figure 3.6. The maximum range achieved by EPC Gen 2, Dewdrop, Buzz, QuarkNet, and a battery assisted node. QuarkNet operates at ranges close to the battery assisted node.

3.6.2 Benefits of μframe adaptation

We now turn to the benefits of adapting the inter-μframe gap to maximize throughput.

3.6.2.1 Convergence of gradient descent

How well does the gradient-descent algorithm learn the optimal harvesting rate? Figure 3.7 shows the results for a node placed in three RF+light harvesting combinations that include short and medium range, and low and medium light. In all cases, we see convergence to close to the optimal point — the best inter-μframe gap ranges from 1ms for 350lux at 1 foot, 4ms when the node is moved to 6ft, to 12ms when the light conditions dip further. In all cases, our tracking algorithm converges in very few steps (≤ 4).

3.6.2.2 Throughput benefits

We now know that QuarkNet picks close to the optimal harvesting rate, but what are the benefits in terms of throughput? To understand this, we place a node 3 feet

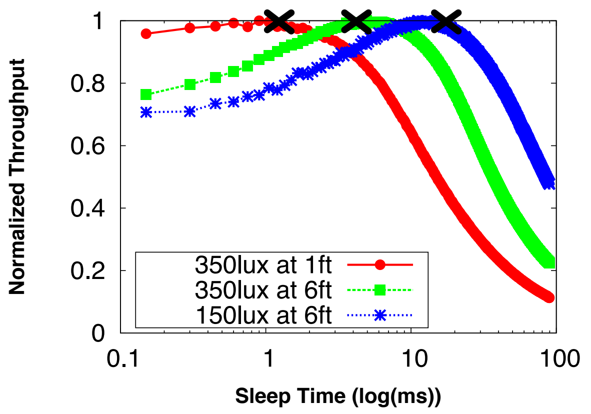

Figure 3.7. Throughput achieved for different sleep times (inter-μframe gaps). The sleep time chosen by QuarkNet is within 98% of the optimal.

from a reader, vary RF power from 17dBm to 26dBm in small steps of 0.3dBm, and inventory the node 2000 times for each scheme. Figure 3.8(a) shows the throughput achieved by EPC Gen 2, Dewdrop, Flit, and QuarkNet. We find that the throughput achieved by QuarkNet is higher than EPC Gen 2, Dewdrop and Flit across all RF power levels. The average communication throughput of QuarkNet is 18kbps, 10.5× higher than EPC Gen 2, 5.8× higher than Dewdrop, and 3.3× higher than Flit. While the figure does not show Buzz's throughput, note that Figure 3.6 already showed that this number is low since the per-slot overhead dominates. The lowest slot size we achieved in our implementation of Buzz is 3ms, which means about 0.3kbps throughput.

The previous experiments were done by varying the RF power level. To be sure that these results translate to the case where nodes are placed at different locations in front of a reader, we measure the throughput achieved by EPC Gen 2, Dewdrop, Flit, and QuarkNet at 30 different randomly chosen locations between 2 to 13 ft in front of a reader. Figure 3.9 shows that the throughput achieved by QuarkNet is higher than the other three schemes across all locations. The average throughput of QuarkNet is 7.8× higher than EPC Gen 2, 6.4× higher than Dewdrop, and 4.4× higher than Flit.

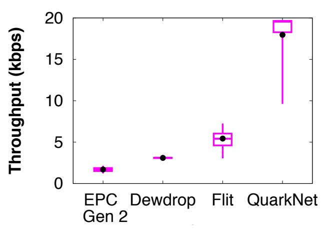

(a) QuarkNet vs micro-powered nodes.

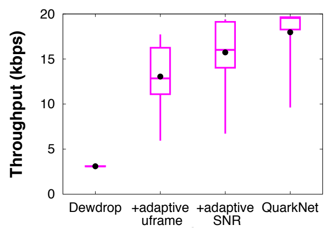

(b) QuarkNet vs Dewdrop.

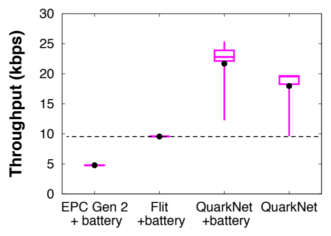

(c) QuarkNet vs battery assisted nodes.

Figure 3.8. For micro-powered devices, QuarkNet improves throughput by at least 3.3× over all other schemes, and even performs better than battery assisted nodes. The benefit comes from reducing overhead, and adapting μframe sizes to energy and SNR.

In particular, QuarkNet continues to operate in many locations where other schemes cease to operate.

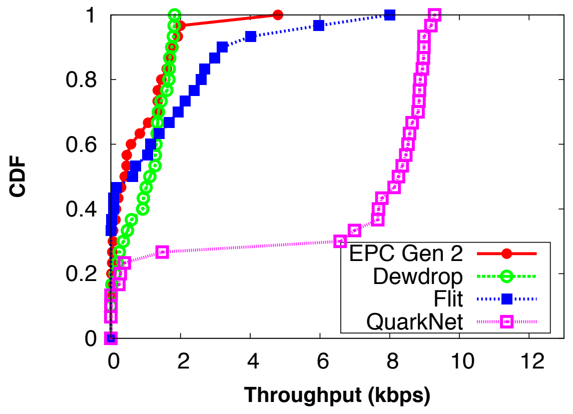

Figure 3.9. Throughput achieved by EPC Gen 2, Dewdrop, Flit, and QuarkNet across 30 locations. QuarkNet has at least 4.4× higher throughput than other schemes.

3.6.2.3 Breaking down the benefits

QuarkNet has a variety of optimizations including reduced overheads, variable-sized μframes, and SNR adaptation. To understand the contributions of these techniques to throughput, we start with the default implementation of Dewdrop, and add one optimization at a time: a) Dewdrop + adaptive frame, which includes variable-length μframes, and b) Dewdrop + SNR adaptation which includes the SNR adaptation. Figure 3.8(b) shows the throughput achieved by the three variants of Dewdrop vs QuarkNet. Clearly, each of the optimizations plays a major role in the throughput improvements observed by QuarkNet. The average communication throughput of μframe is 18kbps, 5.79$\times$ higher than Dewdrop, 1.37$\times$ higher than Dewdrop with adaptive μframes, and 1.14$\times$ higher than the case when SNR adaptation is included. In the final step, we replace Dewdrop's adaptation algorithm with our version that eliminates ADC conversions to get QuarkNet.

3.6.2.4 QuarkNet vs battery-assisted alternatives

Another interesting question is how QuarkNet performs when compared to battery-assisted versions of the other protocols (excluding Dewdrop + battery, which is identical to EPC Gen 2 + battery). Some protocols, such as Flit [45], improve in performance when there is more energy since there is more opportunity for bulk transfer. Would these outperform QuarkNet in battery-assisted scenarios? Figure 3.8(c) shows that throughput achieved by QuarkNet is consistently better. The average throughput of QuarkNet is 18kbps, 3.75$\times$ higher than EPC Gen 2 + battery, and 1.87$\times$ higher than Flit + battery. This result shows the benefit of reducing per-frame overheads in QuarkNet.

3.6.3 Reader-to-node communication

We now turn to an evaluation of reader-to-node communication. We begin by looking at the effectiveness of remote interrupts. We find that remote interrupts are extremely reliable — the reader detects remote interrupts with 100% accuracy across all distances where the node can communicate with the reader, and detection rate directly drops to 0% at roughly 19 – 20 feet where the node cannot detect the signal sent by the reader. While the accuracy will degrade under external interference, we plan to extend remote interruption to include encoded bits to improve robustness.

Next, we look at the throughput of reader-to-node communication when a node is placed at different distances from the reader. Figure 3.10 shows that the throughput achieved by QuarkNet is always higher than fixed 100 bit transfer across all distances. (We chose 100 bits instead of 12 bytes because of the slower baud rate of the reader-to-node link, as a result of which 12 byte transfer ceases to operate even when the node is deployed 1 feet from the reader.) The throughput of QuarkNet is higher than even a battery-assisted EPC Gen 2 node. This shows that the benefit of variable sized μframes is substantial even for reader-to-node communication.

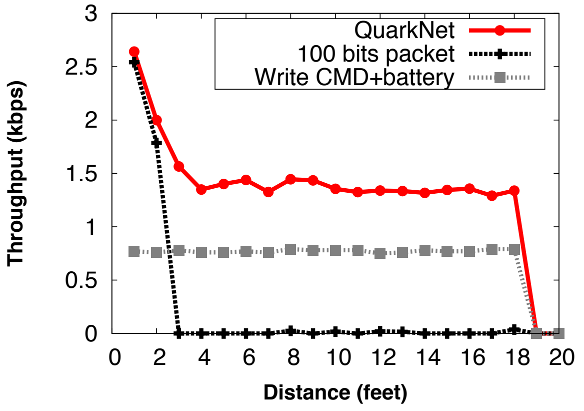

Figure 3.10. Throughput of reader-to-node communication. QuarkNet has 2× higher throughput than battery-assisted EPC Gen 2 Writes.

One trend in the graph that requires a bit more explanation is the fact that throughput decreases rapidly when the node is close to the reader (less than 4 feet), and plateaus until about 18 ft after which it quickly drops to zero. This is because RF-harvesting only works until 4ft (because of the limitations of the USRP reader), and beyond this distance, indoor light harvesting plays the dominant role.

3.6.4 Evaluating the QuarkNet MAC layer

We now turn to the evaluation of our MAC layer that includes all components of the protocol including various co-ordination overheads, frame interleaving, and scheduling. Figure 3.11 shows the communication throughput when we deploy 10

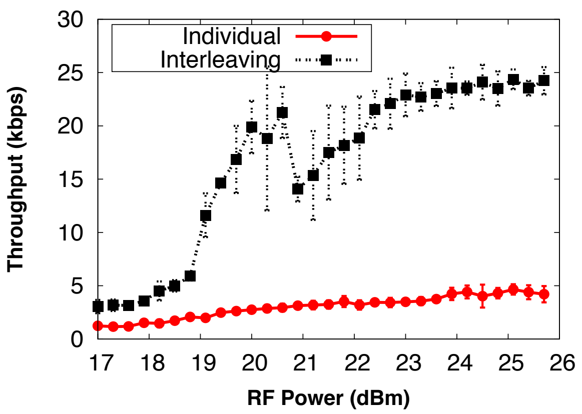

Figure 3.11. Throughput of 10 nodes is 5.4× higher when interleaved than when individually inventoried.

nodes in front of the reader and adjust the RF power from 17dBm to 26dBm. We use a throughput-maximizing scheduling policy in this experiment. For each RF power level, we plot the averaged throughput across the ten nodes and the confidence interval when they are scheduled in an interleaved manner and when they are inventoried individually. The throughput achieved by other MAC layer designs — EPC Gen 2 and Flit — are close to zero, so we do not plot them.

We find that even at the lowest RF power level, almost all nodes get to transmit data to the reader, and the average throughput steadily increases with higher RF power. In addition, the throughput achieved by interleaving the 10 nodes is 5.4× higher than the throughput when those 10 nodes are inventoried individually. These results show that our algorithm scales well across a wide dynamic range of harvesting conditions, and uses gaps between μframes efficiently.

3.6.5 Microbenchmarks

Table 3.2 shows the overhead incurred by different components of QuarkNet. The biggest system overhead is the switch from inactive mode to transmission mode (47.5 us), to configure several registers associated with transmission, such as the hardware timer register and data register. The overhead of the entire μframe size and

Table 3.2. Overhead of μframe transmission.

System overhead (us)		μframe overhead (us)	
TX to inactive	9.9	interrupt config	10.58
inactive to TX	47.5	handle interrupt	9.3
RX to TX	4.08	μframe adaptation	24.3
sleep to wakeup	9.83	voltage detection	3

inter-μframe gap adaptation algorithm (47.2us), is comparable to the total system overhead, and 10× smaller than the cost of an ADC conversion. Overall, the results show that our performance tuning measures have substantial benefits — the sum total of these overheads is smaller than the cost of transmitting 7 bits.

3.7 Discussion

3.7.1 Interoperability with other PHY mechanisms

While our work does not explicitly address co-existence of QuarkNet with other physical layer and upper layer mechanisms, many of these can be easily layered above the methods described in this chapter. For example, rate adaptation is widely used to adapt to wireless channel conditions, thereby maximizing communication throughput. This method operates at the bit-level, where each bit is composed of several symbols. Such an approach can be layered above QuarkNet, with gaps introduced between bits. Similarly, error correction codes or other encoding mechanisms that reduce bit error rate can be implemented above QuarkNet.

3.7.2 QuarkNets role with evolving technology

As micro-harvesters continue to improve in efficiency, one question is whether QuarkNet will continue to remain relevant. We argue that QuarkNet's relevance will increase for two reasons. First, the maximum harvesting rates are fundamentally limited by the physics of the harvesting source and form-factor. For example, RF energy harvesting is limited by the antenna size and the amount power issued by antennas, solar energy harvesting is limited by the panel size and the intensity of illuminance, and thermal energy harvesting is limited by the surface area and the temperature differential. Even if micro-harvesters become extremely efficient (say upwards of 80%), there is still a small amount of energy available, and systems optimizations similar to QuarkNet are critical to using the energy in an efficient manner. Second, trends in nano-electronics and low-power embedded systems are resulting in sensing and computing platforms that consume only tens of micro-watts of power [2]. These trends will make it possible to design many more micro-power based applications such as implantables and on-body sensors, enhancing the relevance of QuarkNet.

3.7.3 Fragmenting other tasks

While our focus in this chapter is on fragmenting the network stack, the abstraction of task fragmentation presented by QuarkNet can be potentially used for breaking down other components of a task such as sensing and computation into smaller atomic units. In our position paper [99], we presented preliminary results that demonstrated the ability to fragment an image sensing task such that the entire sensor can operate with a 3cm$\times$3cm solar panel under natural indoor illuminance. However, many questions remain to fully enable such fragmentation, requiring a combination of architectural modifications to the sensing and computing blocks to facilitate fine-grained fragmentation, systems techniques similar to QuarkNet that can take advantage of the fragmentation capability, as well as data processing techniques to enable useful applications over a layer that dynamically fragments sensing tasks.

3.8 Related Work

We have already discussed Dewdrop, Flit, Buzz, and EPC Gen 2, so we focus on other approaches.

3.8.1 Computational RFIDs (CRFIDs)

There has been increasing emphasis on CRFIDs in recent years given its potential for battery-less perpetual sensing. Ambient Backscatter [63] uses the backscatter of FM signals for short-range communication between tags. This is a severely energy limited platform, and could leverage QuarkNet when harvested energy is low. BLINK [100] is a bit-rate and channel adaptation protocol to maximize communication throughput, which can also leverage QuarkNet for performance. [82] introduces a power-optimized waveform which is a new type of multiple-tone carrier and modulation scheme that is designed to improve the read range and power efficiency of charge pump-based passive RFIDs. [83] presents a system architecture for backscatter communication which reaches 100m communication distance at the cost of slow bit rate (10 bits per second). Such techniques are complementary to QuarkNet — each bit transmitted at slow bit rate can be fragmented into several segments where the information within each bit is still preserved. Also of note is MementOS [76], which uses non-volatile flash storage for checkpoints within a task such that the it can continue execution after an outage. Flash checkpointing is useful for outage tolerance but is more than the cost of transmitting an entire EPC Gen 2 packet, hence it has limited utility in our case.

3.8.2 EPC Gen 2 optimizations

Much of the work on backscatter communication is specific to EPC Gen 2 tags, for example, better tag density estimation [84], better search protocols to reduce inventorying time [59], better tag collision avoidance [66], more accurate tag identification [94], better recovery from tag collisions [21], and more efficient bit-rate adaptation [100]. None of these tackle the problem of maximizing range and throughput from RFID-scale sensors, which have the ability to offload sensing data back to a reader.

EPC Gen 2 supports tag user memory operations in addition to simple EPC queries including the Read and Write command, however they are second-class citizens in the protocol since the main goal is to inventory tags. As a result, both are inefficient primitives for data transfer from tag to reader or vice-versa. In our experiments, we found that the Read and Write commands simply do not work at all under low energy conditions.

3.9 Conclusion

In this chapter, we present a powerful network stack, QuarkNet, that can enable systems to seamlessly scale down to severe harvesting conditions as well as substantial harvesting dynamics. At the core, our approach deconstructs every packet into μframes, handles dynamics with variable-sized μframes, and maximizes throughput via low-cost adaptation algorithms and interleaving of μframes. Results show that QuarkNet provides substantial benefits in pushing the limits of micro-powered devices, and allow them to perform useful work under more extreme environments than previously imagined possible. Our network stack tolerates such conditions, thus makes it valuable to a wide range of emerging micro-powered embedded systems and applications.

CHAPTER 4
HIGH SPEED ULTRA LOW-POWER BACKSCATTER

Existing sensing architectures incur substantial overhead for a variety of computational blocks between the sensor and RF front end — while these overheads were negligible on platforms where communication was expensive, they become the bottleneck on backscatter-based systems and increase power consumption while limiting throughput. In this chapter, we propose a radically new design that is minimalist, yet efficient, and designed to operate end-to-end at tens of μWs while enabling high-data rate backscatter at rates upwards of many hundreds of Kbps.

4.1 Background and Motivation

A fundamental assumption that has driven the design of sensor networks for decades is that communication is the most power-hungry component of an individual sensor system. The power consumption gap between communication and other modules has driven a plethora of design choices in sensor networks, primarily by encouraging designers to reduce data at the source, thereby minimizing the amount of data that needs to be communicated.

We argue that this assumption does not hold when it comes to passive radios such as backscatter. Backscatter requires extraordinarily simple circuitry since the carrier wave is generated by a reader, and a sensor only needs to modulate the signal to transmit information, thereby eschewing power-hungry components of a typical active radio. The simplicity and inherent efficiency of backscatter means that the

Table 4.1. Power consumption of accelerometer, audio, ecg, and image sensors.

	Accel [4]	Audio [5]	ECG [6]	Camera [47]
Power	6μW	15.3μW	60μW	0.7μW

energy gap between communication and other components of a system has narrowed dramatically.

These observations have profound implications on the design of next-generation wireless sensing systems that operate using backscatter. The primary implication is that the bottleneck in terms of power consumption has shifted away from communication to computation and sensing. But sensing is often not the bottleneck as well — the past decade has seen dramatic reductions in the power consumption of sensors such as microphones, cameras, ECG, accelerometers, and others, many of which consume only μWs of power while sampling at high rates (Table 4.1). Thus, both backscatter communication and a variety of low-power sensors can operate at μWs of power, and the key question becomes one of optimizing the rest of the system to match these numbers. This requires that we re-think every component between the sensor and RF interface — data acquisition, data processing, buffering, packetizing, MAC, and many others now become the bottleneck for achieving ultra-low power operation.

In this chapter, we overturn the design principle governing wireless sensor design from one that is focused on minimizing communication to one focused on optimizing the computational elements between the sensor and RF interface. But optimizing computation is easier said than done, and requires an understanding of every module of the sensing platform, in-depth analysis of how to eliminate overhead from these modules, and design of a modified architecture to support an optimized design.

But our efforts to optimize computation raises an unexpected problem. If we do nothing to reduce data at the source, we need the bandwidth to be able to transfer raw data from the sensor to infrastructure. While backscatter communication is efficient in terms of power, throughputs achieved by practical backscatter-based systems have been abysmal. Despite several efforts at improving throughputs of backscatter [45, 100, 29, 86, 44], the best case throughput is still only around 20 kbps even when only a single node is present, and drops dramatically to barely hundreds of bits/second when there are multiple devices sharing the network. These numbers are not encouraging — for example, a microphone sampled at 8-44 KHz requires transmit rates upwards of 704 kbps, a far cry from the throughput that backscatter platforms are able to support today.

This leads us to the central question that we address in this chapter: *how can we design a backscatter-based wireless sensor system that achieves whole-system power consumption of μWs, while simultaneously increasing data rates to support raw data transfer from sensors at several hundreds of kilobits/second.* Our goal is aggressive — as a point of comparison, an existing backscatter-based sensor, the UMass Moo (or the UW WISP) consumes about 2mW of power while transmitting at a few kilobits/second when there are multiple devices present. Thus, we seek to drop the system-wide power consumption by more than two orders of magnitude while simultaneously enabling two orders of magnitude increase in the data rates.

Our contributions are two-fold. First, we present a novel backscatter-based sensor platform, Ekho, that achieves our design goal to optimize power by eliminating computational overhead from the sensor to RF pipeline. We start with a deep dive at what computational modules are present between the sensor and RF interface on a typical low-power sensor platform, and measure their power consumption, before launching into a minimalist design that is optimized for power. Our second contribution is a network stack, EkhoNet, that is designed to be minimalist and enable bandwidth scale up to support data rates of hundreds of Kbps while supporting tens of nodes. While each Ekho node is minimalist, our MAC layer leverages resources at the reader to enable utility-energy and channel-aware optimization of bit rates and slot sizes across nodes.

Our results on a USRP reader and Ekho nodes show that:

- For operating an accelerometer at 400Hz, Ekho consumes 35μW of power, 7.6$\times$ lower than the 266μW of the Moo and 3.3$\times$ lower than the 118μW of WISP5.0. For operating an audio sensor at 44kHz, Ekho consumes 37μW of power, 76$\times$ lower than the Moo and 13.5$\times$ lower than the WISP5.0.

- We show that EkhoNet can scale to a network of several high bandwidth sensors. When a network of ten Ekho nodes equipped with microphones transmit simultaneously to a reader, we achieve a throughput of 780 kbps as a result of interleaving the data streams at the MAC layer. We also use an energy-utility-channel aware scheduler, and show that over 50% of the audio sensors achieve a median MOS score larger than 2, significantly higher than a baseline scheme that assigns sampling rates evenly across all nodes.

4.2 Case for Ekho

In this section, we make the case that backscatter communication is extremely cheap and overturns the widely held premise that communication is more expensive than computation. We focus on the tradeoff between computation and communication since many commonly used sensors are already extremely efficient in terms of power. We begin with a discussion of why backscatter is efficient.

4.2.1 Backscatter radio RF front end

Backscatter radios are designed to enable ultra low power wireless communication. As shown in Figure 4.1, a reader provides a carrier wave, which can be modulated with information to enable ultra low power wireless communication. While the carrier wave can also be rectified by a sensor for energy harvesting, our focus in this chapter is on backscatter as a low-power radio, whether energy is obtained via harvesting or

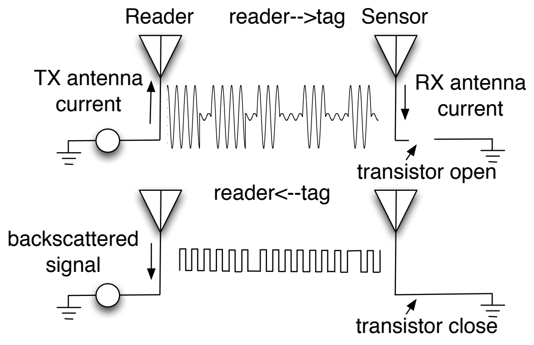

Figure 4.1. Backscatter communication basics.

a battery, hence we focus on the communication rather than harvesting aspects of backscatter.

To transmit data, a sensor toggles the state of a transistor to detune its antenna and reflect the carrier wave back to the reader with its own information bits. Because the sensor does not actively generate RF signal as active radio systems, the power consumption of the backscatter radio is very low. In addition, the on-off transition overhead of backscatter radios is very short because backscatter radios do not have to warm up the RF analog circuits for data transmission unlike active radio systems. As a result, there is little overhead incurred while transmitting via backscatter, even when transmitting at a high rate. For example, one key component of the backscatter analog RF front end of the WISP [18] is a MOSFET transistor (BF1212WR). Its power consumption follows the equation of CV^2F where C is the capacitance of the transistor, V is the digital drain-source voltage, and F is the frequency of operating the transistor. When this transistor is toggled at a slow rate of 10Hz, it consumes 55pW of power, and even when toggled at a high rate of 1MHz, it only consumes 5.5μW of power. Thus, backscatter radios consume of the order of μWs of power, even for high rate data transfer.

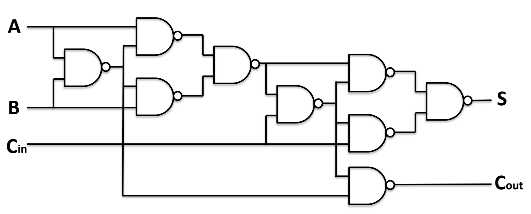

(a) 1 bit adder circuits for computation.

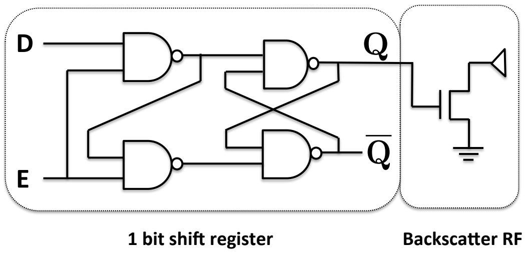

(b) 1 bit shift register controls a backscatter transistor.

Figure 4.2. 1 bit adder and 1 bit shift register circuit.

4.2.2 Why compute if its cheaper to transmit?

The power consumption of backscatter radio has surprising implications on sensor system design, and challenges long-held views about communication vs computation tradeoffs in these systems.

4.2.2.1 Computation vs Communication

A common assumption in designing sensor systems has been that computation is significantly cheaper than communication, often by many orders of magnitude. This view has shaped a plethora of efforts for in-network processing, signal compression, sub-sampling, and other such approaches to reduce data at the source prior to communication. Indeed, this tradeoff has been reinforced by performance/power trends over the past decade — power consumption of embedded processors have dropped dramatically, while power reduction in active radios has been relatively slower.

However, backscatter communication challenges this long-held view. Backscatter is inherently extraordinarily efficient since the carrier wave is generated by the reader, and the tag only backscatters the signal without any additional amplification. Thus, each bit of backscatter is extremely simple, and only requires a handful of gates (Figure 4.2). This implies that for computation to be cheaper energy-wise, the computational operations on each bit would have to use fewer gates than that required to communicate the bit. This is often a tall order due to the simplicity of backscatter.

Consider, for example, a simple aggregation operation that sums ten sensor readings before transmitting the aggregate value over the radio. On traditional sensor platforms, such data reduction would have direct and significant power benefits since communication dominates power, and our aggregation scheme cuts this cost by a factor of ten. The same operation on a backscatter-based platform has dubious benefits. Figure 4.2 shows that the number of NAND gates required for summing two bits is roughly nine (thirty six transistors), but only four NAND gates (sixteen transistors) and an additional transistor for backscattering the signal are needed to transmit the same data via the shift-register controlled backscatter RF! As power consumption is proportional to number of transistors, a nine gate adder consumes 2.1× more power than the shift-register controlled backscatter RF.

It is necessary to add a few caveats to our simplified comparison of computation and communication. The clock rates of communication subsystems are limited by signal to noise ratio considerations, whereas the clock rates of processors can be higher, and thereby reduce power. In addition, low-power processors use many tricks to reduce power consumption including optimized signal processing circuits, different power domains, extremely tight duty-cycling, and so on. Despite these optimizations, the cards are stacked against computation. Backscatter is so incredibly simple in terms of circuitry that even matching the efficiency of backscatter becomes a challenging architectural design problem.

Thus, the crux of our argument is the following: *backscatter drives down the optimal cross-over point between computation vs communication, such that communication of raw data may be preferable to computation in a wider spectrum of real-world scenarios.*

4.2.2.2 Implications on architecture design

This observation has an immediate implication on the architecture of a backscatter-based sensor platform. Traditional sensing platforms add a lot of computational modules between the sensor and the radio for sensor data acquisition, processing, filtering, buffering, etc. The contribution of these components to overall power consumption of an active radio-based sensor system is minimal and can largely be ignored. However, on backscatter-based platforms, these components become the bottleneck.

This raises an intriguing question — with the power consumption of backscatter being so low, would it in fact be more efficient to eliminate all of these modules en-bloc, and just connect the sensor directly to the radio? In other words, would it be better to just stream every bit of data that is sensed directly through the radio?

We take a measurement-driven approach towards answering these questions. First, we look at the computational blocks between sensing and the RF interface on existing backscatter-based sensing platforms to understand how much power they consume, as well as why they suffer in terms of throughput. Second, we build on our empirical study and design a radically new backscatter-based sensor platform that addresses these limitations.

4.3 Investigating existing wireless sensing architectures

In this section, we investigate why current backscatter-based platforms are unable to achieve end-to-end power consumption of μWs for high-rate sensing and transfer. We also investigate why they are unable to achieve high-data rate communication, particularly while operating at low power. To empirically understand these factors, we look at the UMass Moo/UW WISP class platforms that are equipped with sensors, a low-power MCU (MSP 430 family) and a backscatter radio.

4.3.1 Poor energy efficiency

We start with a break down of the power consumed by three key computational modules on a UMass Moo (Figure 4.3): 1) the sensor data acquisition subsystem which handles the protocols for operating sensors, 2) the data handling subsystem on a micro-controller where sensor data is stored, processed (if needed), formatted into packet, and sent to the network stack, and 3) the network stack implemented in a combination of hardware and software.

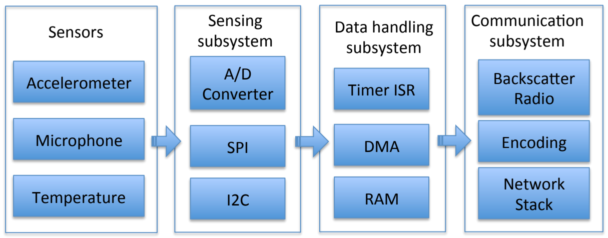

Figure 4.3. Computational blocks on existing backscatter-based sensors.

4.3.1.1 Sensor data acquisition

Sensor data acquisition is a relatively simple operation — some sensors have an on-board ADC, hence data acquisition is via a protocol such as SPI or I2C, whereas other sensors just provide an analog signal which is digitized using the micro-controller's ADC. Despite its simplicity, even these operations are not as cheap as one might expect. For example, sampling an accelerometer via the SPI bus would require periodic wakeup of the MCU to fill the SPI buffer, sending the read command and read address to the sensor, as well as providing the clock for the SPI bus. The overall result is that the MCU is active for about 40% of the time when acquiring data from an accelerometer sampling at 400 Hz. This acquisition operation, in itself, consumes 84μW of power, 14$\times$ higher than the accelerometer (6μW). The cost of acquiring audio data is equally high — when sampling an audio sensor (ADMP803) at 44KHz, acquisition consumes 492μW of power, 14.5$\times$ higher than the audio sensor (34μW).

4.3.1.2 Data handling subsystem

The data handling subsystem is the block that processes the acquired sensor data, formats and packetizes it, and sends it to the network stack. To minimize this overhead, sensor systems typically operate in a duty-cycled mode where the MCU is turned on for a minimal amount of time needed to handle the data, before switching back into sleep mode to conserve energy.

However, this optimization is no longer effective when this subsystem handles high-rate sensors. Figure 4.4 shows the power consumption for executing the timer interrupt service routine to handle each acquired audio sample. At high rate, the MCU is rarely able to switch completely back into the ultra-low power sleep mode due to frequent interrupts. Thus, the overall power consumption of the data handling module is roughly the ballpark of active mode power consumption of the MCU (a few mW), which is several orders of magnitude higher than the power consumed by the sensor.

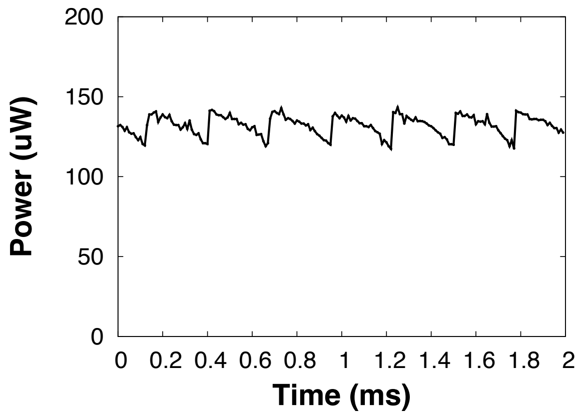

Figure 4.4. Power consumed for handling timer interrupts at 4kHz. The MCU is unable to switch to sleep mode due to frequent interrupts.

One method to reduce power of the data handling subsystem is to use Direct Memory Access (DMA), which allows transfer of data from the sensor to memory without waking up the MCU. This raises the possibility that waking up the MCU

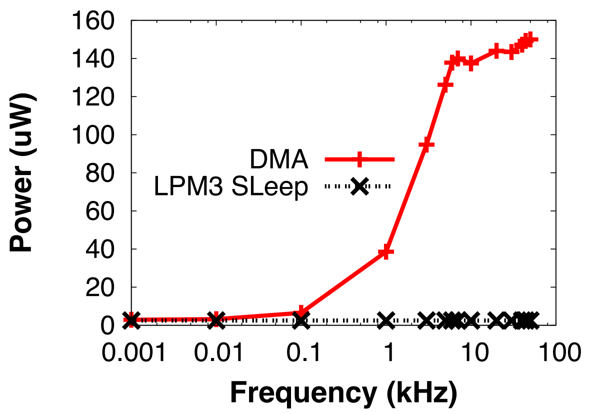

Figure 4.5. The power consumption of DMA transfer at different frequencies.

can, perhaps, be avoided altogether if the data is transferred directly from the sensor to the network queue without any processing.

Surprisingly, DMA does not reduce power consumption. Figure 4.5 shows empirically measured power consumption for DMA transfer on an MSP 430, which moves the sensor data from a sensor to a local memory at different frequencies. We observe that while DMA is efficient at low rates (e..g below 100Hz), it has high power consumption at high transfer rates — for example, DMA transfer consumes 149.2 μW of power at 44 kHz, 60$\times$ higher than the 2.5 μW of LPM3 sleep mode of the MCU. This is surprising since one would expect that the MCU is in sleep mode while DMA operates.

The culprit for high power consumption of DMA turns out to be its tail energy consumption. Figure 4.6 shows the power consumption of repeated DMA transfer at 100 Hz. This experiment is done with an MSP 430 set to LPM3 sleep mode and a timer that periodically triggers DMA transfer. When a DMA transfer is initiated, its power consumption increases to 40μW within 10us, and starts decreasing once the DMA transfer is done. However, the power consumption decays at a relatively slow rate compared to the sharp increase, resulting in a long tail of roughly 3.5ms. When the DMA transfer frequency is high, such as 5kHz shown in Figure 4.5, the long tail

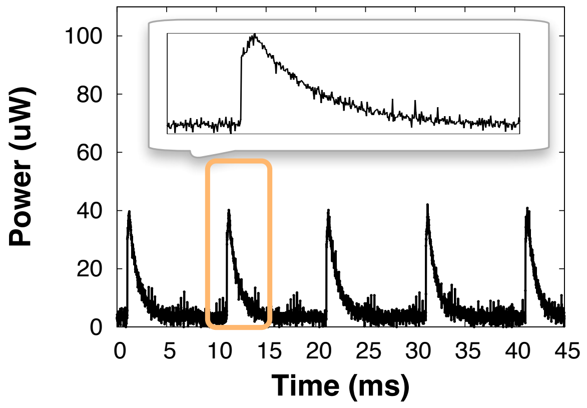

Figure 4.6. Power consumption of DMA transfer at 100Hz. DMA is slow to return to sleep mode.

leads to high power consumption. While we are not certain about the cause of this behavior, one hypothesis is that the system waits for more data before it times out and switches to a lower power mode. This behavior is common in many power savings circuits, for example, in smartphone radios [23, 53], and is typically done to amortize the cost of waking up and shutting down a hardware subsystem.

4.3.1.3 Communication subsystem

The final computational component of a sensor platform is the communication stack, which includes the PHY, MAC and upper layers. While the RF interface of backscatter is extremely low-power, the other layers add more overhead. For example, on the UW WISP or UMass Moo platforms, the backscatter radio is controlled by a hardware timer which needs to be configured and handled in software. In addition, the EPC Gen 2 network stack on these devices is implemented in software, and results in substantial overhead since the MCU needs to handle protocol messages. In fact, the MCU needs to be on for 67% of the time for processing network stack messages at the software layer while only 7% of the time is used for data transmission. As a consequence, the software on UMass Moo platform consumes 2mW of power, which is three orders of magnitude higher than the power consumption of a low-power sensor.

As with the data handling subsystem, the software overhead of the network stack can be reduced by using hardware peripherals to control the radio. One commonly available hardware peripheral on MCUs is the Universal Asynchronous Receiver and Transmitter (UART). This is particularly useful for a backscatter radio since UART generates an ASK signal, which can be directly transmitted via backscatter (which uses OOK). At the first glance, the UART peripheral has the potential to dramatically reduce the cost of running the network stack because it can operate when the MCU stays in deep sleep mode. However, its buffer needs to be filled with sensor data, which in turn needs to be done with either DMA or software, both of which are expensive energy-wise. As a result, even the UART-driven backscatter radio consumes roughly 2mW.

4.3.2 Poor transmission efficiency

The second key drawback of existing backscatter-based sensors is the abysmal throughputs that they achieve. For example, even though there have been many efforts to improve backscatter throughput, the ceiling is still less than 20kbps for a single node [45, 100, 29, 86], and drops to hundreds of bits/second in a network with multiple devices. Clearly, this is far below what is needed for streaming raw sensor data from high-rate sensors.

One factor that limits the throughput is the poor efficiency in clock utilization. For example, the UMass Moo and WISP take 48 clock ticks to send a single bit of data, which causes a 48× reduction of the maximum possible throughput that is achievable with the system clock. We find three reasons for this inefficiency. First, both transmission and reception logic is implemented in software which, naturally, is inefficient in the use of the clock. Although the transmission and reception code on the Moo and WISP platforms are optimized in assembly instructions, one bit transmission and reception still has substantial overhead. Second, EPC Gen 2 PHY-layer encoding further reduces the clock utilization efficiency. To minimize the DC components during data transmission, each bit is encoded into a sequence of pulses using Miller encoding. For example, the Miller-4 encoding used by Moo and WISP platforms uses eight pulses to encode one bit of data, resulting in further drop of throughput by a factor of eight. Third, the EPC Gen 2 MAC layer is extremely inefficient for high bandwidth data transfer. While this is a point that has been made many times before [45, 100, 29, 86], an efficient alternative that achieves high throughput using backscatter is lacking.

4.3.3 Summary

Thus, the limitations of the computational blocks on existing backscatter-based sensor platforms lead us to the following observation. The primary culprit in terms of power is the MCU's active mode power consumption, and the fact that many operations (sensor acquisition, data handling, communication) require execution of instructions on the MCU. Surprisingly, optimizing the system by leveraging hardware peripherals such as DMA and UART do not solve the problem, particularly at high data rates due to tail power consumption, and coupling between different components of the sensing to communication pipeline. In terms of throughput, the primary issues stem from inefficient utilization of the clock due to a combination of software overheads, encoding overheads, and an inefficient MAC layer standard. In conjunction, these limitations call for a *clean-slate re-design of a backscatter-based sensor platform* from the ground up for extremely low power consumption and high data rates.

4.4 The Ekho platform

Our solution is Ekho, a backscatter-based sensor platform that is optimized for ultra low power operation and high-speed streaming from sensors. We outline the platform architecture followed by the MAC layer.

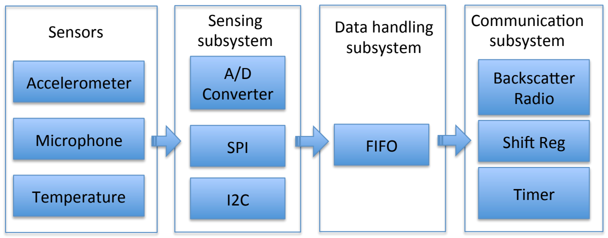

Figure 4.7. The key components of Ekho.

4.4.1 Eliminating computational blocks

At the platform level, the design of Ekho is minimalist. We simply remove as many computational blocks between the sensor and RF analog front end as possible in favor of communicating raw data. Figure 4.7 shows the key components in Ekho.

Ekho reduces the overhead of data acquisition from the sensor by implementing the SPI and ADC sampling logic on a small CPLD (FPGA). Implementing these blocks in hardware means that we can make them as fast as needed without incurring the software overhead of waking up a micro-controller.

Ekho substantially reduces the overhead of handling sensor data by a minimalist approach that uses a FIFO buffer between the sensors with RF analog front end. The FIFO buffer is the minimum element that is needed between sensing subsystem and communication subsystem to deal with short delays in transmitting the data over the backscatter link, for example, due to intermittent scheduling of a device. In this manner, Ekho eliminates software and tail energy overhead that was observed on existing backscatter-based platforms.

The final computational component of the pipeline is the communication subsystem. Unlike EPC Gen 2 that is designed for a broad range of RFID tags, Ekho is designed solely for streaming sensor data from nodes to a reader. A protocol designed solely for streaming data from sensors can be quite simple. The reader informs each node of a timer value that specifies the period with which to transfer data in its FIFO buffer, and a rate that determines how fast to transfer the data. The only hardware component required for this protocol to work is a timer and shift register. Once the timer fires, a shift register converts the input sensor data to an ASK signal that is used to modulate backscatter radios.

In the current instantiation of Ekho, we do not perform any encoding of data. While the need for encoding to deal with harsh wireless conditions and interference is well-known, it also makes the hardware more complex, and consequently more power hungry. For example, the default configuration on the UMass Moo/UW WISP platforms is Miller-4 encoding incurs overhead of several hundreds of gates. Thus, while encoding may be useful in some cases, we do not employ it in Ekho.

4.4.2 The EkhoNet MAC layer

We now turn to the second part of our performance puzzle — achieving high throughputs that are upwards of many hundreds of kilobits/second across different nodes in the network. A high speed MAC is important for supporting an architecture where raw data transfer is the norm rather than the exception.

MAC layer designs are very well understood, particularly in cases such as ours where a central controller performs TDMA-like scheduling of sensor nodes. However, the key point in our design is two-fold: a) even though the sensor node is designed to be extremely simple, the decision making logic can be placed at the reader, thereby enabling surprisingly complex scheduling mechanisms across a network of extremely simple sensor nodes, and b) our MAC is holistic in that it takes into account utility of data, channel-awareness, energy consumption, as well as other hardware considerations, in-order to maximize throughput.

4.4.2.1 MAC Design Considerations

At the heart of EkhoNet is the logic that is used to determine when each node should transfer, and what rate they should transfer. Before we answer this question, we need to understand several characteristics of Ekho including: a) how do MAC-layer parameters impact the energy-efficiency of the platform? b) what are the signal-to-noise ratios at which data transmitted by Ekho can be successfully decoded? c) what criteria should we use to decide what sampling rate to use when sufficient bandwidth is not available? and d) what are the implications of platform considerations such as clock drift and buffer size? We now empirical examine these considerations in greater detail, and discuss the implications on selection of MAC layer parameters.

- **Bits/Joule:** The first question we ask is how energy-efficiency of data transfer depends on the bit rate. Figure 4.8 shows the efficiency of a shift register controlled backscatter radio across different bit rates. At low rates, there is a steep increase in efficiency as bit rate increases due to the fact that constant power consumption by the system is amortized over more bits being transferred. However, improvements in efficiency diminish once the bit rate increases beyond 1Mbps since the relationship between power and frequency of the shift register is roughly linear, hence there are not much improvements possible. The power curve suggests that, from energy perspective, we should choose the fastest bit rate possible for data transmission.

- **Signal to Noise Ratio:** While faster bit rates are preferable due to higher energy efficiency of transfer, SNR degrades as bit rate increases. Figure 4.9 shows the SNR when we deploy a transmitter 1 meter from the reader and change its transmission bit rate. As bit rate increases, the SNR decreases steadily as one would expect. When the SNR is lower than 10dB, decoding becomes difficult on our software-defined radio based reader platform, which gives us an upper

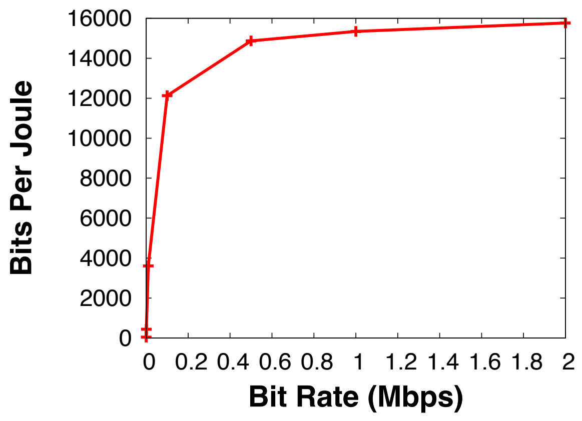

Figure 4.8. Efficiency of backscatter radio (in bits/joule).

bound on the fastest bit rate that can be supported by the system without losing bits.

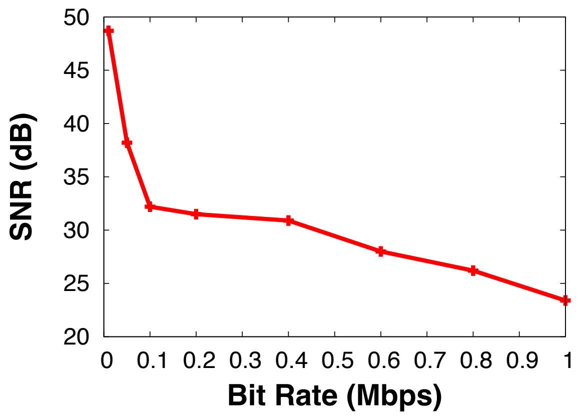

Figure 4.9. SNR at different bit rates when device is placed 1m from a reader.

- **Utility of data:** Since EkhoNet is designed for high-rate sensors, one question that needs to be addressed is how to decide on appropriate sampling rates when the overall data rates at full sampling rates exceed capacity. On our existing system, we are limited to 1Mbps aggregate transfer rate across all nodes since the SDR-based reader is only able to support 8M samples per second due to the limitations of the realtime signal processing logic. This means that we can easily reach the SDR limit when we operate a network of sensors. For example, a network of five audio sensors sampling at 44 KHz, and transmitting raw data generates an aggregate bandwidth of 3.5Mbps, well above what can be supported by EkhoNet.

Our solution is to take into consideration the utility of data generated by the different sensor nodes. Figure 4.10 shows an example of one utility function, Mean Opinion Score (MOS), which is a commonly used metric for characterizing the quality of transmitted audio [11]. The MOS score can be used to guide decisions regarding which node is allocated bandwidth.

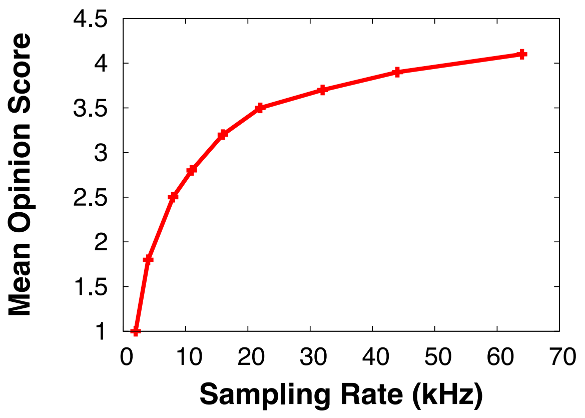

Figure 4.10. Mean Opinion Score (MOS) at different sampling rates for a microphone.

- **Clock drift:** Another consideration in determining slot sizes is clock drift. For example, in our implementation of Ekho, we use a crystal oscillator driven system clock that can drift at upwards of 50 ppm. If two nodes transferred at 1 Mbps, then they would drift by 1200 clock cycles each minute. The reader can handle clock drift in two ways. First, when assigning slots, it can allocate guard bands in each slot to allow for some drift. However, guard bands should be kept to a minimum to reduce bandwidth wastage. Second, the reader has the luxury of observing how the gap between slots varies as nodes transfer, and can detect when collision occurs by looking at the constellation plot of the signal

[86]. Thus, when the reader suspects that slots have bled into each other, it can send a reset pulse that informs all nodes to reset their timers. Note that this is possible for backscatter because reader messages are broadcast and received by all nodes. A reset pulse is simply implemented by shutting off the carrier for a short, pre-defined duration, which is detected by each node. While reset pulses can be short, it should be used infrequently since there can be robustness issues if a node does not receive the pulse. This can result in further collisions resulting in more reset pulses until the network synchronizes.

- **Buffer size:** One additional constraint introduced by the Ekho hardware platform is that the FIFO buffer size on the device is limited, hence if the slot sizes are too long, samples will be lost since the buffer will overflow.

4.4.2.2 Channel-Utility-Energy aware Rate Selection

Given the above constraints, the overall problem that the reader faces can be described as follows: select the optimal bit rate and slot size such that aggregate utility of received data is maximized and aggregate energy consumption minimized, subject to constraints on the buffer sizes, SNR, and guard bands. We formalize this problem below.

We assume that the following parameters are given:

- The minimum SNR, 10 dB in our system, at which the reader can decode bits with low bit-error rate.
- The maximum achievable bit-rate r_i that is higher than the minimum SNR.
- The maximum sampling rate of each node $s_{max}(i)$.
- The size of each sample in bits, b, bits/sample.
- The fraction of each slot that should be a guard band δ.

Given these values, we need to choose the sampling rates for each sensor s_i, and the fraction of time allocated to each node t_i by taking into account the following objective:

- $\sum_{i=1}^{n} U(\mathbf{s})$ which is a measure of the aggregate utility obtained from all sensor data received from the nodes.

The constraints are the following:

- $\sum_i t_i \leq 1$, i.e the fraction of time allotted to nodes sum up to at most one (less than one if the network is operating below its limit).
- $s_i \leq s_{max}(i)$, which restricts the sampling rate for a sensor to be below the maximum.
- $(1-\delta)t_i r_i = b\, s_i$, which ensures that the production of data from the sensor, and transmission of data from the radio are matched i.e. the node can transmit what is being sensed. The term $(1-\delta)$ is present since there's a guard band for each slot.

The overall optimization is shown below (in vector form for compactness). Here, $\mathbf{s}$ and $\mathbf{t}$ are the vectors of sampling rates and the fraction of time allocated to each node, which need to be determined, and $\mathbf{r}$ is the vector of bit rates chosen for each node based on SNR. The symbol $\preceq$ stands for element-wise inequality (i.e. one for each node).

$$\begin{aligned} \underset{\mathbf{s},\mathbf{t}}{\text{maximize}} \quad & \mathbf{1}^{\mathbf{T}} U(\mathbf{s}) \\ \text{subject to} \quad & \mathbf{t}^{\mathbf{T}}\mathbf{1} \leq 1 \\ & \mathbf{s} \preceq s_{max}\mathbf{1} \\ & (1-\delta)\text{diag}(\mathbf{t})\mathbf{r} = b\,\mathbf{s} \end{aligned}$$

Typically, the utility function is concave, for example in the case of MOS score (Figure 4.10). Hence, the objective is to maximize the sum of concave utility functions, and the constraints are linear, hence the optimization can be solved by standard convex optimization methods. Note that the optimization returns the fraction of time for each node — this can be converted to an actual slot size by scaling by an appropriate period such that each node is capable of buffering the data in its local FIFO buffer.

4.5 Implementation

Figure 4.11 shows the prototype of Ekho, which implements all the design elements described in section 4.4. The current prototype measures 1.8 by 2.4 inches, but we believe future revisions can shrink this even further. We now briefly describe the key sub-components used in the prototype.

4.5.1 Hardware

The first key hardware element is an ultra low power FPGA (Igloo Nano AGLN250) that manages the various sub-components of the Ekho platform. Most key components of the Ekho architecture, including the sensing, data handling, and communication subsystems, are implemented within the FPGA. The particular FPGA was chosen because it has low static current consumption and has a 32k bits (2KB) RAM, which also determines the maximum size of our FIFO buffer.

The next key design element is the backscatter circuit that can operate at high speed. As the device toggles the state of a transistor that connects to the antenna, an OOK signal that carries modulated information is generated. However, on existing backscatter platforms, the static current of the transistor is provided by the harvested RF energy, which might vary across time. The varying RF power affects the amount current that is provided to the transistor and leads to unstable edges of the generated

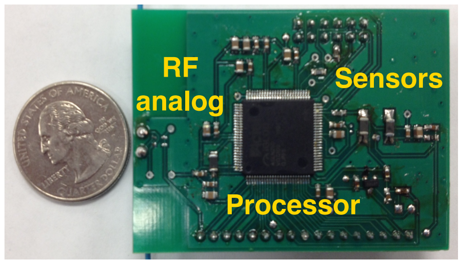

Figure 4.11. Ekho is implemented as a low-profile printed circuit board with small form factor.

OOK signal. Therefore, decoding becomes challenging when the data rate is high. Our backscatter circuit directly provide a small bias current to the transistor and retains a sharp edge for the generated OOK signal.

A critical element of our hardware design is the clock system which drives the FPGA logic. The core of our clock system is a 1MHz ultra low power crystal oscillator that directly feeds into the FPGA. The 1MHz clock is divided to drive different components of the architecture because sensing, data handling, and communication subsystems operate at different speeds. Our clock system is different from the Moo and WISP platforms, where a digital generated clock (DCO) is used. Although the DCO can also be divided for driving different components, it couples the operational modes of the system and its clock speed, as a result of which the high speed clock is only available when the system operates as a whole in a high power mode.

4.5.2 Software defined backscatter reader

We used the USRP N210 mother board and the SBX RF daughterboard to build our software defined backscatter reader for receiving high speed backscatter signals from Ekho. We construct a signal processing pipeline that is able to track the amplitude of the carrier wave that is used as the reference for decoding the OOK signal generated by Ekho. Our decoding is different from Moo and WISP platforms where Miller-4 encoding is used on top of the OOK signal and a decoding template can be

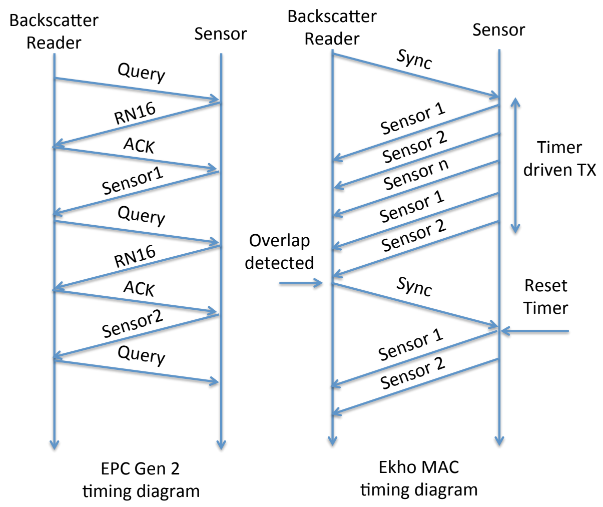

Figure 4.12. Timeline of Ekho MAC.

used for correlating the received signal and output a bit when the template matches the received signal. In Ekho, the data is sent directly via OOK and encoding is not used. Therefore, we need to track the amplitude of carrier wave to determine whether the received signal is a high or low pulse.

4.5.3 MAC layer protocol

Figure 4.12 shows the timing diagram of the Ekho MAC layer. The first stage is to inventory the nodes in the network, and obtain information about their SNR and other sensor-related information. This phase executes very similar to an EPC Gen 2 singulation phase, where nodes can select a slot to transfer in, and send a short sequence of bits with the appropriate information. After the singulation phase, the reader executes the optimization algorithm described in §4.4 and determines the time period and bit rate for each sensor, which is then relayed to the sensor. The reader initiates the singulation phase under several circumstances: a) when significant changes are observed in SNR, which might signify changes in position or orientation, and b) when collisions are detected, which might signify that a new node is attempting to join the network.

Once the reader informs each sensor of its bit rate and period, it initializes slots by sending a synchronization signal during which it shuts down the carrier for a short 10 μs window. This pulse informs all nodes simultaneously that they should start their timers, thereby initiating the TDMA schedule. The length of the sync message needs to be chosen small enough to amortize overhead, but large enough to be detectable at the sensor, hence our choice of 10μs.

When the reader detects that data transmitted during adjacent slots are overlapping into each other (due to clock drift), it re-issues a synchronization pulse to restart the timers on all nodes. Overlap between sensors can be detected by looking at the constellation map of the received signal — if two clusters are present, it indicates that a collision-free signal is received and if more clusters are present, it indicates that a collided signal is observed [86]. If multiple synchronization pulses fail to eliminate collisions, the reader switches back into inventory mode.

4.6 Evaluation

We now evaluate the overall performance of EkhoNet including 1) demonstrating the power benefit of the Ekho architecture, 2) benchmarking the performance of the EkhoNet MAC, and 3) evaluating EkhoNet's ability to support high-rate streams from many sensors while operating at extremely low power consumption.

4.6.1 Experimental setup

We deploy 10 Ekho nodes 1 feet to 9 feet from a backscatter reader. Our experiments do not cover distances larger than 9 feet because of the poor signal quality beyond 9 feet. This is a result of the 100mW maximum power issued by the SBX RF daughterboard, which is 10× smaller than commercial RFID readers.

To understand the power benefits of Ekho, we compare against the UMass Moo (equivalent of Intel WISP 4.0) and the WISP5.0 platforms. Since the WISP5.0 platform is not currently available, we evaluate its power consumption with a prototype that uses the same MCU (MSP430FR5969). Since the MCU is the main power hog in the system, this provides a good proxy for measuring power consumption.

4.6.2 Ekho power benchmarks

We begin our evaluation by validating the claim that the power optimizations on Ekho can substantially reduce the overheads incurred by existing platforms. We follow the organization in §4.4, and show benchmarks for each module — sensor data acquisition, sensor data handling, and network stack.

Figure 4.13 measure the power of the sensing subsystem when Ekho interacts with two types of sensors — an accelerometer with on-board ADC that connects to the MCU via a SPI interface, and an audio sensor where the MCU's ADC is used to sample the sensor. We compare Ekho versus a WISP/Mote-class sensor device (i.e. a device where the sensor connects to an MCU that acquires data). In both cases, we can see that Ekho reduces power consumption substantially — for sampling the accelerometer, Ekho reduces power by 1.5× at 400Hz by eliminating the overhead of software-controlled SPI, and for sampling the audio sensor, Ekho reduces power by 22× by trimming the overhead of running the software-controlled ADC at 44kHz.

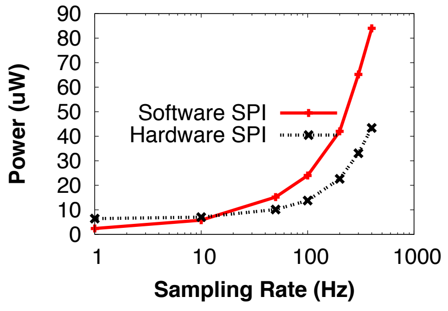

(a) Accelerometer.

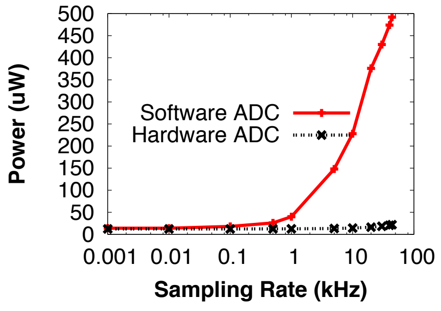

(b) Microphone.

Figure 4.13. Power reduction for sensing subsystem: a) sampling an accelerometer, b) sampling a microphone.

Figure 4.14 measures the power consumption of the data handling subsystem of Ekho, which is composed by a 2kB FIFO buffer for connecting sensors to the RF analog front end. The 2kB FIFO buffer only consumes 26.5μW of power when data is written into the FIFO at 500kHz, 14.4$\times$ lower than the 384μW consumed by DMA driven data migration and 92$\times$ lower than the 1.5mW consumed by timer driven data migration.

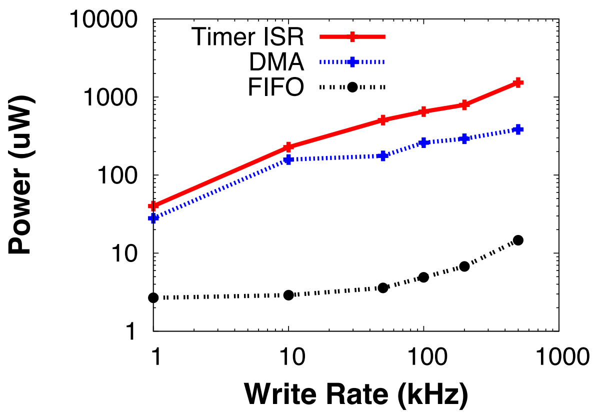

Figure 4.14. Power reduction for data transfer to network queue.

Figure 4.15 shows the power consumption of the communication subsystem which is composed of a shift register and backscatter radio. At 1Mbps, Ekho's communication subsystem consumes only 77μW of power, 13.4$\times$ lower than a UART controlled backscatter radio implemented on the WISP and 44$\times$ lower than a software controlled backscatter radio implemented on the WISP. For software and UART controlled backscatter radios, we do not measure power at bit rates higher than 6Mbps because the maximum clock on rate on WISP platform is 24MHz, which limits the maximum achievable bit rate.

4.6.3 Whole-system power consumption

Having looked at power benchmarks for individual components of Ekho, we turn to a whole-system power measurement from sensing to transmission. We look at the

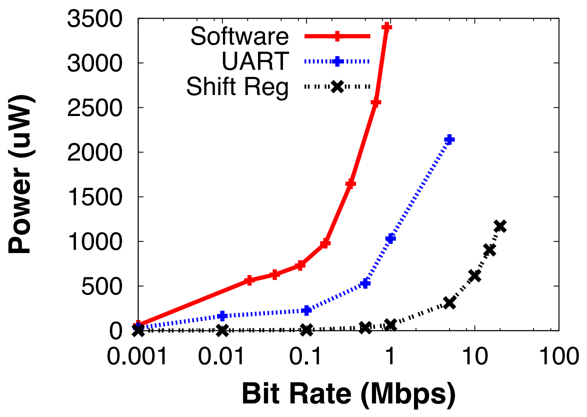

Figure 4.15. The power consumption of operating a backscatter radio.

overall power consumed by Ekho when operating the same two sensors as earlier — accelerometer and microphone.

We start with a measurement of Ekho with an accelerometer. The sensor has a built-in ADC and talks via SPI to the sensor platform. Figure 4.16 shows that at 1Hz, the power consumption of Ekho is higher than Moo and WISP5.0 platforms. This is because the static current consumption of the FPGA at the core of Ekho is 8.9μA, much higher than the 0.1μA static current draw of Moo and WISP5.0. However, when the frequency of operating the accelerometer increases, the power consumed by Moo and WISP5.0 platforms increases significantly while the Ekho system still consumes only tens of μW. At 400Hz, the Ekho system consumes 35μW of power, 7.6$\times$ lower than the 266μW of Moo and 3.3$\times$ lower than the 118μW of WISP5.0.

We now turn to power measurements when Ekho is connected to a microphone. An external ADC is used to sample the audio sensor, and send a digital signal to the core platform (Moo, WISP5.0, or Ekho). Figure 4.17 shows the power consumption of the three platforms. At 44kHz, the Ekho system only consumes 37μW of power, 76$\times$ lower than the Moo and 13.5$\times$ lower than the WISP5.0.

In conclusion, Ekho is particularly efficient when using higher rate sensors that sample at frequencies of hundreds of Hz. A crucial observation is that even when the

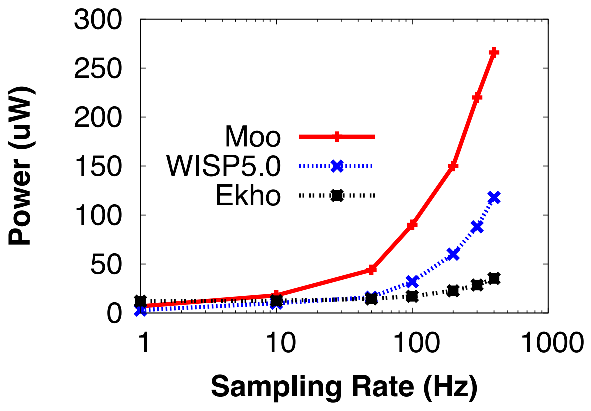

Figure 4.16. Whole-system power consumption for operating an accelerometer sensor.

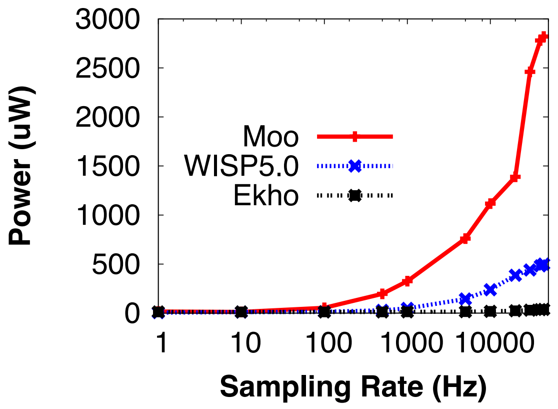

Figure 4.17. Whole-system power consumption for operating an audio sensor.

sensing rate increases by two orders of magnitude from the accelerometer at 400Hz to the microphone at 44kHz, the overall power consumption remains almost the same. This shows that Ekho scales up very well as sampling rate increases. In addition, Ekho is able to operate with sensors that use SPI or provide an analog signal while retaining high efficiency.

4.6.4 Evaluating EkhoNet's throughput

Having discussed the power benefits of Ekho, we now turn to look at the performance of Ekho's transfer rate.

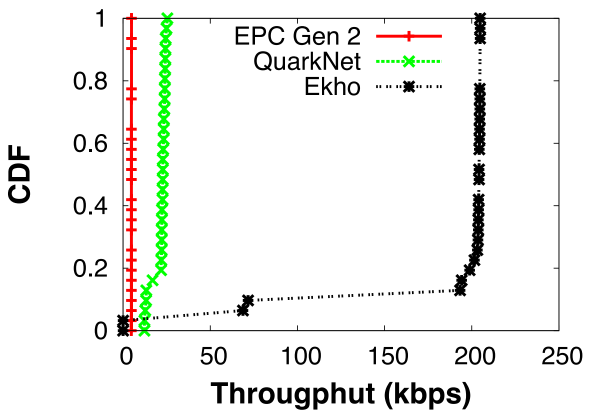

Figure 4.18. Comparing throughputs of EPC Gen 2, QuarkNet on Moo vs Ekho across 30 locations.

We start with the throughput achieved by a single node. Since the Moo and WISP platforms currently support only a 256Kbps baud rate, we fix Ekho's clock to operate at the same rate. We then compare Ekho's throughput against the Moo executing EPC Gen 2 [96], and QuarkNet [97]. Figure 4.18 shows the cumulative throughput across 30 locations. The 30 locations are chosen randomly between 1 feet to 9 feet from a backscatter reader.

There are two key observations. First, we see that the throughput achieved by Ekho is 45× higher than Gen 2 and 8× higher than QuarkNet on the Moo. EPC Gen 2 suffers greatly due to protocol overhead, and therefore achieves abysmal overall throughput. Although QuarkNet is a highly optimized system that is designed for micro powered sensors, its throughput is limited by the fact that the PHY layer (encoding, etc) is implemented in software on Moo, which reduces throughput. Second, we see that there are a few locations where our design decision to eschew encoding hurts us. At those locations, the received signal can still be decoded by EPC Gen 2 and QuarkNet because of the SNR benefit of Miller-4 encoding. However, it can be seen that this is a small fraction of the overall range of the reader. (Note that if encoding is essential, it is possible to add this module to Ekho at the cost of some additional power consumption and reduced throughput.)

We now turn to the throughput achieved by a network of nodes, and evaluate the benefits of our energy and utility function aware bit rate selection algorithm. We deploy 10 Ekho nodes with microphones at three locations (3 feet, 6 feet, and 9 feet from a backscatter reader). The maximum sampling rate of each audio sensor is 44kHz and each sample data is 16 bits. As a result, an audio sensor can generate up to 706k bits data per second. In contrast, the overall network transmission capacity of EkhoNet is 1Mbps in our current instantiation since each device is equipped with a 1Mbps clock. Thus, 10 audio sensors in front a backscatter reader can saturate the 1Mbps network easily, which means that adapting the bit rate as well as the sampling rate of each sensor is necessary.

When channel is saturated, the selection of bit rate is intuitive because maximum bit rate which meets the lowest SNR decoding threshold (10dB) should be used. The selection of sampling rate follows the energy-utility joint optimization we formulated in §4.4.

Figure 4.19 shows the MOS score obtained by 10 audio sensors at 3 locations. Our optimization framework attempts to allocate bandwidth such that sensors with higher SNR can get the bandwidth they need for achieving higher MOS scores. As a baseline, we compare against a scheme that allocates bandwidth equally across all sensors. The median and mean MOS scores achieved by EkhoNet is higher than the baseline scheme — 50% of the nodes have MOS scores higher than two, which is acceptable audio quality, whereas the uniform allocation scheme has MOS scores of about 1.7, which means poor audio quality. A breakdown across nodes shows that our algorithm assigns higher sampling rate to sensor 1 to 5 because they have higher SNR. While other application-specific utility functions are possible, these results demonstrate that

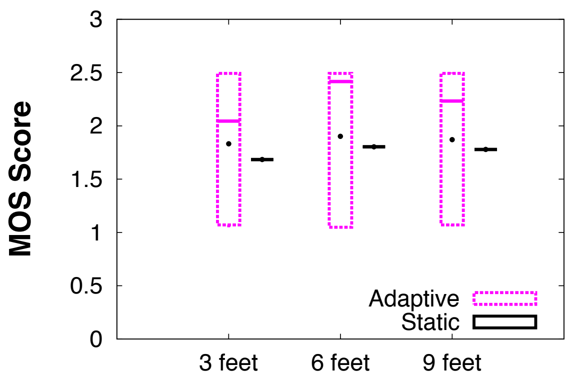

Figure 4.19. Boxplot of the MOS scores for 10 Ekho nodes with microphones at 3 locations (3 ft, 6 ft, 9 ft).

despite the simplicity of Ekho platforms, the EkhoNet MAC can be more complex and optimize network-wide throughput, energy and utility.

4.7 Related Work

4.7.1 Backscatter communication

There has been much recent emphasis on backscatter communication. Some efforts have explored bandwidth limitations of backscatter communication in terms of throughput including Flit [45], Buzz [86], and Blink [100]. While there are interesting ideas underlying each of these, the overall throughput achieved by EkhoNet is orders of magnitude higher than the above systems as a result of a clean-slate design. Other efforts have focused on using harvested power in an efficient manner including QuarkNet [97][99] and Dewdrop [29] — these approaches are complementary to EkhoNet and can be used in conjunction with the ideas in this chapter.

In addition to the above, there have been many interesting ideas on using backscatter for real-world applications. Ambient Backscatter [63] uses the backscatter of FM signals for short-range communication between tags to enable credit-card transactions. AllSee [58] explores the backscattered signal for gesture recognition. These ideas can potentially benefit from an Ekho-like platform that is designed to reduce power consumption while increasing bandwidth.

Much literature has explored the design of MAC layer protocols for RFIDs, and several of these approaches specifically address data collection from RFID-scale sensors [30, 45, 86, 97]. Viewed in isolation, our MAC layer protocol is simplistic since its merely a stripped down version of TDMA, hence it relates to most of the above protocols. However, our work should be viewed not just as a MAC layer, but a system-wide re-design to strip computational overhead from backscatter-based sensors, and thereby achieve higher efficiency.

4.7.2 Optimized sensing platforms

There have been many highly optimized sensor hardware designs proposed over the past decade. At a high level, these can be separated into two classes — optimized hardware platforms designed for specific applications, and optimized hardware platforms that are intended as a building block for research and applications. One example in the former class is the NeuralWISP [50], a wireless neural interface that operates on harvested RF energy. Some examples in the latter class are the Michigan M^3 [61], an impressive mm^3 sensor that operates at low power, and the Epic Mote [34], which is a modular mote-class platform for enabling low-power wireless sensor network applications.

EkhoNet differs from these efforts in that it is designed for raw data transfer from high-rate sensors at extremely low power levels. Thus, it is a general-purpose platform for sensors similar to the second class of devices, but focused on backscatter and high-rate sensors. As a result, the underlying design principles and optimizations are completely different from those that drive the other class of platforms.

4.8 Discussion

While Ekho provides substantial performance benefits over the state-of-art in backscatter-based sensor platforms, there are several questions that we have not completely addressed in our evaluation. We discuss these in this section.

4.8.1 FPGA v.s. MCU

One of the design choices in Ekho is the use of an FPGA rather than MCU — this choice greatly reduces the computational and data migration overheads between the sensor and radio, but in the process, it sacrifices ease of programmability. While FPGA programming has become easier in recent years due to improved IDEs and GUI interfaces [10], it requires familiarity with logic design at the circuits level. MCUs, on the other hand, are much more natural to program using commonly used high-level languages such as C, which is one of the reasons for its wide use on sensor platforms.

We believe that the greater difficulty in programming FPGAs is not as much of an issue for Ekho as for other platforms. Wireless sensors are designed to be intelligent, autonomous nodes that can adapt to dynamics in energy levels, channel conditions, routing changes, and others. In contrast, Ekho is designed to be a "dumb" peripheral for a powerful reader that simply forwards the raw sensor data over a backscatter link. Much of the decision-making logic that is traditionally implemented on the sensor side are performed at the reader. Thus, Ekho can be viewed as just another sensor, with an interface that allows the reader to set sampling rates and bit rates (as shown in §4.4).

4.8.2 Power benefits

The results presented in this chapter compare Ekho against existing backscatter-based sensing platforms such as the WISP, but one question is whether we would have significant power benefits if we compared against an FPGA implementation of the WISP. Our evaluation did not address this question since re-implementing the entire sensing, computation, and communication pipeline of the WISP on an FPGA is a substantial effort, but we provide a qualitative comparison.

Existing research work [72] on RFIDs suggests that an EPC Gen 2 tag implemented on FPGA usually consumes 5K to 10K logic gates. Clearly, an EPC Gen 2 tag does not perform any operation related to sensing. Therefore, sensor sampling, data migration, buffering, and other tasks would incur additional overhead. For example, Touhafi and Glesner et al [33, 49] investigate an FPGA (Spartan3-2000) based sensing platform which consumes 1200K gates, several orders of magnitude higher than an EPC Gen 2 tag. Our Ekho implementation consumes only 6K gates, which is comparable to an EPC Gen 2 tag and significantly less than what we would expect with an FPGA version of the WISP. Since the power consumption of an FPGA depends on the number of gates used, Ekho should still be significantly more efficient.

4.8.3 Encoding

Another design decision that needs more discussion is that Ekho eschews encoding in an effort to be minimalist. Unsurprisingly, this can be problematic in scenarios where the wireless channel is noisy. Figure 4.20 shows a simple experiment where we place a tag at 20 locations between 1–9 ft in front of a reader, and look at the SNR with EPC Gen 2's Miller-4 encoding, and without encoding. The decoding threshold for our backscatter reader is 10dBm, so any signal lower than this threshold cannot be decoded correctly. As expected, there is about a 10dB difference between encoded and uncoded signal. The SNR is higher than 10dB in 80% of the locations for uncoded data, and higher than 10dB in about 90% of the locations after encoding. This comes at a high cost, however, since the node consumes 8$\times$ more power for achieving the same bit rate.

Thus, our point is simply that encoding is yet another computation block on a backscatter-based sensor platform. While the power consumption of techniques like

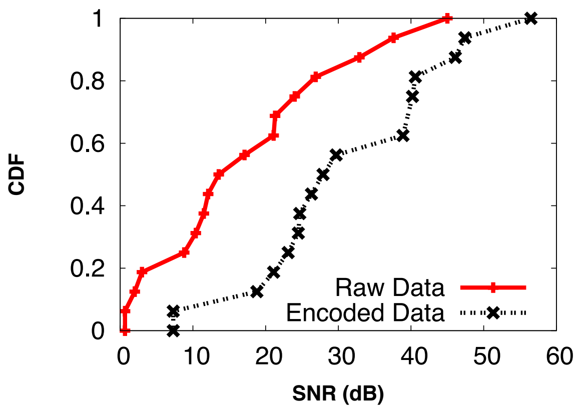

Figure 4.20. SNR of transmitting encoded and raw data across 20 locations

encoding are insignificant in most radios, the pros and cons deserve to be examined more carefully for ultra-low power platforms such as Ekho.

4.8.4 Applications

Finally, this chapter does not focus on applications of Ekho, but we view our work as an enabler for a variety of applications. While the idea of backscatter-based sensing is not new [91], many existing efforts are about networking simple, low rate sensors (e.g. temperature, pressure, etc). But the need for backscatter in such scenarios is debatable — active-radio based wireless sensors operate for years on coin cells at low sensing and communication rates. But rich sensors such as microphones and cameras operate primarily in a tethered manner since data rates are far too high for continuous communication. Our work seeks to bridge the gap, and enable camera networks or microphone networks to stream data continuously in an untethered manner. The benefits of streaming raw sensor data to internet-connected infrastructure is immense since one can use vast amount of computational resources to jointly process the data streams and enable smart applications. A simple example would be continuous speaker recognition and transcription of meeting notes by deploying a tethered reader and dozens of untethered Ekho nodes at different locations in a conference room.

4.9 Conclusion

In this chapter, we present a powerful backscatter wireless sensing architecture, Ekho, that can sample sensors at tens of kHz and transmit data wirelessly at several hundreds of kbps, while only consuming tens of μWatts of power. The key observation in Ekho is that backscatter wireless communication is energy-wise much cheaper than computation. Therefore, by eliminating the overheads of sensing subsystem, data handling subsystem, and communication subsystems, we enable the whole sensing-communication pipeline to operate at extremely low power. Over the Ekho platform, we design a MAC layer that allocates bit-rates across nodes while taking into account energy-efficiency, utility of data, and a variety of platform-level considerations. We believe that EkhoNet can enable new explorations in backscatter-based sensing systems, and enable new applications that use ultra-low power high-rate sensors.

CHAPTER 5

ENABLING PRACTICAL BACKSCATTER COMMUNICATION FOR ON-BODY SENSORS

Deploying backscatter on mobile and wearable devices is hard because of the lack of an incident carrier for backscatter. Existing mobile and wearable devices do generate a carrier. However, this carrier is not directly transmitted. Instead, it is used to modulate a baseband signal before transmission. To make matters worse, backscatter readers are not already widely deployed. As a result, we cannot just leverage existing infrastructure for backscatter. In this chapter, we address this challenge by leveraging multiple ambient wireless signals, such as WiFi and BLE, for carrying backscattered information. We explore key factors that enable backscatter using commercial WiFi and BLE radios.

5.1 Introduction

The ultra low-power nature of backscatter communication makes it a compelling technology for the design of wearable and on-body sensors that operate on tiny energy budgets. Today, most such sensors use Bluetooth Low Energy (BLE) for low-power communication, but BLE consumes tens of milliwatts when operating in active mode i.e. when transmitting data. In contrast, a backscatter tag consumes a few micro-watts in active mode, and enables the design of on-body sensors that continually stream data at an end-to-end power budget of tens of micro-watts [101]. The tiny energy budget combined with the simplicity of the hardware components needed to design backscatter-based sensors opens up a range of possibilities including micro-powered on-body sensors [95], miniature implantable sensors [93], thin and flexible wearables [69], and others.

But when we attempt to make backscatter practical for on-body sensors, we face a conundrum. Unlike built environments where backscatter-enabled access points or readers can conceivably be deployed, we have limited options in a mobile environment. We can perhaps modify radio chipsets in smartphones and wearables to include backscatter support, but this will not be immediately deployable and their widespread use will hinge on market forces. Ideally, we would leverage existing mobile and wearable devices that people already use as a source of continuous carrier and backscatter receiver. But these devices are not designed to support backscatter, and therefore do not embed crucial building blocks such as self-interference cancelation. This is particularly problematic when dealing with a link as fickle and sensitive as backscatter — reverse link path loss and backscatter antenna reflection losses create a dicey decoding scenario even with perfectly tuned hardware [78], and the constraints of commercial transceivers on mobile devices only exacerbates the situation.

Consider the case of WiFi Backscatter [57], a recent attempt at resolving this conundrum. In this technique, a receiving WiFi device looks at the RSSI values for each packet, and first smoothes these values to remove natural variations in the WiFi signal. It then uses signal strength variations in the averaged signal to extract a lower rate backscattered signal. But this approach is difficult to tune precisely in a mobile scenario where the WiFi signal is continuously changing due to movement and body blockage variations. This makes it hard to cleanly average away the WiFi signal variations, and leads to low signal to noise ratio (SNR), and consequently less performance in terms of range and throughput. Thus, the challenge that we face is how to use commercial transceivers while also effectively dealing with carrier interference.

Our key insight in this paper is that backscatter can be made practical for wearables using a simple but effective trick — if a backscatter tag can *shift an incident WiFi or Bluetooth carrier to a clean WiFi or Bluetooth band*, then that the receiver can see a clean, carrier-interference free backscattered signal in the shifted band. The tag can perform on-off keying (OOK) at the shifted frequency to transfer information in the shifted frequency band. This method is practical on devices that many users already use in mobile settings. For example, a mobile phone can act as a Bluetooth carrier, an on-body sensor can be a tag that shifts the signal by 20MHz while modulating it, and a Bluetooth receiver on a wristband (like a Microsoft Band) can receive this shifted signal in the adjacent band.

There are two reasons why frequency shifting allows us to improve backscatter performance. The first is that the receiver sees a clean signal and does not need to deal with any other interference in the same channel. The lower noise level means that we can achieve higher performance than methods that try to separate the primary carrier from backscatter signal in a single channel without assistance of self-interference cancelation techniques. The second reason is that the receiver can use the structure of the primary carrier (i.e. WiFi or Bluetooth packet preamble) to be able to detect the shifted signal at very low SNRs. For example, typical WiFi and Bluetooth chipsets have receive sensitivity of -90dBm to -95dBm, much lower than the threshold of detecting the RSSI of a signal with unknown structure. This allows us to operate at longer ranges than RSSI-based methods, albeit at lower bitrates since we can modulate information only at the rate at which packets are transmitted. Thus, our method leverages both the benefits of frequency shifting as well as the high receive sensitivity of modern radio chipsets.

Frequency shifting also opens up some interesting new possibilities. We often have multiple portable devices in our vicinity including phones, smartwatches, tablets and laptops. In these scenarios, we can leverage multiple transmitters and receivers to improve the throughput and reliability of the link. This is possible since the tag simply reflects any incident signal that resonates with its antenna unlike active radios that need to filter signals into specific bands before transmission.

While frequency shifting has many benefits, it opens up a fundamental challenge of tag-side power consumption. Shifting to an adjacent WiFi band necessitates a 20MHz oscillator at the tag, whereas existing RFIDs and computational RFID-scale devices only need slow oscillators that operate at several Kilohertz. High speed oscillators typically consume milliwatts of power, which is incompatible with our goal of operating at micro-watts of power. We tackle this challenge by sacrificing precision for power — we design a low-power ring oscillator-based clock generator for the FS-Backscatter tag which operates at tens of micro-watts but also has temperature-induced frequency variations. However, we show that FS-Backscatter is robust to such temperature-induced frequency variations that we might expect for on-body sensors.

In summary, our system, FS-Backscatter, has several novel contributions.

- First, we design, implement and evaluate a practical backscatter system for on-body devices that enables ultra-low power communication while also being compatible with commercial WiFi and Bluetooth transceivers. We show that FS-Backscatter can operate up to 4.8m distance and provide throughputs ranging from tens of bits/second to tens of kilobits/second depending on the specific transmitter – receiver configuration.

- Second, we show that FS-Backscatter can take advantage of the plethora of radios that are available on portable devices and combine transmitters or receivers to boost performance. We show that throughputs increases by 25% to 100%, and we can achieve up to 48.7kbps throughput in two transmitter and two receiver scenarios.

- Third, we show that an FS-Backscatter tag operates at a power budget of 45μW through the use of a ring-oscillator based clock design, and is robust to frequency variations induced by environmental changes.

5.2 Case for FS-Backscatter

Several recent efforts have proposed ways to make backscatter communication practical by leveraging either existing wireless infrastructure or existing wireless-enabled devices. The mobile scenario, which is the target of our work, adds an additional wrinkle in that the method should work on-the-go and not just in built settings. We discuss prior work from this perspective and understand how they fare in our problem domain.

5.2.1 Infrastructure-assisted Backscatter

Several existing techniques rely on tethered infrastructure either for carrier generation or for decoding the backscattered signal or both. Of course, all RFID readers operate in this manner in that they generate a narrowband carrier, and perform self-interference cancelation to separate the backscattered signal from the carrier. But RFID reader infrastructure is not ubiquitous, so a few recent methods have designed innovative ways to embed reader functionality into existing devices.

BackFi [26] modifies a WiFi Access Point (AP) by augmenting it with the ability to cancel the OFDM carrier signal. The benefit of this technique is that it keeps the tag very simple — a simple ASK-transmitting tag can simply backscatter the AP-generated WiFi signal without worrying about the complexity of the underlying OFDM signal structure.

BLE-Backscatter [35] flips this method and provides infrastructural support such that a backscatter tag can communicate with a commodity BLE radio receiver. Here, the infrastructure component is a simple continuous wave (CW) transmitter, and a backscatter tag modulates the CW tone to emulate a BLE transmitter, thereby allowing commodity BLE receivers to receive the modulated signal. The BLE-Backscatter tag saves power because it no longer needs to generate the carrier, but it emulates a BLE stack and is therefore more complex and power-hungry than an ASK-modulating backscatter tag.

Neither of these methods are viable in a mobile context since they use infrastructure-assistance, and require additional hardware for self-interference cancelation or CW generation that is not embedded in existing radios.

5.2.2 Infrastructure-less Backscatter

A second class of methods leverages an ambient carrier (e.g. TV or WiFi carrier), and backscatter this signal so that it can be received at a commodity receiver. Of these, we do not consider the TV carrier signal used by Ambient Backscatter [63] since its availability is very spotty and the signal strength decays significantly a few miles away from a TV tower station. But WiFi Backscatter [57] appears more practical since it uses a commodity WiFi transmitter and receiver, which is plausible in a wearable scenario where we might use a phone as the transmitter and smartwatch as receiver. The tag side retains the simplicity of ASK-based backscatter.

From a signal processing perspective, the key challenge is separating the ambient carrier from the backscattered information without the benefit of self-interference cancelation. Instead, these methods rely on the fact that changes in the WiFi or TV carrier occur at a much higher rate than changes in the backscatter modulation. Therefore if the received signal is averaged over a long enough window, the backscatter modulated information can be recovered. This averaging can be done using an envelope detector in the analog domain (used in Ambient Backscatter [63]), or low pass filter in the digital domain (used in WiFi Backscatter [57]), after which one can

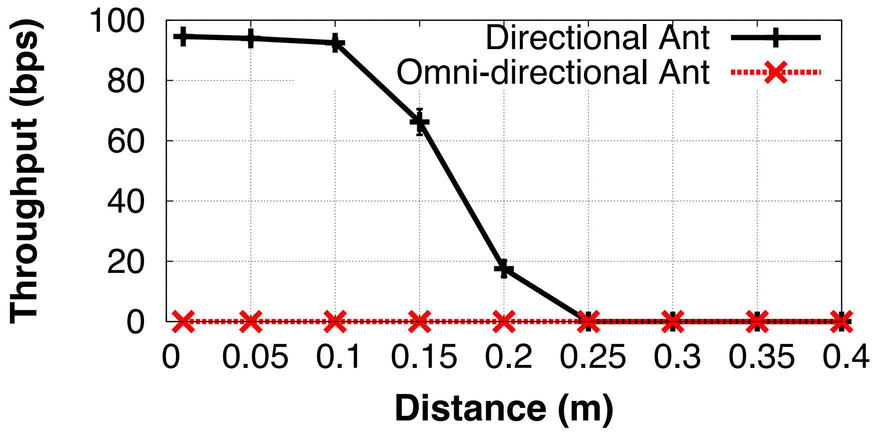

Figure 5.1. Throughput of WiFi Backscatter across distance with 3dBi Omni-directional [7] and 9dBi directional [17] antennas.

measure how a backscattered signal changes the propagation characteristics of the incident signal.

While WiFi Backscatter appears practical for the mobile scenario, it is quite difficult to get the scheme to work in practice. The design presents two issues: a) the primary exciter is much louder than the backscatter signal and, despite averaging, reduces signal to noise ratio to such an extent that range is extremely low, and b) the temporal variations due to typical human movements and corresponding channel variations in mobile environments requires dynamic tracking of signal and noise thresholds, which in turn makes decoding sensitive to the chosen thresholds.

To illustrate the downsides to this design, let us empirically measure WiFi Backscatter throughput across distance. We use a bi-static backscatter deployment similar to that in [57], and place a CC3200 WiFi transmitter 1m away from a backscatter tag while moving the CC3200 WiFi Backscatter decoder away. The results are shown in Figure 5.1.

Our first observation is that when a tag is equipped with a standard 3dBi omni-directional antenna [7], WiFi Backscatter simply does not work, even at close ranges. We then try to equip the tag with a 9dBi directional antenna [17] to see how performance improves. Indeed, WiFi Backscatter does work, but achieves only up to 0.2m operational distance and 19bps data rate even with a 9dBi directional antenna. Let us dig in a bit further to understand why WiFi Backscatter has low performance.

5.2.2.1 Low signal-to-noise ratio

The first key issue is the strong interference from the ambient carrier, which limits operational range as well as data rate. To measure interference, we set up a deployment similar to the one in [57], and place a 0dBm WiFi transmitter 3m away from a backscatter device. One difference is that our tag is equipped with an omnidirectional antenna, unlike [57] which uses a custom multi-antenna array. The main reason for this change is that the 18.5cm×15.7cm[1] custom multi-antenna array is too large for on-body sensor tags. We move the WiFi receiver away from the backscatter tag and measure the TX signal strength as well as the backscattered signal strength.

Figure 5.2 shows empirically measured SNR and SINR of WiFi Backscatter across distance. Even when the receiver is 0.1m from the backscatter device, the SINR measured is -47dB i.e. the transmitted WiFi signal strength is 47dB higher than the backscattered signal strength. When the receiver is moved further, the SINR decreases even more. The SINR at 2m decreases to -71dB, which makes backscatter decoding extremely challenging. As a result, the system can achieve respectable data rates only at extremely short ranges of a few centimeters, and decoding range is typically a meter or less while the data rate is reduced to a few bits/second.

5.2.2.2 Mobility-induced dynamics

The second issue is that mobility changes the propagation characteristics of an incident signal, which makes decoding highly sensitive to the chosen threshold. Fig-

[1]We can measure the antenna size using the picture shown in [57] because the size of each patch element is 4.06cm×3.09cm.

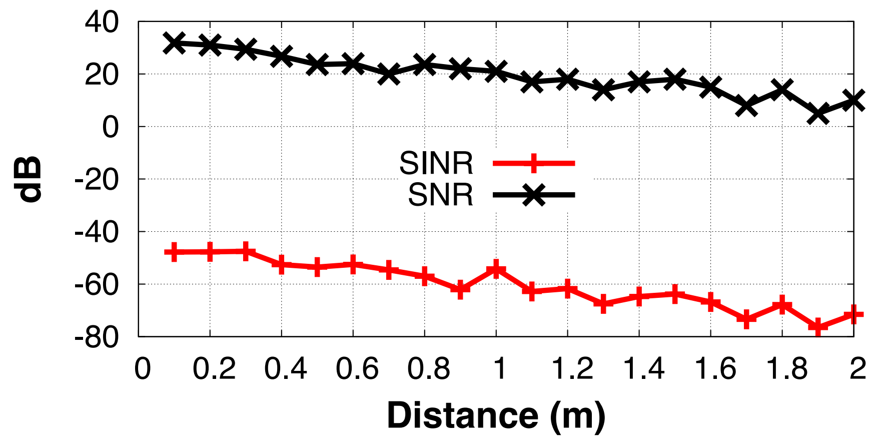

Figure 5.2. SNR and SINR of backscatter across distance.

ure 5.3 shows the CDF of the received signal strength of a WiFi transmitter when it is placed 1m away from a receiver. When the transmitter and receiver are static, the environment does not change and we can observe a stable WiFi signal with a median strength of -35dBm. However, when a person carries both the transmitter and receiver and moves around, the received signal strength varies significantly from -80dBm to -20dBm. Such dramatic signal variations will introduce significant decoding errors if the pre-calibrated threshold is not adapted accordingly. But adaptive re-calibration of the threshold is also very hard due to the large dynamic range of the variability, and will require complicated channel estimation and adaptation that is well outside the regime of what can be done on an ultra-low power backscatter tag.

5.2.3 FS-Backscatter: Key Ideas and Challenges

The essential idea underlying FS-Backscatter is quite simple — if a tag can shift-and-modulate a carrier signal in one frequency band into an adjacent non-overlapping frequency band where a receiver is listening, then the receiver has a clean channel within which to recover the modulated backscatter signal. This model is quite different from existing methods for backscattering which either use ASK or FSK modula-

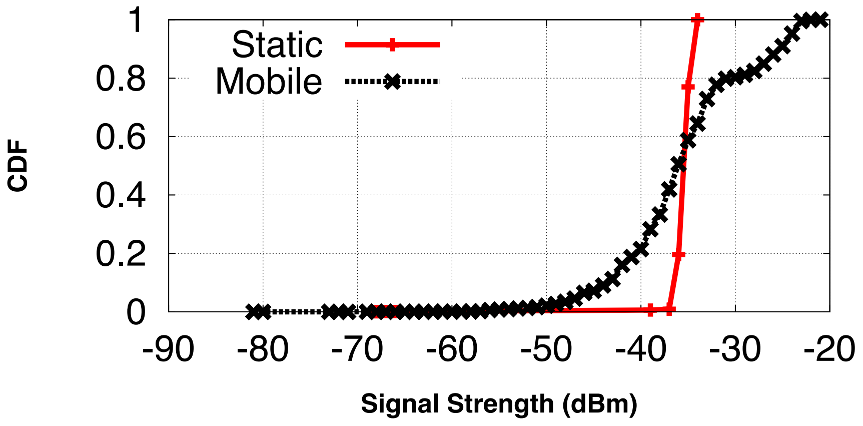

Figure 5.3. Received WiFi signal strength in static and mobile deployment.

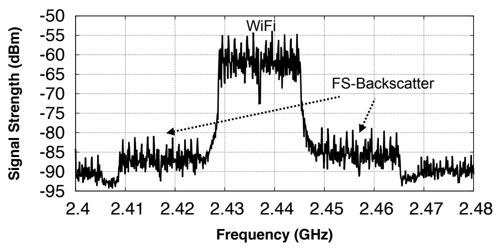

(a) FS-Backscatter reflects a WiFi signal

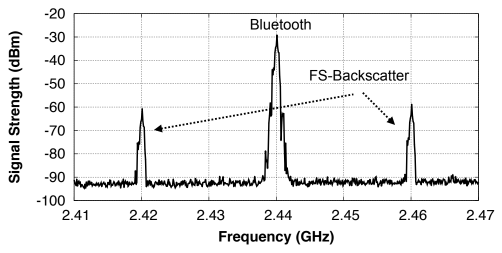

(b) FS-Backscatter reflects a Bluetooth signal

Figure 5.4. FS-Backscatter reflects a WiFi signal and a Bluetooth signal to adjacent non-overlapping channels.

tion; instead, our method involves a fixed frequency shift to a clean band followed by amplitude modulation.

Why would we expect this method to work well? The first reason is simply that the backscattered signal is shifted into a clean band where we are no longer affected by the interference from the carrier. Figure 5.4(a) shows the effect of shifting a WiFi signal, and Figure 5.4(b) shows the same result for a BLE signal. It is clear that the shifted signal is quite distinct from the primary carrier.

A second reason is that modern WiFi and Bluetooth receivers are designed to be extremely sensitive to structured weak signals, such as the preamble in a packet. For example, the CC2560/CC2564 Bluetooth receivers are able to detect packets at

-95dBm which allows them to work at a few tens of meters while only consuming tens of milliwatts. We can leverage this sensitivity to combat signal losses due to reflection (typically 30dB) and due to path loss on the reverse link. The distance we need to operate under in typical mobile scenarios is only a couple of meters, which is much shorter than the receive range of either Bluetooth or WiFi and gives us room to have additional signal losses due to body attenuation.

While frequency shifting opens up an array of possibilities, it introduces some practical questions and challenges. The first question is one of practicality - is this technique viable in practice? If it is viable, how well does it perform? When does it work and when does it fail? Do commodity radios expose APIs that allow us to tap into this method? The second is one of power — since non-overlapping WiFi bands are separated by 20MHz, we need a 20MHz oscillator at the tag. This is substantially higher than what is needed for simple ASK modulation at a few tens or hundreds of kilobits/second, and higher frequency clocks incur more power. But how much power efficiency do we lose at the tag? Are there ways to mitigate the loss of efficiency and keep it to tens of micro-watts? In the rest of this section, we discuss answers to these questions.

5.3 Frequency-Shifted Backscatter

In this section, we look at the practicality of FS-Backscatter on existing commodity radios and the implications on the design of the tag. We start with single transmitter to receiver scenarios, then at multiple transmitters to receivers scenarios, and finally discuss the design of the tag.

5.3.1 FS-Backscatter on Commodity Radios

The first question we ask is: If we take a commodity WiFi or Bluetooth Low Energy (BLE) chipset operating in broadcast mode, and shift the carrier to the adjacent frequency band while simultaneously modulating the carrier in this band, can a receiver listening on the adjacent band decode the backscattered signal?

5.3.1.1 Packet-level FS-Backscatter

Our first set of experiments look at the packet-level RSSI information that most WiFi and BLE chipsets provide, and see whether this can be used to decode the backscattered signal.

- **WiFi-to-WiFi Backscatter:** In this experiment, a CC3200 WiFi transmitter transmits a stream of packets in channel 1, and a WiFi receiver (CC3200) is configured to listen to packets in the next non-overlapping channel 5. The transmitter transmits at 1200 packets/second, and a FS-Backscatter tag is configured to shift by 20MHz and then perform on-off keying of its RF transistor at half the frequency of the transmitter packet rate i.e. 600 bits/second. The idea is that the WiFi receiver successfully receives a packet when the tag shifts by 20MHz, and does not receive a packet when the tag does not shift. This binary sequence of bits is the information being transmitted by the backscatter tag.

  Figure 5.5(a) shows the results when the WiFi transmitter is 1m away from the tag and we move the receiver away from the tag. The frequency shifted signal can clearly be decoded by the receiver. FS-Backscatter is able to operate up to 4.8m when it leverages packet-level RSSI information for decoding and has average throughput of 627.7bps across all distances.

- **Bluetooth-to-Bluetooth Backscatter:** The same underlying method for frequency shifting can also be used with a TI CC2650 BLE transmitter and a BLE receiver listening on the channel that is 20MHz away. The transmitter broad-

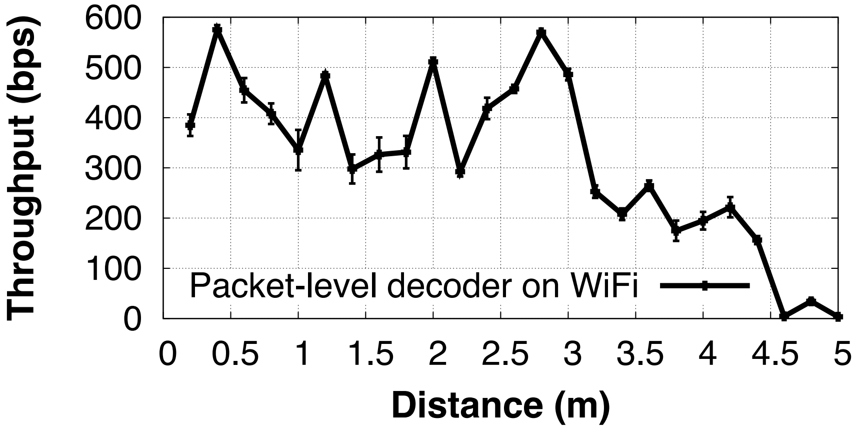

(a) Packet-level decoding on reflected WiFi.

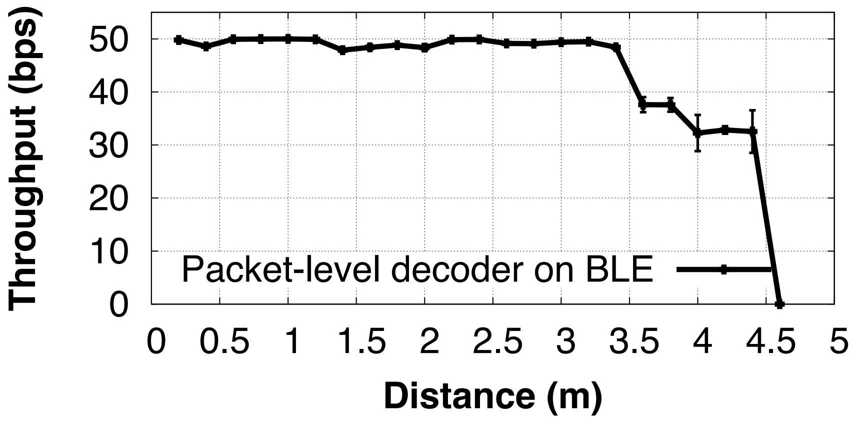

(b) Packet-level decoding on reflected BLE.

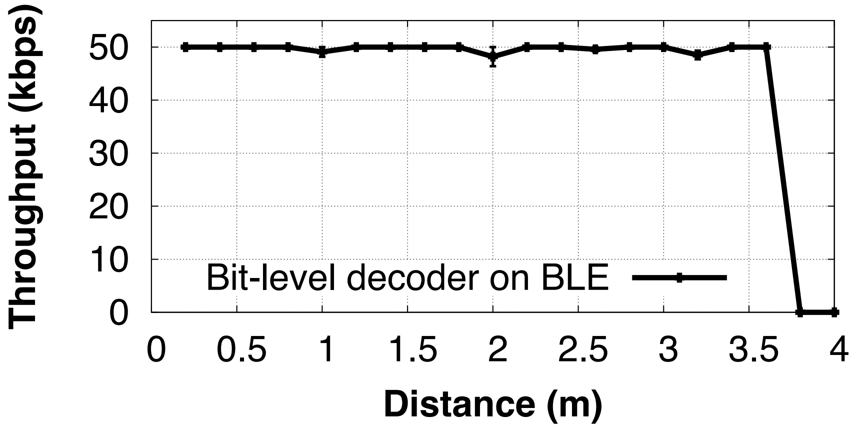

(c) Bit-level decoding on reflected BLE.

Figure 5.5. FS-Backscatter throughput across distance when leveraging WiFi and Bluetooth signals.

casts at 100 packets/second. Figure 5.5(b) shows that FS-Backscatter is able to operate up to 4.4m, with an average data rate of 45.8bps.

5.3.1.2 Bit-level FS-Backscatter

The above approach shows feasibility, but throughput is quite low since we are limited to one piece of information (RSSI) per packet. This means that any backscatter modulation scheme is limited by the packet rate on commodity radios — WiFi can broadcast about 3K packets/second, while BLE only broadcasts ∼100 packets/second. These rates are comparable to what was achieved in WiFi Backscatter, but given that we have a clean band to work with, we should be able to go a lot faster. But to achieve this, we need information at a layer lower than packet-level RSSI i.e. we need sub-packet RSSI information.

To explore this option, we use a commercial TI BLE radio that exposes a slightly lower level interface [16]. This radio provides an option for bypassing the BLE stack and directly obtaining RSSI values of the channel at a finer granularity. This physical layer interface can be used for detecting the presence (or absence) of a backscattered signal in the band at rates that are considerably faster than packet-level backscatter.

In this experiment, we use a Bluetooth transmitter, and configure an FS-Backscatter tag to modulate at a rate of 50kbps. We sample RSSI information at 100KHz from the CC2541 BLE receiver to decode the signal. Thus, each RSSI reading is an average of the channel readings over a duration of 10μs, and provides a measure of whether or not the backscattered signal is present in the adjacent channel.

Figure 5.5(c) shows the results. We can see that FS-Backscatter is able to achieve ∼50kbps data rate at close range and can operate up to 3.6m. The range is shorter than packet-level backscatter since we are not able to exploit structure in the backscattered signal that is used for packet-level decoding. But we are able to take advantage of the fact that we are working in a clean channel with limited noise, and thereby operate much longer than techniques that use ASK backscatter without frequency shifting.

5.3.1.3 What if no channels are available?

In the previous discussion, we assumed that the channel adjacent to the carrier is unoccupied, but one question is what if none of the channels are free. Our backscattering method works only when two adjacent non-overlapping channels are available i.e. the transmitter channel, and either the channel at the next lower non-overlapping frequency band or the higher non-overlapping frequency band. Note that both are viable options since frequency shifting shifts the carrier into both adjacent channels. But it is not unusual for many wireless channels to be occupied, so what happens if that is the case.

We note that even if there is a significant amount of WiFi traffic, some channels are highly unlikely to be used for active transmission. 2.4GHz WiFi has 14 allocated channels, whereas only 11 are used in practice since channels 12 and 13 have strict requirements regarding emission limits to avoid spilling over to adjacent restricted frequency bands [32]. However, since the backscattered signal is very weak, it is well below these emission limits, and hence we can shift the carrier from Channel 9 and listen in Channel 13.

We verify the emissions from FS-Backscatter in Channel 12 and 13 when a WiFi transmitter is operating in Channel 9. Figure 5.6 shows that the backscattered signal strength at Channel 13 is only -85dBm[2], 30dB lower than the WiFi carrier signal and close to the noise level. Therefore, FS-Backscatter will not cause interference to radios operating close to Channel 13 because its signal strength is too weak.

[2]Measured at the FS-Backscatter tag antenna.

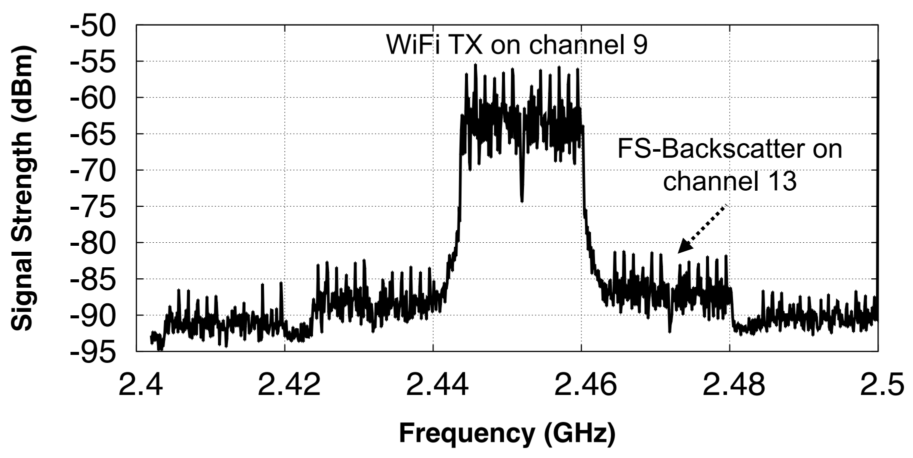

Figure 5.6. FS-Backscatter spectrum when leveraging 2.4GHz WiFi channel 13 for carrying backscattered information.

5.3.1.4 Can we improve robustness by using multiple transmitters or receivers?

So far, we have discussed the case where there is a single incident carrier and a single receiver. But in many mobile scenarios, we have the possibility of using more than two radios. For example, we often have multiple bluetooth-enabled accessories including tablets and headsets, so we may be able to repurpose these as an additional backscatter carrier or receiver. These additional radios can potentially be used as multiple carrier emitters and receivers to improve robustness since backscattered signals are generally weak and more sensitive to noise.

Can FS-Backscatter leverage more than two radios? One of the benefits of FS-Backscatter is that it is not limited to backscattering a single carrier. The backscatter tag's analog RF front end includes only an RF transistor and antenna, and unlike other radios, has no filters to limit the band where the radio can operate. As a result, a backscatter tag is able to reflect multiple incident signals at the same time as long as these signals can resonate with the backscatter antenna. Since both WiFi, Bluetooth, Zigbee and many other ISM-band radios share the same 2.4-2.483GHz spectrum, a backscatter device is able to reflect some combination of these at the same time. This feature provides several potential benefits where we can leverage multiple ambient carriers and multiple receivers to enhance backscatter performance.

We can leverage multiple transmitters and receivers quite easily in FS-Backscatter. Multiple transmitters can simply turn off carrier sensing and broadcast in the same band to increase the reflected signal strength. Note that this method would not work if we use ASK backscatter in the same channel as the carrier, since the additional transmitter would also add interference. But in FS-Backscatter, the backscatter signal strength is boosted in the shifted channel.

If we use multiple receivers, we can simply combine the signals to improve decoding performance. In an ideal scenario, one could combine the analog signals via maximal ratio combining, but since we operate over a commercial transceiver, we are restricted to the RSSI information coming from the radio. Thus, in our case, the two receivers can measure the signal strength (RSSI) of a backscattered bit on each receiver, and exchange this information. Then, we can simply add the signal strength received by each receiver for determining the actual bit transmitted by a backscatter tag.

5.3.2 Low-power FS-Backscatter Tag

A major question that remains is the design of the FS-Backscatter tag. The main consideration is that the tag needs to be able to shift by 20MHz such that it can shift both WiFi and Bluetooth carriers into a non-overlapping frequency band. This is a key difference between an FS-Backscatter tag and previous work on RFIDs (and Computational RFIDs) since previous work focuses either on ASK or FSK modulation around the center frequency of the carrier, whereas we require the the tag to shift the carrier by 20MHz prior to modulation. Thus, the question we need to answer is whether an FS-Backscatter tag can operate at micro-watts of power while shifting the carrier by such a substantial amount.

5.3.2.1 What is the power bottleneck?

Intuitively, more power will be consumed when we have to shift the carrier by larger frequencies. We look at three subsystems on a backscatter tag — RF transistor, transmission logic and clock generator, to determine which of these consume the most power as the shifted frequency increases.

- **RF Transistor:** The RF transistor is a MOSFET transistor with a capacitance around 2.1pF (ADG902). Its power consumption can be calculated using the equation $\frac{1}{2}CV^2F$ where C is the capacitance of the transistor, V is the gate voltage, and F is the frequency of operating the transistor. Even when toggled at a high rate of 20MHz, the RF transistor only consumes 21μW. Thus, the power consumption of the RF transistor itself is low and has a linear relationship with F.

- **Transmission logic:** The second subsystem, transmission logic, is a hardware module that toggles the backscatter RF transistor based on data transmitted. We use a digital circuit to implement the transmission logic, and the power consumption of this module increases linearly with the rate of transmission [101]. While the precise power consumption depends on the logic, we expect that this module consumes around 15μW of power given that we can open and close the transistor via an NAND gate [12], which has a capacitance of around 1.5pF.

- **Clock generator:** The third subsystem is the clock generator which provides the clock for timing the whole system. Oscillators are typical sources for generating clocks. Table 5.1 shows the power consumed by the lowest power commercially available oscillators that we could find at different frequencies and accuracies. We find that once we begin shifting by several MHz, the power consumption also rises to a few milliwatts.

Table 5.1. Power consumed by commercial oscillators operating at different frequencies and different accuracies.

Oscillators	Frequency	Accuracpy	Power
ASH7K	32 kHz	±10ppm	1.48μW
LTC6990	1 MHz	±50ppm	326μW
LTC6900	10 MHz	±40ppm	2.04mW

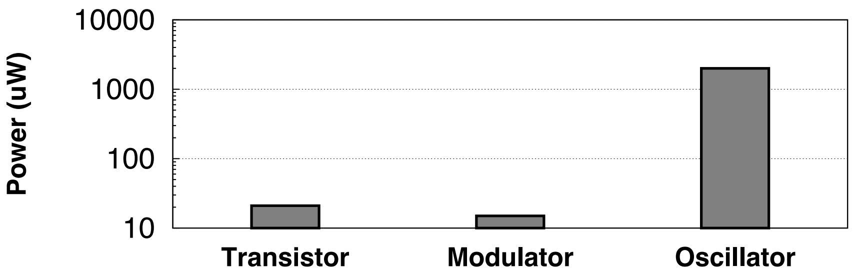

Figure 5.7. Backscatter tag power consumption breakdown.

Figure 5.7 shows a power consumption breakdown of the three subsystems. Its clear from the above breakdown that the clock generator is the highest power consumer in the entire system and consumes two orders of magnitude of more power compared to the RF transistor and the transmission logic. So we turn our attention to this component and ask whether there is a way to make our oscillator circuit operate at μWs of power.

5.3.2.2 Can we shift by 20MHz while consuming μWs?

A key question in designing a low-power oscillator is the precision that we are willing to tolerate. Active radios choose their oscillators based on several considerations including reducing leakage outside the channel to permitted levels, lowering phase noise, and minimizing power consumption. But if FS-Backscatter can tolerate less precision in the oscillator output, we can design significantly lower power oscillators.

In particular, one attractive design for an ultra-low power oscillator is a ring oscillator, which is used in some integrated digital and communication systems [55] [79] [60]. Our design of a 20MHz ring oscillator looks as shown in Figure 5.8. A

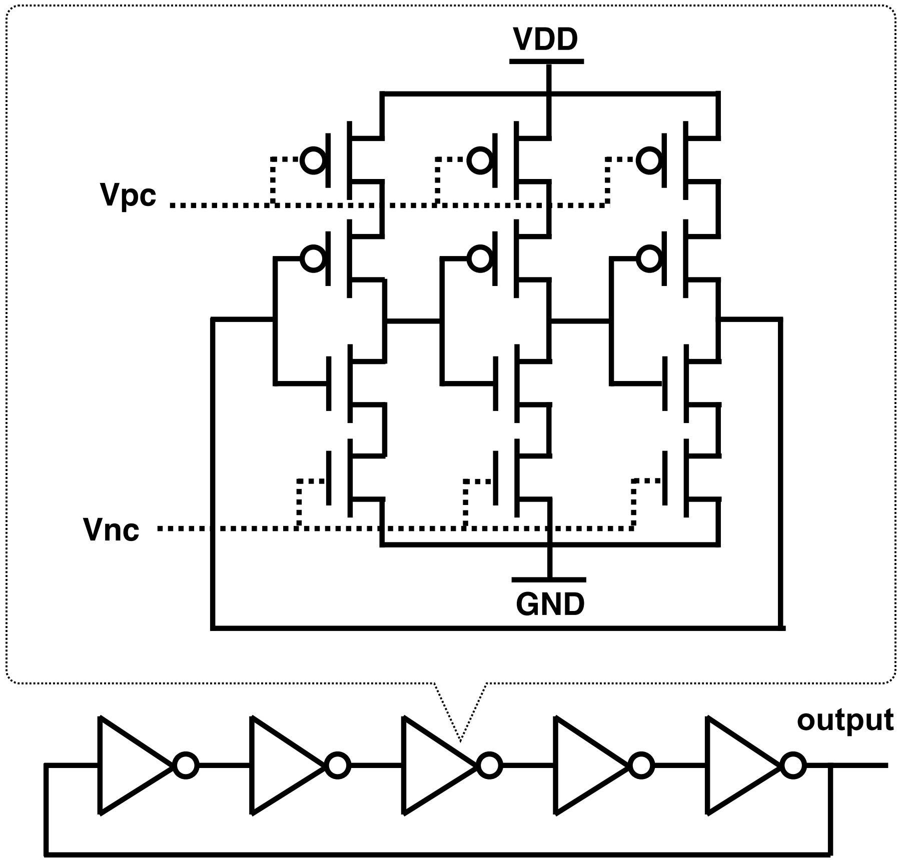

Figure 5.8. Ring oscillator circuit diagram.

ring oscillator leverages an odd number of inverters and connects them in a serial sequence. Since the last stage inverter outputs a signal that has a reversed logic as the input of the first stage inverter, the whole circuit can oscillate. The frequency of the ring oscillator is determined by the propagation delay of each inverter. We use two approaches to control the propagation delay of each stage. First, we use a voltage controlled inverter where we adjust the gate voltage (V_{nc} and V_{pc}) of two PMOS and NMOS transistors in an inverter to control its propagation delay. Second, we use an RC circuit between the inverters to add additional delay. We simulate a 20MHz ring oscillator in HSPICE and see that we are able to achieve 20MHz by tuning the control voltage V_{nc} and V_{pc} and the RC parameters.

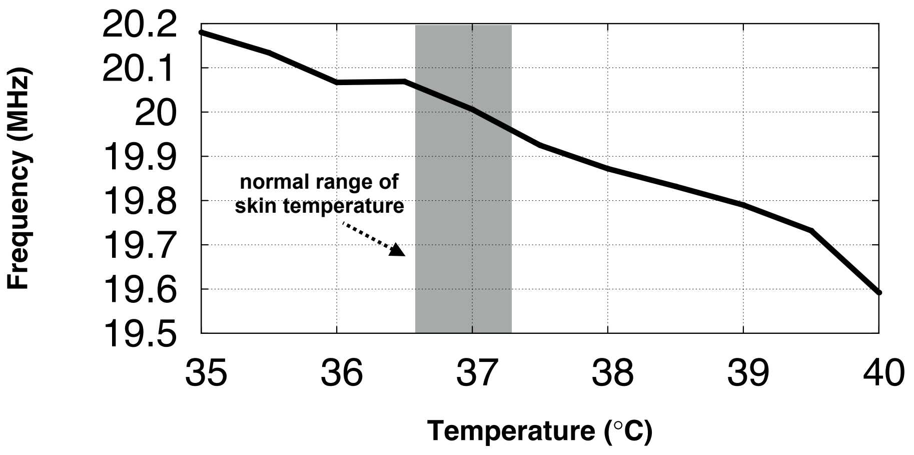

Figure 5.9. Ring oscillator frequency when temperature changes. The normal range of skin temperatures is fairly tight (typically between 36.6^{o}C and 37.2^{o}C).

While attractive from a power perspective, a ring oscillator is typically not used in active radios because its frequency can vary a fair bit with temperature variations. In general, the frequency can vary by a few MHz if there is a significant temperature swing of more than a few tens of degrees (C). Such variation is typically going to be a showstopper for many radio designs.

However, a ring oscillator may still be suitable for FS-Backscatter since it is specifically intended for on-body sensors. The normal range of skin temperatures is fairly tight (typically between 36.6°C–37.2°C), and even sweating and physical exercise only induce small temperature changes of less than 1°C due to thermal regulation [28]. Figure 5.9 shows an HSPICE simulation of our ring oscillator design at temperatures around the human range. We use our HSPICE implementation of the 20MHz ring oscillator to measure the effect of such temperature shifts, and find that the frequency changes by roughly 69$\sim$210kHz. We then modify the shifted frequency of FS-Backscatter by20MHz $\pm$ 250kHz to see its effect on the packet-level and bit-level decoders described earlier.

Figure 5.10 shows the effect on a packet-level decoder when leveraging a WiFi signal. When an FS-Backscatter tag experiences a frequency offset that is smaller

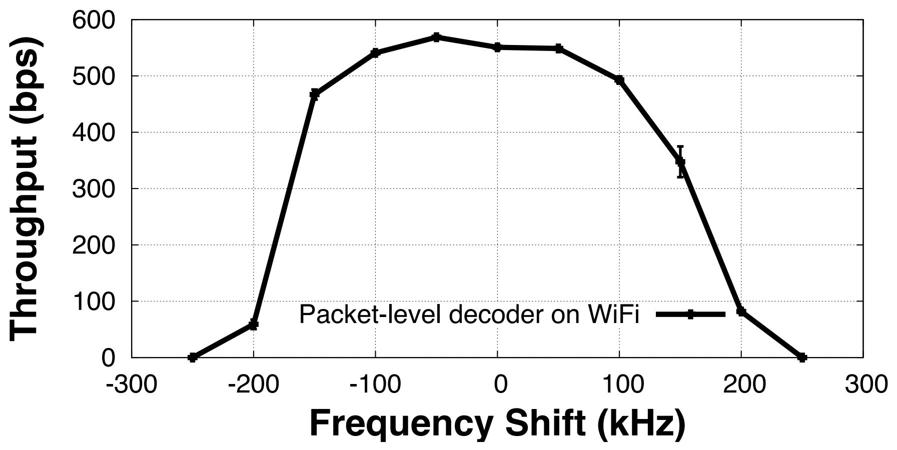

Figure 5.10. Packet-level decoder throughput on a WiFi signal when a tag experiences ±250kHz frequency offset.

than 100kHz, we can achieve similar throughput as the one without any frequency offset. However, when the frequency offset is larger than 150kHz, FS-Backscatter throughput starts degrading. When the frequency offset is larger than 250kHz, FS-Backscatter throughput degrades to zero. While not shown in the figure, we also see that BLE packet-level decoder is more robust to frequency shifts, and can tolerate roughly 450kHz frequency shift before the throughput degrades.

Note that even if the packet-level decoder does not work when the sensor is not attached to the body or when the temperature swing is large, we can still use the bit-level decoder that uses RSSI information. Bluetooth channels are 2MHz apart, so a temperature-compensated decoder can listen on the appropriate channel where the backscattered signal is strongest.

5.3.2.3 Reducing operating voltage

Another optimization that we make is to reduce the voltage range in which the FS-Backscatter tag operates and thereby reduce power. Let us first look at the voltage needed for toggling an RF transistor. The minimum voltage needed for powering an ADG902 RF transistor is $V_{DD} = 1.65V$. However, it does not mean that we need

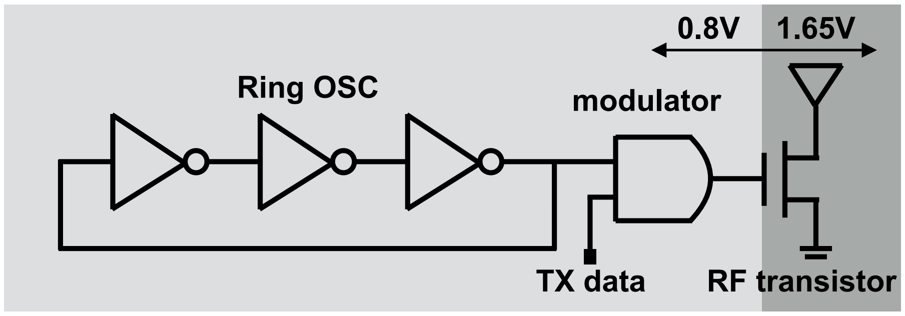

Figure 5.11. FS-Backscatter tag diagram.

to feed a 1.65V signal into the gate of the transistor for opening and closing the gate. In fact, an ADG902 can be opened and closed by switching between $0.65V_{DD}$ and 0.35V. As a result, instead of switching between 1.65V and 0V, we can switch between 1.0725V and 0.35V to toggle the transistor. Such smaller operational voltage range will reduce the power consumed for toggling the RF transistor.

Similarly, we do not have to run the ring oscillator and the data modulator at high voltage either. Instead of running the whole system at 1.65V, we can operate these two subsystems at 0.8V. Then, we use a 0.3V voltage shifter to move the 0.8V/0V signal output by the modulator to 1.1V/0.3V, high enough for toggling the RF transistor. By operating the ring oscillator and modulator at 0.8V, we can significantly reduce the overall system power consumption. Our final tag design is shown in Figure 5.11.

5.4 Implementation

In this section, we describe our implementation of FS-Backscatter.

- **FS-Backscatter Tag:** Our prototype of an FS-Backscatter tag is designed to be flexible in connecting different types of antennas to understand the effect of antenna gain. The backscatter analog front end that allows us to explore these design options is shown in Figure 5.12. We use an ADG902 transistor to tune and detune the antenna. The antenna is connected to the transistor via an SMA

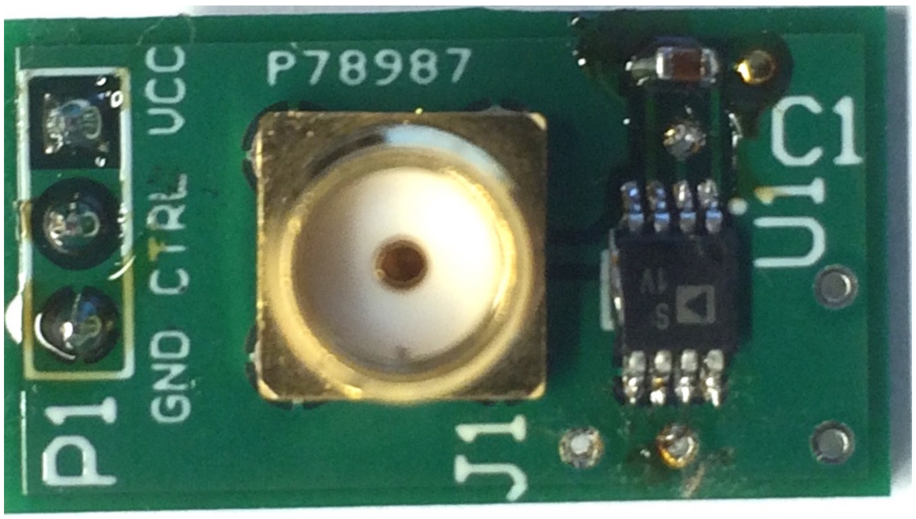

Figure 5.12. FS-Backscatter radio analog front end

connector, which allows us to directly connect different types of antennas. For example, we connect to a VERT2450 and a TL-ANT2409A 2.4GHz antenna for reflecting 2.4GHz wireless signals in our implementation. Our flexibility comes at a cost, however, since we do not tune matching circuits to the specific antenna. Hence, we might expect some performance improvement in a more integrated version.

In addition to the above prototype, we also have a full simulation of FS-Backscatter in HSPICE, which allows us to evaluate the power and performance of our ring oscillator circuit and voltage rails optimizations. We use three voltage controlled inverters to implement the ring oscillator. The control voltages for PMOS and NMOS are $V_{pc} = 0.1V$ and $V_{nc} = 0.75V$ respectively. We add one RC circuit ($R = 1.008K, C = 1.84pF$) in the second stage of the ring oscillator to introduce additional delay. When we use 0.8V to drive the PMOS and NMOS inside of the ring oscillator, we are able to obtain 20.006MHz oscillating frequency, accurate enough for modulating our information. Before feeding the

20MHz clock into the modulator, we put two additional inverters after the ring oscillator to shape the signal output by the ring oscillator.

- **Active transmitter and FS-Backscatter decoder:** Our carrier transmitter and receiver implementations use standard radios with standard antenna configurations to keep the setup similar to what we can expect in a mobile scenario. The transmitter is simply a Bluetooth/BLE or WiFi transmitter that continuously broadcasts data in a specified channel. Our packet-level decoders are implemented on a commercial TI CC3200 WiFi receiver and TI CC2650 BLE receiver. Packet-level reception is designed to work on commercial WiFi and BLE receivers without modification. Our bit-level decoder is implemented on a TI CC2541 BLE chipset which, in addition to the normal BLE mode, also supports a proprietary mode that bypasses the Bluetooth stack and allows us to directly access channel RSSI. While this API is not widely available on all BLE chipsets, we note that this mode is only needed at the receiver i.e. only one endpoint needs modification. So, one potential path to widespread use may be to have next-generation fitness bands or smartwatches swap BLE chipsets to use one with low-level channel access (or otherwise provide API access to the raw channel RSSI values) so that we can also use it as a high-rate backscatter receiver.

  When we observe an incident WiFi signal on the ith channel and a Bluetooth/BLE signal on the jth channel, we configure CC3200 and CC2650/CC2541 to detect packets on the $i + n$th and $j + n$th channels where n indicates the number of channels shifted by an FS-Backscatter tag. Signals detected by each radio are reported to the joint decoder for deciding the actual bit transmitted by a backscatter tag. CC3200, CC2650, and CC2541 have similar sensitivity (-95dBm) for detecting a backscattered signal.

- **WiFi Backscatter setup:** Since the code for WiFi Backscatter is under license from UW to a licensee company, we re-implement this scheme using parameters provided in the paper. We use a 9dBi directional gain antenna at the tag in experiments where we compare against this scheme because WiFi Backscatter does not work with a monopole antenna (as described in §5.2). But in all other experiments, we use a standard 3dBi omni-directional antenna [7] for FS-Backscatter. The WiFi/Bluetooth transmitter and receivers are equipped with standard onboard chip or PCB antennas.

5.5 Evaluation

We now turn to an evaluation of the various aspects of FS-Backscatter.

5.5.1 FS-Backscatter: Throughput and BER

Our goals in this experiment are two-fold. First, we want to tease apart the benefits of shifting to a clean band, and leveraging structure of WiFi/Bluetooth packets. Packet-level decoding allows us to take advantage of both whereas bit-level decoding only allows us to take advantage of the clean band. Second, we want to understand the differences in obtained throughput if we use the two types of decoding methods. Packet-level decoding gets one bit of information per packet, whereas bit-level decoding can go much faster.

In this experiment, we place a backscatter tag 1m away from a CC3200 WiFi/CC2650 BLE transmitter and then move the backscatter decoder away from the tag. We show two versions of this experiment — the first with a 9dBi directional antenna [17] on the tag to ensure that we obtain throughput numbers for WiFi Backscatter, and the second using a more standard 3dBi antenna [7]. We then evaluate the throughput for FS-Backscatter across distance for packet-level and bit-level decoding in FS-Backscatter as well as WiFi Backscatter.

Figure 5.13(a) shows the results. Packet-level decoding generally gives us the highest range of ∼5m, demonstrating the benefits of leveraging both a clean band as well as signal structure. We get this range even when using a more typical monopole antenna, which shows that leveraging both benefits has huge implications on range and makes backscatter practical even in challenging environments. FS-Backscatter can achieve 4.8m maximum operational distance, 16× longer than the WiFi backscatter system. In addition, the average throughput achieved is 627.7bps, 12.5× higher than WiFi Backscatter. These results clearly show the benefits of moving the backscattered signal into an adjacent clean spectrum rather than trying to separate WiFi signal variation from the backscatter modulated signal within the same band.

We turn to a comparison of packet-level decoding v.s. bit-level decoding. We use a BLE transmitter, and show results for the two decoding schemes in Figure 5.13(b). When bit-level RSSI information is used for decoding, the maximum operational distance achieved is 3.6m and the throughput increases to 50kbps, 79× higher than FS-Backscatter when packet-level RSSI is used because intra-packet RSSI detection allows us to detect the presence of reflected signal faster. The achieved maximum operational distance is slightly shorter because bit-level RSSI does not leverage the packet structure for decoding.

Figure 5.13(c) shows the bit error rate (BER) of FS-Backscatter across distance. We use the same experimental setting as Figure 5.13(b). FS-Backscatter with bit-level decoder can achieve 10^{-3} BER at 3.6m with 50kbps data rate and packet-level decoder can achieve 10^{-2} BER at 3.2m. When the FS-Backscatter tag is further, bit-level decoder BER increases to one sharply while packet-level decoder BER increases gradually. Such difference comes from the fact that packet-level decoder can leverage the structure of a packet for detecting the reflected signal. As a result, it is more tolerant to the degradation of reflected signal strength.

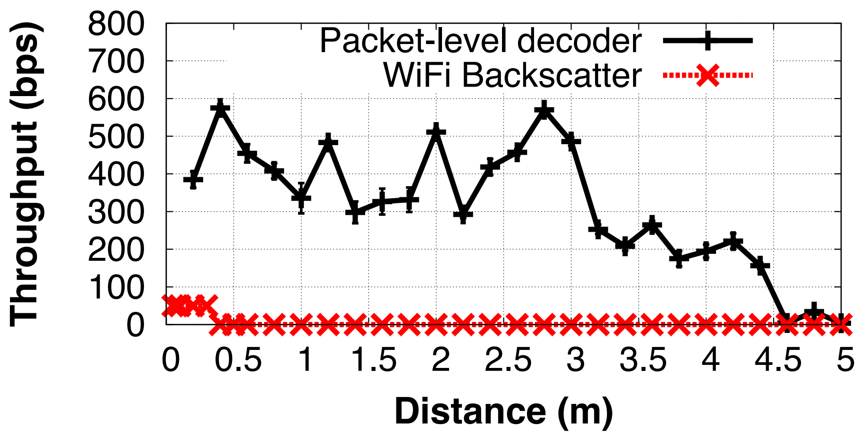

(a) Throughput when reflecting WiFi.

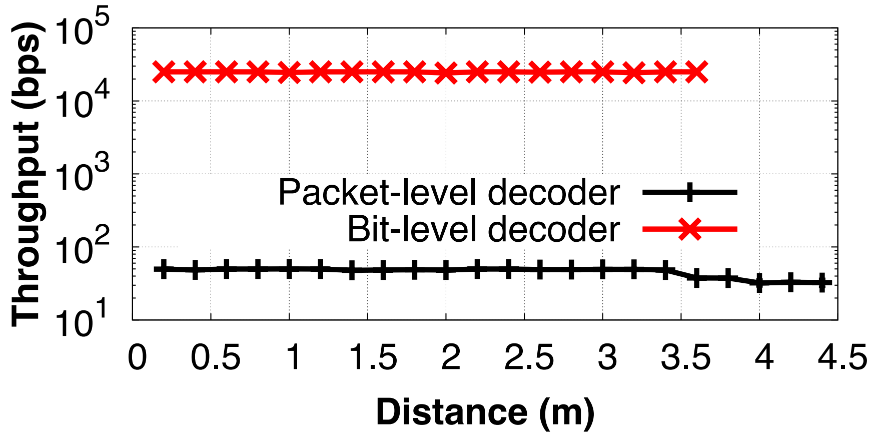

(b) Throughput when reflecting BLE.

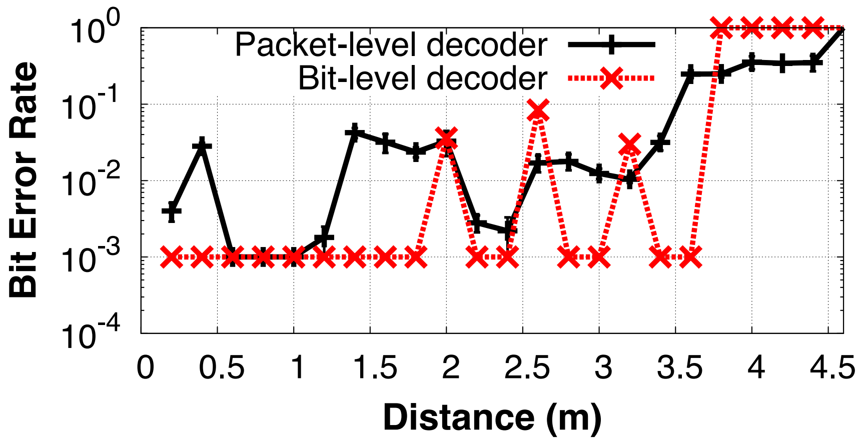

(c) BER when reflecting BLE.

Figure 5.13. FS-Backscatter throughput and BER across distance when leveraging WiFi and Bluetooth signals.

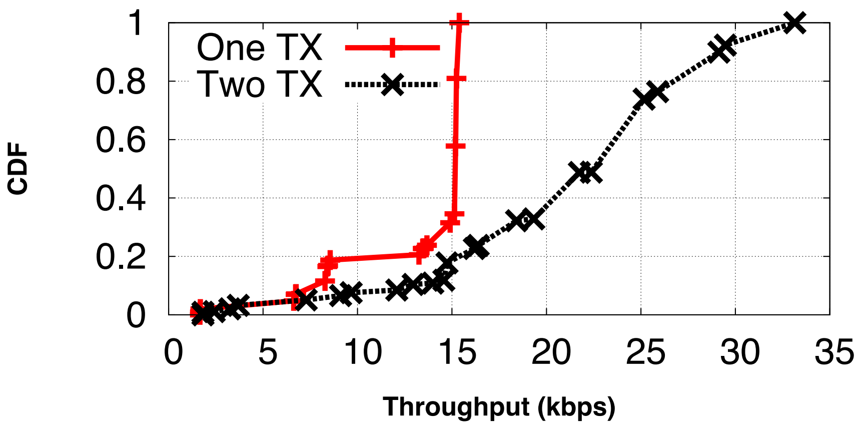

(a) Leveraging two active transmitters.

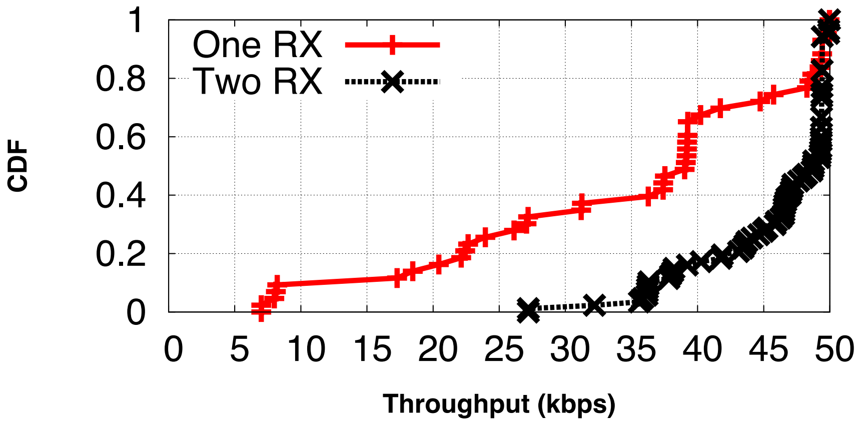

(b) Leveraging two active receivers.

Figure 5.14. FS-Backscatter throughput benefit when leveraging multiple active transmitters and receivers.

5.5.2 Multiple Carriers and Receivers

Let us now look at the benefits of leveraging multiple carrier signals for carrying backscattered information and multiple receivers for joint decoding. This set of experiments considers scenarios where we might have three or more radios on a phone, wristband, and tablet, and where multiple transmitters or receivers may be leveraged.

5.5.2.1 Leveraging multiple carriers

First, we investigate the benefit of multiple carriers where two Bluetooth signals are simultaneously leveraged by FS-Backscatter. We deploy two Bluetooth transmitters 0.2m away from each other and a FS-Backscatter tag in five locations in the department building, run a 2-minute experiment at each location, and compute throughput once every 10 seconds. Figure 5.14(a) shows the cumulative throughput of FS-Backscatter. When we only leverage a single Bluetooth signal, median throughput of 15.1kbps is achieved. However, FS-Backscatter is able to achieve 22.3kbps median throughput when leveraging both transmitters, 1.47× higher than leveraging a single Bluetooth signal. The throughput improvement is for reasons described in S5.3.1.4 — since Bluetooth transmitters are limited to a maximum output power of 0dBm, two transmitters naturally increases the signal strength at the decoder.

5.5.2.2 Leveraging multiple receivers

In our second experiment, we look at the case where two receivers are leveraged for joint decoding. We use two Bluetooth receivers 0.2m away from each other, each of which is configured to decode by using bit-level RSSI information. We measure the cumulative throughput and show the results in Figure 5.14(b). When a single Bluetooth receiver is used, we achieve 39.1kbps median throughput. When we jointly decode using two Bluetooth receivers, we can achieve 48.7kbps throughput, 1.24× higher than the single receiver case. We can achieve such throughput improvement because the reflected signal at one receiver can be strong while the reflected signal at the other is weak. In these cases, joint decoding is helpful and improves SNR.

5.5.3 Power consumption

Let us now look at the power consumption of an FS-Backscatter tag. We provide a breakdown of power for each component (ring oscillator, modulator, RF transistor), as well with and without DC voltage shifting. The results are shown in Figure 5.15.

We first look at the tag power consumption without DC voltage shifting where the whole system operates at 1.65V, which is the minimum voltage required for toggling an ADG902 RF transistor. The three hardware components of an FS-Backscatter

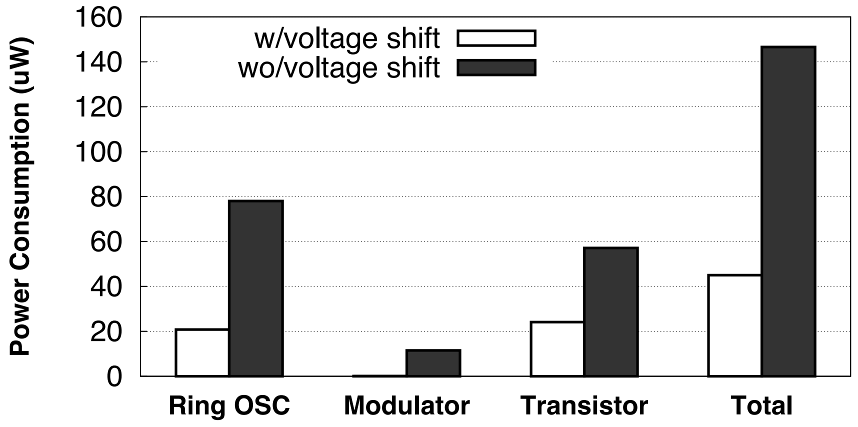

Figure 5.15. Benchmarking the power consumption of a FS-Backscatter tag.

tag: ring oscillator, data modulator, and RF transistor consume 78μW, 11.5μW, and 57.1μW respectively when transmitting at 50kbps and the overall tag power consumption is 146.6μW.

We reduce the tag power consumption by configuring the ring oscillator and data modulator to operate at lower voltage (0.8V) and shift the signal voltage output by the data modulator before feeding into the RF transistor. In this case, the ring oscillator, data modulator, and RF transistor consume 20.8μW, 0.1μW, and 24.1μW respectively with DC voltage shifting. The overall tag power consumption is 45μW, 3.25$\times$ lower than the case without DC voltage shifting. As shown, the major power reduction comes from the ring oscillator, which consumes 3.75$\times$ less power when operating at a lower voltage.

5.5.4 FS-Backscatter vs BLE/Zigbee

In this section, we compare the performance of FS-Backscatter against low-power active radios such as BLE and Zigbee. Low-power radios for wearable devices need to be compared along two axes. The first is bits/joule i.e. how many bits can be transmitted for a fixed amount of energy. This gives a measure of how much data can be transferred via a particular radio given an energy budget. However, more

Table 5.2. FS-Backscatter energy efficiency. Pkt refers to packet-level decoding, and Bit refers to bit-level decoding.

	Bits/μJ	Peak Power
BLE(CC2650)	54.6	18.3mW(0dBm)
ZigBee(CC2630)	13.7	18.3mW(0dBm)
FS-Backscatter (Pkt-WiFi)	25.5	45μW
FS-Backscatter (Pkt-BLE)	2.2	45μW
FS-Backscatter (Bit)	1100	45μW

powerful radios with higher bitrates will generally have higher efficiency in bits per joule, but will also consume more power in active mode. To account for this effect, another metric that is useful is peak power draw of the radio. Higher peak power draw implies worse lifetime from batteries, since battery decay curves are linked to not just the average power draw but also the peak power draw [38] [37] [22]. It also means that tags would need more complex batteries with built-in power management circuits to be able to sustain the burst during active mode. In addition, higher peak power also means that operating on harvested power is unlikely since additional voltage boosting and energy buffering circuits increase quiescent power draw.

Table 5.2 shows the peak power consumption and bits per μJ of a CC2650 BLE radio, a CC2630 ZigBee radio, and FS-Backscatter operating in three modes. FS-Backscatter has three orders of magnitude smaller peak power consumption compared to BLE and ZigBee. Therefore, FS-Backscatter is beneficial when we design a system that requires small peak power consumption, for example, in energy harvesting-based tags. When leveraging packet-level decoding, FS-Backscatter has smaller bits per μJ compared to BLE and ZigBee because its data rate is slow. However, when operating in bit-level decoding mode, FS-Backscatter energy efficiency significantly improves and can achieve 1100bits/μJ, 20.3$\times$ higher than BLE.

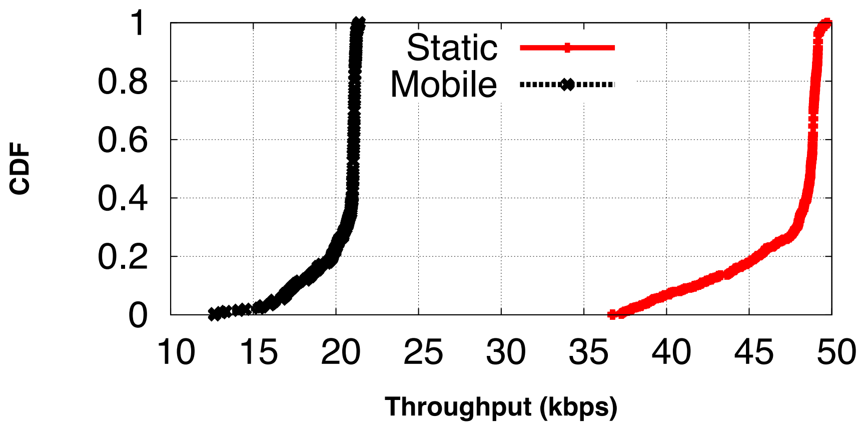

Figure 5.16. FS-backscatter throughput in static and mobile deployment.

5.5.5 Mobile and static deployment

We now look at the overall system performance in an on-body sensing scenario where we place a BLE transmitter in the pocket, a BLE receiver on the wrist, and the FS-Backscatter tag on the chest. This scenario corresponds to a scenario where a user has a phone and smartwatch, and wears an on-body sensor. The FS-Backscatter sensor tag transmits data at 50kbps, and a wristband receives and decodes the reflected signal using bit-level decoding. We look at a static case where the user is static for 10 minutes, and a mobile case where the user moves around for 10 minutes. We plot CDFs of the throughput numbers taken for each 10 second interval.

Figure 5.16 shows the results. We are able to achieve 48.7kbps and 21kbps median throughput when the person is static and mobile respectively. These numbers are very encouraging since many on-body sensors generate data rates far lower than this number. For example, a 3-axis accelerometer [3] sampled at 100Hz has a data communication rate requirement of 4.8kbps, whereas a ECG electrode [19] sampled at 250Hz has data rate requirements of 2kbps.

Between the static and mobile cases, we observe higher and more stable FS-Backscatter throughput in static deployment, as we might expect. In contrast, FS-Backscatter throughput is lower in the mobile deployment because body movement leads to significant channel variations and degrades throughput. However, the throughput in the mobile case is also quite promising, and worst case throughput is already more than 10kbps. This means that FS-Backscatter should generally be able to provide a continuous communication link from an on-body sensor to a phone/smartwatch combination.

5.5.6 Mutual Interference

One potential issue that we have not touched upon so far is how FS-Backscatter might interfere or be interfered by active radio traffic. Understanding mutual interference is important because FS-Backscatter operates in the 2.4GHz ISM band where spectrum occupancy is high. To answer this question, we first look at the interference by a WiFi radio on FS-Backscatter when both operate on the same channel. We deploy both a BLE transmitter and a FS-Backscatter decoder 1m away from an FS-Backscatter tag. We then adjust the distance of a WiFi interferer to understand how WiFi interferes with the FS-Backscatter data transmission. We use the bit-level decoder in this experiment since this is most likely to be impacted by cross-traffic.

Figure 5.17(a) shows that FS-Backscatter can achieve 49.7kbps median throughput when the WiFi interferer is not present. However, we observe that throughput degrades to 31.7kbps and 47.4kbps when the WiFi interferer is 10m and 15m from the FS-Backscatter decoder. This is because the power of the backscatted signal is only around -80dBm, whereas the power of the WiFi interferer is at least 20dB higher at close range. When the WiFi transmitter is 15m away, FS-Backscatter is able to achieve 47.4kbps throughput, close to the case when the WiFi interferer is not present. When WiFi transmitter is closer than 10m, FS-Backscatter throughput degrades to zero because WiFi interference is too strong.

Let us now look how FS-Backscatter interferes on an ongoing WiFi transmission. In this experiment, we deploy a WiFi transmitter 5m away from a WiFi receiver.

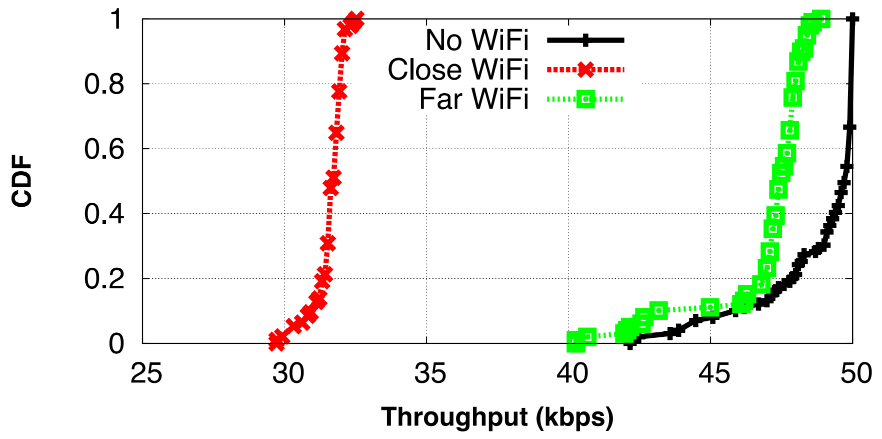

(a) FS-Backscatter throughput when WiFi interference is present.

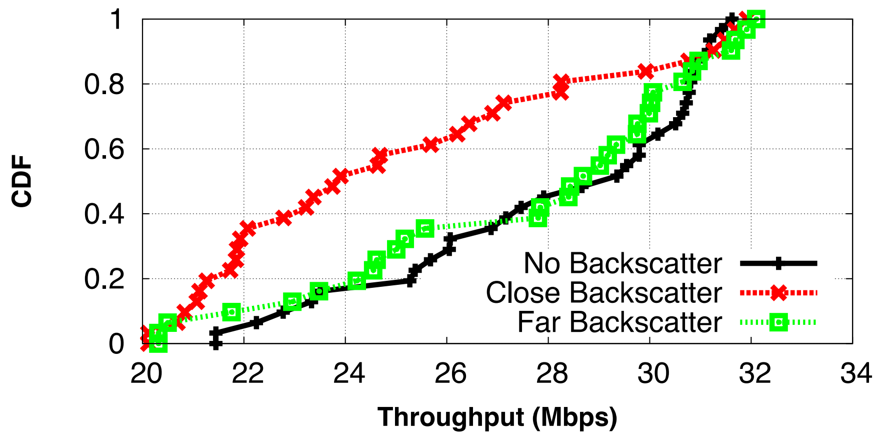

(b) WiFi throughput when backscatter interference is present.

Figure 5.17. Mutual interference between FS-Backscatter and WiFi.

Figure 5.17(b) shows that WiFi is able to achieve 29Mbps when FS-Backscatter is not present. When a FS-Backscatter tag is 0.2m from the WiFi receiver, the median WiFi throughput degrades to 23.9Mbps, 1.21× smaller. When the FS-Backscatter tag is 1m away, we observe 28.7Mbps median WiFi throughput, close to the case when FS-Backscatter is not present. Therefore, FS-Backscatter has only a relatively small interference range, and even then does not seem to have a substantial effect on WiFi throughput.

5.6 Related Work

There has been a lot of interest and activity in the area of backscatter-based communication and sensing in recent years [101, 71, 97, 45, 100, 64, 86, 87, 85, 88, 48, 52, 51, 71]. The interest has been spurred by the booming industry for embedding tiny sensors in virtually anything that we wear, touch, use or even ingest, ranging from the Internet of Things, on-body and implantable sensors, wearables, mobile devices, urban sensing, and others [42, 81, 93, 65, 25].

In particular, our work is inspired by recent progress on enabling backscatter with commodity radios or with some infrastructure support. Among the earliest efforts at approaching the problem in this manner is Ambient Backscatter [63] and WiFi backscatter [57]. More recently, there have been interesting infrastructure-assisted approaches such as BLE-Backscatter [35] and BackFi [26]. We have discussed these methods extensively in §5.2, and will not go into the details here. These are terrific ideas but they do have their limitations either in terms of robustness or practicality in the mobile environment. We build on these ideas and look at how to make backscatter practical for on-body devices. We also note that prior work does not look at the possibility of leveraging multiple incident signals, which we can take advantage of in FS-Backscatter.

FS-Backscatter is also inspired by previous work on interference cancellation. Recent work has looked at this problem in the context of full-duplex radios[54, 73, 68, 27, 31, 54]. However, these efforts require additional hardware components that are not present on many existing commercial radios. Other recent work use signal processing techniques over the analog signal to minimize interference [56, 40, 62, 41, 39, 46]. However, such analog signals are not available on many existing commercial radios. FS-Backscatter is designed to work on commercial radios and their constraints, and uses frequency shifting rather than interference cancelation.

FS-Backscatter tag is also inspired by previous work on RFID tag ASIC designs [90, 67, 77]. The main difference between an FS-Backscatter tag and an RFID tag is that FS-Backscatter requires a higher speed local clock for shifting the incident carrier signal. To achieve this, we leverage ring oscillators designs [70, 36, 75] and tune the circuit to enable 20MHz oscillating frequency while only consuming $\sim$20μW of power.

5.7 Conclusion

In summary, we discuss the design of FS-Backscatter, a system that enables backscatter communication between on-body sensor tags and commercial WiFi and Bluetooth radios. The key idea of FS-Backscatter is that we can reduce carrier signal interference by shifting the backscattered signal to a clean band that does not overlap with the carrier. We demonstrate that a 20MHz frequency shift is enough for enabling an FS-Backscatter tag to communicate with commercial WiFi and Bluetooth radios. Such frequency shift does not come with high power consumption at the tag side because we leverage a ring oscillator circuit to design a FS-Backscatter tag that only consumes 45μW. Our empirical evaluation shows that an FS-Backscatter tag is able to communicate with commercial WiFi and Bluetooth radios up to 4.8m and achieve 50kbps data rate. We believe that FS-Backscatter paves the way toward enabling practical deployment of backscatter-based low power on-body sensor tags.

CHAPTER 6
CONCLUSION AND FUTURE WORK

6.1 Thesis Summary

This thesis explores fundamental factors that limit the range, power reduction, and deployability of backscatter systems. I have employed a set of techniques, including hardware design, wireless communication, and operating systems, to significantly improve the performance of backscatter systems.

We propose a hardware sensing architecture that minimizes computational blocks between the sensors and the backscatter RF interface. Its design is inspired by studying a variety of computational blocks between sensors and backscatter RF interface. We find that these overheads were negligible on platforms where communication was expensive. However, because of the ultra-low power consumption of backscatter radios, they become the bottleneck on backscatter-based systems and increase power consumption while limiting throughput. Therefore, we overturn the design principle governing wireless sensor design from one that is focused on minimizing communication to one focused on optimizing the computational elements between the sensor and RF interface. FPGA instantiation demonstrates $\geq$1Mbps backscatter transmission while only consuming $\leq 100\mu$W of power, two orders of magnitude improvement over the state of the art.

We propose a network stack that fragments any network task into its smallest atomic units to enable the system to scale down to resource impoverished regimes. Its design is inspired by the observation that communication tasks executed by micro-powered sensors are simply too large to fit into the extreme energy constraints of this regime. For example, the core primitive of a network stack — packet transfer — can involve hundreds of instructions and bits. A packet transfer might not be successfully executed simply because it is too large compared to the extreme energy constraints of resource impoverished regimes. Therefore, we employ a simple but powerful abstraction — by fragmenting any network task into its smallest atomic units, we can enable the system to operate in resource impoverished regimes. The instantiation enables packet transfer when the whole system is powered by a 3cm$\times$3cm solar panel under natural indoor light condition.

In the last part, we look at how to deploy backscatter systems on mobile and wearable devices. Our key idea is leveraging multiple existing wireless signals for carrying backscattered information. To achieve the goal, we have to deal with several challenges, such as strong self-interference, slow data rate, and low power consumption. Our design follows two rules. First, we leverage existing wireless signals for backscatter since we do not need to deploy additional backscatter readers. Second, we use commercial radio receiver for decoding backscattered information because these radio already exist on mobile and wearables. Our empirical evaluation with an FPGA controlled backscatter radio, TI CC3200 WiFi chip, and TI CC2560 BLE chip shows that our system is able to achieve 500bps throughput and 5m operational distance when reflecting a WiFi signal respectively. Similar results can be observed when reflecting a bluetooth signal where we achieve 50kbps throughput and 5m operational distance.

6.2 Future Work

I would like to continue to explore research problems related to wearable and mobile systems. Below I describe three research directions I will pursue in the near future.

6.2.1 Applications enabled by backscatter

Backscatter has the potential to enable low-power video gaming on mobile devices. Video game applications usually involve complex graphics processing, including object segmentation and 3D rendering, and thereby require significant amount of computational resources and energy. For example, running the "Need for Speed" game on an iPhone consumes 90% of its CPU. To make matters worse, the iPhone cannot last for more than 2 hours when a user continuously plays the game. With the aid of ultra low-power backscatter radios, many graphics processing tasks can be offloaded to a base station which is connected to the cloud. Once graphics processing is done at the cloud, the computed results will be pushed back to mobile devices via backscatter. Because a mobile device only acts as a display for cloud-computed results, the proposed scheme will significantly reduce the energy and computational resources needed for running video gaming. There are several research challenges I will address to enable this application, including omni directional backscatter, partitioning tasks between mobile devices and cloud, and providing software and hardware abstractions for ease of application development.

6.2.2 Passive sensing via backscatter

Backscatter also has the potential to enable passive gesture identification and human activity recognition. To identify gestures and recognize activities, several recent research work [74] [20] exploit the key observation that any motion changes the propagation characteristics of backscattered signal. For example, a "wave" gesture will generate a doppler frequency shift on the received signal of a WiFi AP. [74] detects the doppler shift via physical layer signal processing, and uses it as the indicator of the presence of a gesture. However, detecting gestures presented by fingers via backscatter is challenging. Because of the small movement of fingers, doppler shift introduced is tiny and hard to detect. Instead, I am going to explore frequency domain features to identify fine-grained finger gestures. Specially, I am planning to use Frequency Modulated Continuous Wave (FMCW) radar. The intuition is that tiny finger movement will introduce large frequency offset on the backscatter signal received by a FMCW radar. Therefore, fine-grained finger gesture identification is possible. Realizing this capability requires research efforts from multiple perspectives, including customizing FMCW systems on a commercial WiFi AP, distinguishing finger gestures versus multi path interferences, etc.

6.2.3 Mobile health

Backscatter has the potential to enable ubiquitous and non-obtrusive health monitoring, which is hard to achieve with existing wearable and implantable devices. Let us look at a specific mobile health application — hearing aids, which grants hearing to people who otherwise would be unable to do so. One type of hearing aids is cochlear implants. However, existing cochlear implants require a disk-shaped transmitter about an inch in diameter, with a wire snaking down to a joint microphone and power source around the patient's ear. We think that backscatter can help significantly shrink down the form factor of cochlear implants. It provides RF energy for operating the whole cochlear system. In addition, the measured electrical signal can be offloaded to a base station via ultra low-power backscatter. By eliminating the battery, the whole cochlear implant has a smaller form factor and can be encapsulated into the middle ear. In addition to cochlear implants, many other mobile health applications will benefit from backscatter as well. For example, an RF-powered glucose monitoring system can be embedded in a contact lens.

BIBLIOGRAPHY

[1] 33 Billion Internet Devices By 2020: Four Connected Devices For Every Person In World. www.strategyanalytics.com.

[2] Advanced Self-Powered Systems of Integrated Sensors and Technologies. http://assist.ncsu.edu.

[3] Adxl362 mems accelerometer.

[4] Analog devices adxl362 accelerometer sensor. http://www.analog.com/static/imported-files/data_sheets/ADXL362.pdf.

[5] Analog devices mems microphone admp803. http://www.analog.com/static/imported-files/data_sheets/ADMP803.pdf.

[6] The cbvs ecg-on-chip. http://www.clearbridgevitalsigns.com/chip.html.

[7] Ettus research vert2450 antenna.

[8] Five Challenges For The Internet of Things Ecosystem. http://www.forbes.com/sites/rakeshsharma/2013/11/12/five-challenges-for-the-the-internet-of-things-ecosystem/.

[9] Gradient descent. http://en.wikipedia.org/wiki/Gradient_descent.

[10] Libero ide. http://www.microsemi.com/products/fpga-soc/design-resources/design-software/libero-ide.

[11] Mean opinion score. http://en.wikipedia.org/wiki/Mean_opinion_score.

[12] Nxp 74hc1g00 nand gate.

[13] Source code of QuarkNet. https://github.com/pengyuzhang/QuarkNet.

[14] The Impinj UHF Gen 2 Speedway RFID Reader. http://www.impinj.com.

[15] ThingMagic Bistatic Antenna. http://buyrfid.com/.

[16] Ti cc2541 simplelink bluetooth smart and proprietary wireless mcu.

[17] Tp-link tl-ant2409a antenna.

[18] WISP: Wireless Identification and Sensing Platform. http://seattle.intel-research.net/wisp/.

[19] Zephyr bioharness.

[20] Adib, Fadel, and Katabi, Dina. *See through walls with WiFi!*, vol. 43. ACM, 2013.

[21] Angerer, C., Langwieser, R., and Rupp, M. Rfid reader receivers for physical layer collision recovery. *IEEE Transactions on Communications* (2010).

[22] Badam, Anirudh, Chandra, Ranveer, Dutra, Jon, Ferrese, Anthony, Hodges, Steve, Hu, Pan, Meinershagen, Julia, Moscibroda, Thomas, Priyantha, Bodhi, and Skiani, Evangelia. Software defined batteries. In *Proceedings of the 25th Symposium on Operating Systems Principles* (2015), ACM, pp. 215–229.

[23] Balasubramanian, Niranjan, Balasubramanian, Aruna, and Venkataramani, Arun. Energy consumption in mobile phones: a measurement study and implications for network applications. In *ACM SIGCOMM IMC 2009*.

[24] Bandyopadhyay, S., and Chandrakasan, A.P. Platform architecture for solar, thermal and vibration energy combining with mppt and single inductor. In *VLSI Circuits (VLSIC), 2011 Symposium on* (2011), IEEE, pp. 238–239.

[25] Bandyopadhyay, Supriyo, Mercier, Patrick P, Lysaght, Andrew C, Stankovic, Konstantina M, and Chandrakasan, Anantha P. A 1.1 nw energy-harvesting system with 544 pw quiescent power for next-generation implants. *Solid-State Circuits, IEEE Journal of 49*, 12 (2014), 2812–2824.

[26] Bharadia, Dinesh, Joshi, Kiran Raj, Kotaru, Manikanta, and Katti, Sachin. Backfi: High throughput wifi backscatter. In *Proceedings of the 2015 ACM Conference on Special Interest Group on Data Communication* (2015), ACM, pp. 283–296.

[27] Bharadia, Dinesh, and Katti, Sachin. Fastforward: fast and constructive full duplex relays. In *Proceedings of the 2014 ACM conference on SIGCOMM* (2014), ACM, pp. 199–210.

[28] Bierman, William. The temperature of the skin surface. *Journal of the American Medical Association 106*, 14 (1936), 1158–1162.

[29] Buettner, Michael, Greenstein, Ben, and Wetherall, David. Dewdrop: an energy-aware runtime for computational rfid. In *USENIX NSDI 2011*.

[30] Buettner, Michael, and Wetherall, David. A software radio-based uhf rfid reader for phy/mac experimentation. In *RFID (RFID), 2011 IEEE International Conference on* (2011), IEEE, pp. 134–141.

[31] Choi, Jung Il, Jain, Mayank, Srinivasan, Kannan, Levis, Phil, and Katti, Sachin. Achieving single channel, full duplex wireless communication. In *Proceedings of the sixteenth annual international conference on Mobile computing and networking* (2010), ACM, pp. 1–12.

[32] Commission, Federal Communications. Part 15.247 operation within the bands 902 - 928 mhz, 2400 - 2483.5 mhz, and 5725 - 5850 mhz.

[33] De la Piedra, Antonio, Braeken, An, and Touhafi, Abdellah. Sensor systems based on fpgas and their applications: a survey. *Sensors 12*, 9 (2012), 12235–12264.

[34] Dutta, Prabal, and Culler, David. Epic: An open mote platform for application-driven design. In *IEEE IPSN 2008*.

[35] Ensworth, Joshua F, and Reynolds, Matthew S. Every smart phone is a backscatter reader: Modulated backscatter compatibility with bluetooth 4.0 low energy (ble) devices. In *RFID (RFID), 2015 IEEE International Conference on* (2015), IEEE, pp. 78–85.

[36] Farzeen, Suzana, Ren, Guoyan, and Chen, Chunhong. An ultra-low power ring oscillator for passive uhf rfid transponders. In *Circuits and Systems (MWSCAS), 2010 53rd IEEE International Midwest Symposium on* (2010), IEEE, pp. 558–561.

[37] Feeney, Laura Marie, Rohner, Christian, Gunningberg, Per, Lindgren, Anders, and Andersson, Lars. How do the dynamics of battery discharge affect sensor lifetime? In *Wireless On-demand Network Systems and Services (WONS), 2014 11th Annual Conference on* (2014), IEEE, pp. 49–56.

[38] Furset, Kjartan, and Hoffman, P. High pulse drain impact on cr2032 coin cell battery capacity. *Availab le: http://www. eetimes. com/ContentEETimes/Documents/Schweber C 924* (2011).

[39] Gollakota, Shyamnath, Adib, Fadel, Katabi, Dina, and Seshan, Srinivasan. Clearing the rf smog: making 802.11 n robust to cross-technology interference. *ACM SIGCOMM Computer Communication Review 41*, 4 (2011), 170–181.

[40] Gollakota, Shyamnath, and Katabi, Dina. *Zigzag decoding: combating hidden terminals in wireless networks*, vol. 38. ACM, 2008.

[41] Gollakota, Shyamnath, Perli, Samuel David, and Katabi, Dina. Interference alignment and cancellation. In *ACM SIGCOMM Computer Communication Review* (2009), vol. 39, ACM, pp. 159–170.

[42] Gollakota, Shyamnath, Reynolds, Matthew S, Smith, Joshua R, and Wetherall, David J. The emergence of rf-powered computing. *Computer 47*, 1 (2014), 32–39.

[43] Gorlatova, Maria, Kinget, Peter, Kymissis, Ioannis, Rubenstein, Dan, Wang, Xiaodong, and Zussman, Gil. Challenge: ultra-low-power energy-harvesting active networked tags (enhants). In *Proceedings of the 15th annual international conference on Mobile computing and networking* (2009), ACM, pp. 253–260.

[44] Gummeson, Jeremy, Clark, Shane S, Fu, Kevin, and Ganesan, Deepak. On the limits of effective hybrid micro-energy harvesting on mobile crfid sensors. In *ACM MobiSys 2010*.

[45] Gummeson, Jeremy, Zhang, Pengyu, and Ganesan, Deepak. Flit: a bulk transmission protocol for rfid-scale sensors. In *ACM MobiSys 2012*.

[46] Halperin, Daniel, Anderson, Thomas, and Wetherall, David. Taking the sting out of carrier sense: interference cancellation for wireless lans. In *Proceedings of the 14th ACM international conference on Mobile computing and networking* (2008), ACM, pp. 339–350.

[47] Hanson, Scott, Foo, ZhiYoong, Blaauw, David, and Sylvester, Dennis. A 0.5 v sub-microwatt cmos image sensor with pulse-width modulation read-out. In *JSSCC 2010*.

[48] Hassanieh, Haitham, Wang, Jue, Katabi, Dina, and Kohno, Tadayoshi. Securing rfids by randomizing the modulation and channel. NSDI.

[49] Hinkelmann, Heiko, Reinhardt, Andreas, Varyani, Sameer, and Glesner, Manfred. A reconfigurable prototyping platform for smart sensor networks. In *Programmable Logic, 2008 4th Southern Conference on* (2008), IEEE, pp. 125–130.

[50] Holleman, Jeremy, Yeager, Dan, Prasad, Richa, Smith, Joshua R, and Otis, Brian. Neuralwisp: An energy-harvesting wireless neural interface with 1-m range. In *BioCAS'08* (2008), IEEE, pp. 37–40.

[51] Hu, Pan, Zhang, Pengyu, and Ganesan, Deepak. Leveraging interleaved signal edges for concurrent backscatter. In *Proceedings of the 1st ACM workshop on Hot topics in wireless* (2014), ACM, pp. 13–18.

[52] Hu, Pan, Zhang, Pengyu, and Ganesan, Deepak. Laissez-faire: Fully asymmetric backscatter communication. In *Proceedings of the 2015 ACM Conference on Special Interest Group on Data Communication* (2015), ACM, pp. 255–267.

[53] Huang, Junxian, Qian, Feng, Gerber, Alexandre, Mao, Z Morley, Sen, Subhabrata, and Spatscheck, Oliver. A close examination of performance and power characteristics of 4g lte networks. In *ACM MobiSys 2012*.

[54] Jain, Mayank, Choi, Jung Il, Kim, Taemin, Bharadia, Dinesh, Seth, Siddharth, Srinivasan, Kannan, Levis, Philip, Katti, Sachin, and Sinha, Prasun. Practical, real-time, full duplex wireless. In *Proceedings of the 17th annual international conference on Mobile computing and networking* (2011), ACM, pp. 301–312.

[55] Kamalinejad, Pouya, Keikhosravy, Kamyar, Molavi, Reza, Mirabbasi, Shahriar, and Leung, Victor. An ultra-low-power cmos voltage-controlled ring oscillator for passive rfid tags. In *New Circuits and Systems Conference (NEWCAS), 2014 IEEE 12th International* (2014), IEEE, pp. 456–459.

[56] Katti, Sachin, Rahul, Hariharan, Hu, Wenjun, Katabi, Dina, Médard, Muriel, and Crowcroft, Jon. Xors in the air: practical wireless network coding. In *ACM SIGCOMM Computer Communication Review* (2006), vol. 36, ACM, pp. 243–254.

[57] Kellogg, Bryce, Parks, Aaron, Gollakota, Shyamnath, Smith, Joshua R, and Wetherall, David. Wi-fi backscatter: internet connectivity for rf-powered devices. In *Proceedings of the 2014 ACM conference on SIGCOMM* (2014), ACM, pp. 607–618.

[58] Kellogg, Bryce, Talla, Vamsi, and Gollakota, Shyamnath. Bringing gesture recognition to all devices. In *USENIX NSDI 2014*.

[59] Law, C., Lee, K., and Siu, K.Y. Efficient memoryless protocol for tag identification. In *Proceedings of the 4th international workshop on Discrete algorithms and methods for mobile computing and communications* (2000), ACM, pp. 75–84.

[60] Lee, Kin Keung, Granhaug, Kristian, and Andersen, Nikolaj. A study of low-power crystal oscillator design. In *NORCHIP, 2013* (2013), IEEE, pp. 1–4.

[61] Lee, Y., Kim, G., Bang, S., Kim, Y., Lee, I., Dutta, P., Sylvester, D., and Blaauw, D. A modular $1mm^3$ die-stacked sensing platform with optical communication and multi-modal energy harvesting. In *ISSCC 2012*.

[62] Lin, Kate Ching-Ju, Kushman, Nate, and Katabi, Dina. Ziptx: Harnessing partial packets in 802.11 networks. In *Proceedings of the 14th ACM international conference on Mobile computing and networking* (2008), ACM, pp. 351–362.

[63] Liu, Vincent, Parks, Aaron, Talla, Vamsi, Gollakota, Shyamnath, Wetherall, David, and Smith, Joshua R. Ambient backscatter: wireless communication out of thin air. In *ACM SIGCOMM 2013*.

[64] Liu, Vincent, Talla, Vamsi, and Gollakota, Shyamnath. Enabling instantaneous feedback with full-duplex backscatter. In *Proceedings of the 20th annual international conference on Mobile computing and networking* (2014), ACM, pp. 67–78.

[65] Mercier, Patrick P, Lysaght, Andrew C, Bandyopadhyay, Saurav, Chandrakasan, Anantha P, and Stankovic, Konstantina M. Energy extraction from the biologic battery in the inner ear. *Nature biotechnology 30*, 12 (2012), 1240–1243.

[66] Namboodiri, V., and Gao, L. Energy-aware tag anticollision protocols for rfid systems. *Mobile Computing, IEEE Transactions on 9*, 1 (2010), 44–59.

[67] Nikitin, Pavel V, Rao, KV Seshagiri, Lam, Sander F, Pillai, Vijay, Martinez, Rene, and Heinrich, Harley. Power reflection coefficient analysis for complex

impedances in rfid tag design. *IEEE Transactions on Microwave Theory and Techniques 53*, 9 (2005), 2721–2725.

[68] Nikitin, Pavel V, and Rao, KVS. Antennas and propagation in uhf rfid systems. *challenge 22* (2008), 23.

[69] Pantelopoulos, Alexandros, and Bourbakis, Nikolaos G. A survey on wearable sensor-based systems for health monitoring and prognosis. *Systems, Man, and Cybernetics, Part C: Applications and Reviews, IEEE Transactions on 40*, 1 (2010), 1–12.

[70] Park, Sunghyun, Min, Changwook, and Cho, SeongHwan. A 95nw ring oscillator-based temperature sensor for rfid tags in 0.13μm cmos. In *Circuits and Systems, 2009. ISCAS 2009. IEEE International Symposium on* (2009), IEEE, pp. 1153–1156.

[71] Parks, Aaron N, Liu, Angli, Gollakota, Shyamnath, and Smith, Joshua R. Turbocharging ambient backscatter communication. In *Proceedings of the 2014 ACM conference on SIGCOMM* (2014), ACM, pp. 619–630.

[72] Peris-Lopez, Pedro, Hernandez-Castro, Julio Cesar, Estevez-Tapiador, Juan M, and Ribagorda, Arturo. Lameda prng for epc class-1 generation-2 rfid specification. *Computer Standards & Interfaces 31*, 1 (2009), 88–97.

[73] Pozar, David M. *Microwave engineering.* John Wiley & Sons, 2009.

[74] Pu, Qifan, Gupta, Sidhant, Gollakota, Shyamnath, and Patel, Shwetak. Whole-home gesture recognition using wireless signals. In *Proceedings of the 19th annual international conference on Mobile computing & networking* (2013), ACM, pp. 27–38.

[75] Qu, Gang, and Yin, Chi-En. Temperature-aware cooperative ring oscillator puf. In *Hardware-Oriented Security and Trust, 2009. HOST'09. IEEE International Workshop on* (2009), IEEE, pp. 36–42.

[76] Ransford, Benjamin, Sorber, Jacob, and Fu, Kevin. Mementos: System support for long-running computation on rfid-scale devices. *ACM SIGPLAN Notices 47*, 4 (2012), 159–170.

[77] Rao, KV Seshagiri, Nikitin, Pavel V, and Lam, Sander F. Impedance matching concepts in rfid transponder design. In *Automatic Identification Advanced Technologies, 2005. Fourth IEEE Workshop on* (2005), IEEE, pp. 39–42.

[78] Sample, Alanson P, Yeager, Daniel J, Powledge, Pauline S, Mamishev, Alexander V, and Smith, Joshua R. Design of an rfid-based battery-free programmable sensing platform. *Instrumentation and Measurement, IEEE Transactions on 57*, 11 (2008), 2608–2615.

[79] Song, F, Yin, J, Liao, HL, and Huang, R. Ultra-low-power clock generation circuit for epc standard uhf rfid transponders. *Electronics Letters 44*, 3 (2008), 199–201.

[80] Sundstrom, Kurt E, Cooper, Scott A, Sarajedini, Amir, Esterberg, Aanand, Humes, Todd E, and Diorio, Christopher J. Rfid reader systems detecting pilot tone, Jan. 8 2013. US Patent 8,350,665.

[81] Talla, Vamsi, Kellogg, Bryce, Ransford, Benjamin, Naderiparizi, Saman, Gollakota, Shyamnath, and Smith, Joshua R. Powering the next billion devices with wi-fi. *arXiv preprint arXiv:1505.06815* (2015).

[82] Trotter, Matthew S, Griffin, Joshua D, and Durgin, Gregory D. Power-optimized waveforms for improving the range and reliability of rfid systems. In *RFID, 2009 IEEE International Conference on* (2009), IEEE, pp. 80–87.

[83] Vannucci, Giovanni, Bletsas, Aggelos, and Leigh, Darren. A software-defined radio system for backscatter sensor networks. *Wireless Communications, IEEE Transactions on 7*, 6 (2008), 2170–2179.

[84] Vogt, H. Efficient object identification with passive rfid tags. *Pervasive Computing* (2002), 98–113.

[85] Wang, Jue, Adib, Fadel, Knepper, Ross, Katabi, Dina, and Rus, Daniela. Rf-compass: robot object manipulation using rfids. In *Proceedings of the 19th annual international conference on Mobile computing & networking* (2013), ACM, pp. 3–14.

[86] Wang, Jue, Hassanieh, Haitham, Katabi, Dina, and Indyk, Piotr. Efficient and reliable low-power backscatter networks. In *ACM SIGCOMM 2012*.

[87] Wang, Jue, and Katabi, Dina. Dude, where's my card?: Rfid positioning that works with multipath and non-line of sight. In *ACM SIGCOMM Computer Communication Review* (2013), vol. 43, ACM, pp. 51–62.

[88] Wang, Jue, Vasisht, Deepak, and Katabi, Dina. Rf-idraw: virtual touch screen in the air using rf signals. In *Proceedings of the 2014 ACM conference on SIGCOMM* (2014), ACM, pp. 235–246.

[89] Yakovlev, A., Kim, S., and Poon, A. Implantable biomedical devices: wireless powering and communication. *Communications Magazine, IEEE 50*, 4 (2012), 152–159.

[90] Yeager, Daniel, Zhang, Fan, Zarrasvand, Azin, George, Nicole T, Daniel, Thomas, and Otis, Brian P. A 9 a, addressable gen2 sensor tag for biosignal acquisition. *Solid-State Circuits, IEEE Journal of 45*, 10 (2010), 2198–2209.

[91] Yeager, Daniel J, Powledge, Pauline S, Prasad, Richa, Wetherall, David, and Smith, Joshua R. Wirelessly-charged uhf tags for sensor data collection. In *RFID, 2008 IEEE International Conference on* (2008), IEEE, pp. 320–327.

[92] Yeager, D.J., Holleman, J., Prasad, R., Smith, J.R., and Otis, B.P. Neuralwisp: A wirelessly powered neural interface with 1-m range. *Biomedical Circuits and Systems, IEEE Transactions on 3*, 6 (2009), 379–387.

[93] Yip, Marcus, Jin, Rui, Nakajima, Hideko Heidi, Stankovic, Konstantina M, and Chandrakasan, Anantha P. A fully-implantable cochlear implant soc with piezoelectric middle-ear sensor and arbitrary waveform neural stimulation. *Solid-State Circuits, IEEE Journal of 50*, 1 (2015), 214–229.

[94] Zanetti, D., et al. Physical-layer identification of uhf rfid tags. In *ACM MobiCom* (2010).

[95] Zappi, Piero, Lombriser, Clemens, Stiefmeier, Thomas, Farella, Elisabetta, Roggen, Daniel, Benini, Luca, and Tröster, Gerhard. Activity recognition from on-body sensors: accuracy-power trade-off by dynamic sensor selection. In *Wireless sensor networks*. Springer, 2008, pp. 17–33.

[96] Zhang, H., Gummeson, J., Ransford, B., and Fu, K. Moo: A batteryless computational rfid and sensing platform. Tech. rep., Tech. Rep. UM-CS-2011-020, 2011.

[97] Zhang, Pengyu, and Ganesan, Deepak. Enabling bit-by-bit backscatter communication in severe energy harvesting environments. In *NSDI 2014*.

[98] Zhang, Pengyu, and Ganesan, Deepak. Enabling bit-by-bit backscatter communication in severe energy harvesting environments. Tech. rep., School of Computer Science, UMass Amherst. URL: `http://cs.umass.edu/~pyzhang/papers/QuarkNet-tech-report.pdf`, 2014.

[99] Zhang, Pengyu, Ganesan, Deepak, and Lu, Boyan. Quarkos: Pushing the operating limits of micro-powered sensors. In *Proceedings of the 14th USENIX conference on Hot Topics in Operating Systems* (2013), USENIX Association, pp. 7–7.

[100] Zhang, Pengyu, Gummeson, Jeremy, and Ganesan, Deepak. Blink: a high throughput link layer for backscatter communication. In *ACM MobiSys 2012*.

[101] Zhang, Pengyu, Hu, Pan, Pasikanti, Vijay, and Ganesan, Deepak. Ekhonet: high speed ultra low-power backscatter for next generation sensors. In *Proceedings of the 20th annual international conference on Mobile computing and networking* (2014), ACM, pp. 557–568.